MICROCOPY RESOLUTION TEST CHART
NATIONAL BUREAU OF STANDARDS 1963 A

UNDERKEEL CLEARANCE STUDY

prepared for

NAVAL FACILITIES ENGINEERING COMMAND

Alexandria, Virginia

by

Dr. A. B. Rudavsky
Wei-Yih Chow
James C. Wang
Jen-Men Lo

HRS Inc. *HYDRO RESEARCH SCIENCE*

.3334 VICTOR COURT   ■   SANTA CLARA, CALIFORNIA 95050   ■   408 – 988-1027

UNDERKEEL CLEARANCE STUDY

prepared for

NAVAL FACILITIES ENGINEERING COMMAND

Alexandria, Virginia

Cover photo illustrates one cause of CVN Fouling Problem.

by

Dr. A. B. Rudavsky

Wei-Yih Chow

James C. Wang

Jen-Men Lo

March 31, 1981

REPORT DOCUMENTATION PAGE	READ INSTRUCTIONS BEFORE COMPLETING FORM

1. REPORT NUMBER	2. GOVT ACCESSION NO.	3. RECIPIENT'S CATALOG NUMBER
N00014-80-C-0395		

4. TITLE (and Subtitle)	5. TYPE OF REPORT & PERIOD COVERED
Underkeel Clearance Study prepared for Naval Facilities Engineering Command Alexandria, Virginia	Final, March 1980 – September 1981
	6. PERFORMING ORG. REPORT NUMBER
	1124

7. AUTHOR(s)	8. CONTRACT OR GRANT NUMBER(s)
Dr. A. B. Rudavsky Jen-Men Lo Wei-Yih Chow James C. Wang	N00014-80-C-0395

9. PERFORMING ORGANIZATION NAME AND ADDRESS	10. PROGRAM ELEMENT, PROJECT, TASK AREA & WORK UNIT NUMBERS
Hydro Research Science (HRS, Inc.) 3334 Victor Court Santa Clara, CA 95018	Element 64567N Task 23702

11. CONTROLLING OFFICE NAME AND ADDRESS	12. REPORT DATE
PCO ONR Dept Navy 800 N. Quincy St. Arlington, VA 22217	published September 1981
	13. NUMBER OF PAGES
	170

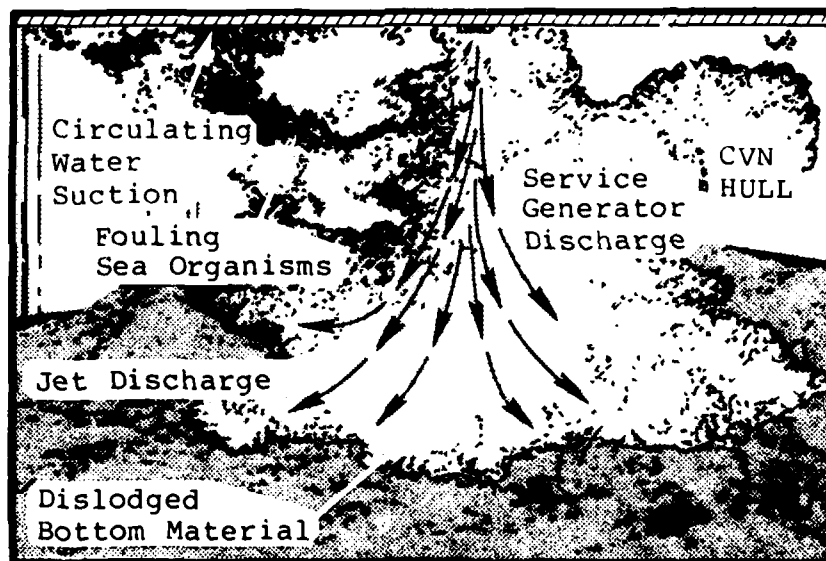| 14. MONITORING AGENCY NAME & ADDRESS(if different from Controlling Office)	15. SECURITY CLASS. (of this report)
Commander Atlantic Division Naval Facilities Engineering Command Attn: Mr. W.F. Gasser, Code 1025 Bldg W-5, Naval Station, Norfolk, VA 23511	Unclassified
	15a. DECLASSIFICATION/DOWNGRADING SCHEDULE

16. DISTRIBUTION STATEMENT (of this Report)

DISTRIBUTION STATEMENT A

Approved for public release;
Distribution Unlimited

17. DISTRIBUTION STATEMENT (of the abstract entered in Block 20, if different from Report)

18. SUPPLEMENTARY NOTES

19. KEY WORDS (Continue on reverse side if necessary and identify by block number)

Fouling   Hydraulic Models
Marine Organisms   Numerical Models
Sediments   Discharge Diffusers
Jets

20. ABSTRACT (Continue on reverse side if necessary and identify by block number)

Hydraulic model study was conducted to characterize the dynamic process of deep-draft vessel's sea-chest fouling, and to assess the flow patterns generated by suction and discharge of the sea chests in confined spaces. Onboard solutions were developed to minimize fouling of the sea chests by introducing diffuser structures at the discharge sea chests. A numerical model for assessing the flow patterns and suction foulings was also developed.

DD FORM 1473   EDITION OF 1 NOV 65 IS OBSOLETE
1 JAN 73

CONTENTS

CONTENTS (continued)

CONTENTS (continued)

CONTENTS (continued)

CONTENTS (continued)

LIST OF FIGURES

LIST OF FIGURES (continued)

LIST OF FIGURES (continued)

LIST OF TABLES

EXECUTIVE SUMMARY

THE PROBLEM -- DECREASED OPERATIONAL READINESS OF CVN CLASS VESSELS

The operational readiness of aircraft carriers has for years been reduced by what would seem to be a minor problem -- the fouling of sea chests due to the ingestion of bottom sediment and marine organisms. Such fouling problems occur at both pier side and upon entering and leaving the berthing areas of certain Naval harbors.

According to one Navy source, serious consequences can result from the inoperability of circulating water systems of CVN class vessels. Some typical problems have been reported [1] to include:

- Delays of flight operations for up to 12 hours following underway time, as catapults cannot be warmed at the pier.

- Underway evolutions cannot be conducted using the main engines, and tug assistance to anchorage is therefore often required.

- Frequent malfunctions of the turbine generator and distilling plant occur, in addition to excessive wear of the ship's machinery and pump components.

Such circulating water-system clogging has been found to occur at either the suction grating on the hull or on the tube sheet inside the condenser head. The exact causal factors were previously unknown, but were assumed to

Reference:

- Text Section 3.1

- Text Sections 1.1, 3.1
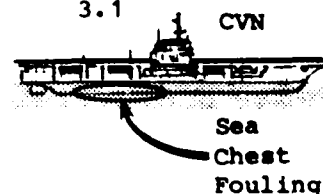
CVN

Sea Chest Fouling

-a-

be: underkeel "migration" of marine organisms,
sea chest suction, inadequate underkeel clear-
ance, or a combination of these factors.

- Text Sections 3.2.3,
  3.2.4

Before this study, little was known about
the underkeel clearance required to alleviate
such fouling problems. Prior to dredging to
the proposed 50- plus 2-foot berthing depth
for carriers, Norfolk Naval Base authorities
wanted to be assured that the planned depth
would alleviate the fouling problem.

Proposed 50' Depth
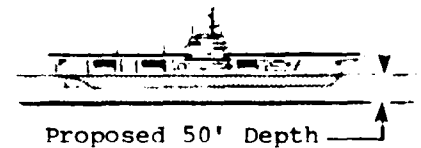
OBJECTIVES OF THE CURRENT STUDY

A Technology Development project was
initiated by Naval Facilities Engineering
Command (NAVFACENGCOM) to determine the
underkeel clearance required to alleviate
the fouling problem. The project was sub-
sequently awarded to Hydro Research Science
(HRS, Inc.) in the form of ONR Contract Num-
ber N00014-80-C-0395 dated 17 MAR 80.

- Text Sections 1.2,
  3.8
- Figure 3-4

The underlying objectives of the result-
ing HRS study were to: (a) investigate the
underkeel requirements of aircraft carriers
as related to the sea chest fouling problem,
and (b) develop an on-board technology to
control the fouling problems experienced by
aircraft carriers in certain parts of Norfolk
Harbor.

PHYSICAL MODEL PREPARATION

Precision-constructed scale models of the
selected CVN class service generator and main
circulating cooling systems were then con-
structed. The models were placed in the HRS

- Text Section 4.1
- Appendix B
- Figures 4-1, 4-2,
  4-3

Berthing Tank and fully instrumented for experimental purposes. The tank bottom was filled with sized walnut shell grains to simulate mud and algae to simulate marine organisms, and a dye probe was installed in the recirculating system to enable observation of the flow patterns.

IDENTIFICATION OF THE PRIMARY CAUSAL FACTOR

As a result of an intense hydraulic modeling investigation of the circulating cooling system fouling problems of Naval aircraft carriers during berthing and light off operations at port...the primary causal factor was identified as the sea-chest discharge jet.

- Text Section 4.2
- Figure 4-4

The impingement of the jet on the berthing floor was found to cause dislodgement of bottom material. When the resuspended materials approached the suction sea chest, they were ingested and fouling occurred. Hydraulic model experimentation using an assumed average draft of 39 ft, with underkeel clearances of 5, 13, and 21 ft, corresponding to slip depths of 44, 52, and 60 ft, respectively, indicated that a strong "jet" persisted throughout the entire jet path.

An in-depth study was then conducted to characterize the velocity and pressure fields of the jets. It became obvious that onboard modifications would be potentially effective in controlling condenser fouling problems.

THE DIFFUSER AS THE
ONBOARD SOLUTION

As the outcome of April/May 1980 meetings between HRS, NAVSEASYSCOM, NAVFACENGCOM

- Text Section 1.2.2

and LANTNAVFACENGCOM at the HRS Laboratory, it was agreed that HRS should pursue sea-chest "diffusers" as a viable onboard solution to the fouling problem.

The concept of diffuser design is to spread the flow through various physical arrangements such that the flow velocity is reduced and a uniform exit velocity obtained.

● Text Section 6.2

It was further agreed that the resulting diffuser designs were to be tested by HRS at potential underkeel clearances of 5 and 13 ft, corresponding to slip depths of 44 and 52 ft, utilizing physical-model test procedures.

● Text Section 1.2.2

THE ORIGINAL
NAVSEASYSCOM DIFFUSER DESIGNS

NAVSEASYSCOM provided HRS with two preliminary sea-chest diffuser designs for evaluation. The diffuser impact chamber consisted of two semicircular cups concaved upward and located directly under the discharge line. The guide vanes located on the sides of the diffuser were designed to change the flow direction.

● Text Sections 6.3, 6.4

NAVSEA
Diffuser

Rotational flow patterns were found in diffuser tests, the flow was branching into two streams due to the design of the two semicircular cups. It was evident that further modification of the diffuser was needed to achieve better flow distributions.

THE IMPROVED DIFFUSER DESIGNS

Onboard solutions were subsequently developed to obtain the optimized sea-chest dif-
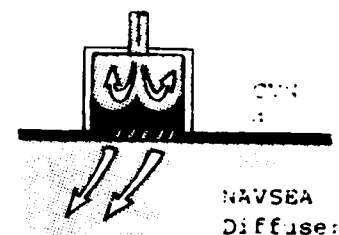
● Text Section 6.0

fuser designs for the Service Generator (SG)
cooling system. The optimized diffuser de-
signs reduced the jet-produced disturbance of
the berthing floor—also reducing the sub-
sequent ingestion of suspended materials into
the suction sea chest.

ASSESSMENT OF 5-FOOT KEEL CLEARANCE

The existing 5-foot keel clearance or
44-foot slip depth was found to pose fouling
problems because of the following reasons:
(1) marine organisms usually "remain" within
6 ft from the sea floor, and (2) inadequate
dispersions of the jet flow result from such
"very confined" underkeel spaces.

- Text Sections 2.1, 6.7
- Appendix B

With the installation of the proposed
diffuser, satisfactory reduction of flow
velocity was accomplished. However, the 5-
foot underkeel clearance will still impose
potential sea-chest fouling problems.

It was therefore concluded that the
existing 5-foot underkeel clearance is in-
adequate to prevent fouling of aircraft-
carrier circulating cooling systems in the
Norfolk Harbor environment.

THE SUPPORTING NUMERICAL-MODEL STUDY

The objective of the numerical-model study
was to develop a state-of-the-art numerical
model relating the underkeel clearance of an
aircraft carrier to the dynamics of sea-chest
flow fields and related berthing floor behav-
ior.

- Text Section 5.0
- Appendix C, F
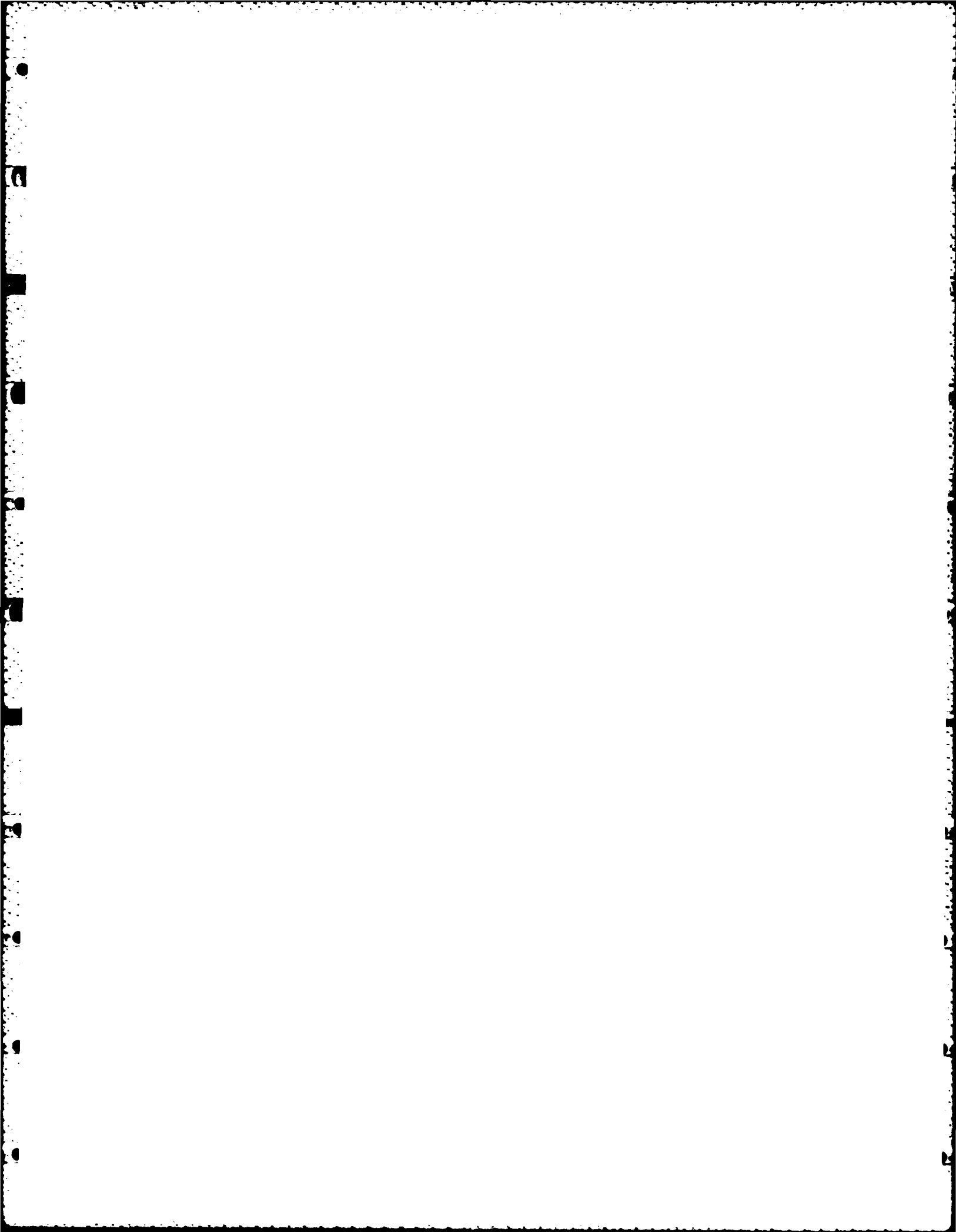
APPLICATIONS OF THE NUMERICAL MODEL

The numerical model was developed for the following purposes:

- Judging the stability of the bottom material by comparing the shear stress with the critical shear stress from Shields curve.

- Understanding the influence of under-keel clearance as it relates to the impingement of a jet.

- Estimating the volume of bottom material or marine organisms which could be ingested given a specified concentration and distribution of the organisms.

- Determining the jet center to suction center distance required to reduce the volume of ingested materials.

THE RESULTING CONCLUSIONS

The following conclusions resulted from this study:

- The jet discharge from the sea chest causes the marine life to be suspended and catapulted into the zone of influence of suction sea chest.

- The existing 5-foot underkeel clearance results in extreme jet strength, and extensive resuspension and insufflation of material.

- Text Section 2.1
- Figure 2-1

- Dredging the existing slips to 50 plus 2 ft to produce a 13-foot underkeel clearance would be beneficial, but would not cure the problem. A combination of onboard (diffuser installation) and offboard (dredging and facility modification) measures should provide the optimal means of reducing the problem.

- The discharge velocity of the main circulation pumps, although less than the service generators, is still sufficiently great to cause fouling when the pumps are operated at full capacity. It is technically feasible to diffuse the jet, but this study does not evaluate this option. If operationally acceptable, the fouling caused by the main circulation pumps could be reduced by throttling back when operating pier side. The main circulating cooling system was further investigated under reduced flow rates of 20,000 gpm and 8,750 gpm. Test results indicated that under low flow rate, the disturbance of sea floor was reduced.

- The diffuser designed for the service generator will reduce the strength of the discharge jet. Similar diffusers could be designed for other discharge openings. If desired by the Navy, the diffuser could be designed for

-7-

even smaller exit velocities. How-
ever, the louvered exit area would
have to be expanded.

- Installation of the service generator
diffuser must be considered as a
partial solution. Deepening the
berthing area by dredging, and pos-
sible additional facility modifica-
tion measures to be investigated in
a follow-on HRS study, are expected
to solve the suction fouling problem.

RECOMMENDATIONS

Our recommendations for solving the suction
fouling problems are:

- Text Section 2.2

- Deepening the berthing area to 50
plus 2-foot overdredge to achieve
a 13-foot underkeel clearance.

- Installing the single-barrel and
double-barrel diffusers designed for
the service generator cooling system
to suit the ship hull application.
With the installation of the dif-
fuser, the service generator dis-
charge jet will be reduced in
strength which will aid in alleviat-
ing sea-chest fouling.

- Utilizing other onboard and offboard
remedial measures such as throttling
back main circulation system pumps
and modifying existing waterfront
structures to minimize the dislodge-
ment/transportation of organisms and
sediment.

It is further recommended that a much larger
scale sea-chest model be studied (model-to-
prototype scale ratio of 1:4) to provide ad-
ditional detailed information on flow patterns,
back pressures, velocities, and localized
phenomena not clearly revealed by the 1:10
hydraulic model study.

1.0 Introduction

1.0   INTRODUCTION

1.1   THE UNDERLYING PROBLEM

During "berthing" and "light off" operations in some ports, aircraft carriers sometimes experience heavy fouling of sea chests and condensers due to the ingestion of bottom sediment and marine organisms.   [1] [2]*

Such clogging has been found to occur at either the suction opening grate on the hull bottom or on the tube sheet inside the condenser head.   The causal factors were previously unknown, but were assumed to be: underkeel "migration" of marine organisms, sea-chest suction, inadequate underkeel clearance, or a combination of these factors.

1.2   THE CURRENT STUDY

Before this study, little was known about the underkeel clearance required to alleviate such fouling problems.   Prior to dredging to the proposed 50- plus 2-foot berthing depth for carriers, Norfolk Naval Base wanted to be assured that the planned depth would alleviate the fouling problem.

A Technology Development project was therefore initiated by Naval Facilities Engineering Command (NAVFACENGCOM) to determine the underkeel clearance required to alleviate the problem.   The project was subsequently awarded to Hydro Research Science (HRS, Inc.) in the form of ONR Contract Number N00014-80-C-0395 dated 17 MAR 80.

1.2.1   The Study Objectives.   The underlying objectives of this study were to: (a) investigate the underkeel requirements of aircraft carriers as related to the sea-chest fouling problems, and (b) develop an onboard technology to control the fouling problems experienced by aircraft carriers in certain parts of Norfolk Harbor, primarily those berthed at Pier 12.

---

* Numbers in brackets [ ] refer to references in
  Annotated Bibliography, Appendix E.

1.2.2 <u>Scope of the Study</u>. As the outcome of meetings between HRS, NAVSEASYSCOM, NAVFACENGCOM, and LANTNAVFACENGCOM conducted in April and May 1980 at the HRS Laboratory, it was agreed that HRS was to pursue development of sea-chest "diffusers" as an onboard solution to the fouling problem. It was further agreed that the resulting diffuser designs were to be tested at underkeel clearances of 5, 13, and 21 ft using physical-model test procedures. The clearances conform to the average existing slip depth of 44 ft, a proposed dredging depth of 50 plus 2 ft, and a theoretical dredging depth of 60 ft, respectively.

> NOTE: HRS has received a subsequent contract
> to pursue the development of <u>offboard</u> fouling
> controls for the proposed Pier 11 and existing
> Pier 12 area at Naval Station, Norfolk, Virginia.
> <u>The current report deals only with the onboard</u>
> <u>solutions developed in satisfaction of the</u>
> <u>cited contract.</u>

1.2.3 <u>Structure of the Study</u>. To ensure satisfaction of the underlying objectives, the project was conducted as several discrete, but interrelated, phases. The primary phases included:

Phase 1 -- Analysis of the underlying problem and identification of potential onboard solution methodologies.

Phase 2 -- Physical-model experimentation to analyze the potential solutions... identifying the "most promising" for additional refinement.

Phase 3 -- Development of a working numerical model to assess underkeel flow fields and berthing floor behavior.

Phase 4 -- Comprehensive documentation of the
project, including a Final Report and
Bibliography, a User's Manual for the
numerical model, and a narrated 16mm
movie.

1.3 SOURCES OF INFORMATION

The following paragraphs identify the primary sources of
information for this study. All of the cited sources were used
extensively for the physical-model construction and test program,
and were also drawn upon in developing this report.

1.3.1 NAVFACENGCOM, NAVSEASYSCOM, and LANTNAVFACENGCOM.
General information on the structural aspects of Naval air-
craft carriers was provided by NAVFACENGCOM. The following
drawings were supplied:

- AOE Drawing No. 120-2286180 -- Sheets 1 and 2

- AOE Drawing No. 120-2287720 -- Sheets 2, 3, and 4

- CVN 69 Docking Drawing No. 845-4636304.

Additional information was obtained from: (a) communica-
tions between HRS and NAVFACENGCOM/NAVSEASYSCOM/LANTNAVFACENGCOM
regarding the design of, and general information about, the
sea chest, and (b) conferences held at HRS to discuss both the
experimental program and the diffuser design.

1.3.2 Virginia Institute of Marine Science (VIMS). HRS en-
tered into a contract with Virginia Institute of Marine
Science (VIMS), performed by Dr. Robert Diaz, to study the
hydrodynamic properties of the identified fouling marine
organisms. The resulting data was utilized by the HRS project
staff and is included as Appendix A of this report.

1.3.3 Literature Searches. Generalized data on hydrologic and sediment conditions near the study area were gathered via an extensive search of the available literature. [3] [4] [5] [6] [7]

1.4 STRUCTURE OF THIS REPORT

The remainder of this report documents the Technology Development project performed by HRS, Inc. For ease of readership, the report has been divided into two parts. Part I consists of a "less technical" summary of the project, and includes Sections 1 through 6. Part II contains more detailed technical information and data, and includes Appendix A through Appendix F. The contents of each section and appendix include:

--PART I--

Section 1 - INTRODUCTION

Section 2 - CONCLUSIONS AND RECOMMENDATIONS
             A concise discussion of the study conclusions
             and the resulting recommendations.

Section 3 - THE PROBLEM
             A summary of the fouling problem in terms of
             the available "pre-study" information and data.

Section 4 - THE ANALYSIS
             A description of the analytical and physical
             model studies conducted by the HRS project
             staff.

Section 5 - THE NUMERICAL MODEL
             Description of the state-of-the-art numerical
             model developed to relate "keel clearance"
             of Naval aircraft carriers to the dynamics
             of the flow field and related berthing floor
             behavior.

Section 6 - THE SOLUTIONS
            Discussions of the HRS-developed solutions
            to the fouling problem, including conclu-
            sions and recommendations.

                    --PART II--

Appendix A - HYDRODYNAMIC PROPERTIES OF MARINE ORGANISMS
            A summary of the data resulting from the
            marine organism investigations conducted
            by Dr. Robert Diaz of VIMS under contract
            to HRS, Inc.

Appendix B - PHYSICAL MODEL TESTS AND RESULTS
            Descriptions of the physical model setup
            and test results.

Appendix C - DEVELOPMENT OF THE NUMERICAL MODEL
            A detailed description of the working numeri-
            cal model developed to permit assessment of
            the flow field beneath an aircraft carrier.

Appendix D - KEY WORDS AND DEFINITIONS
            An alphabetical listing of the key technical
            and scientific terms used in this report,
            along with a concise definition of each term
            or abbreviation.

Appendix E - ANNOTATED BIBLIOGRAPHY
            A state-of-the-art annotated bibliography of
            the primary references used to assess the
            fouling problem, and to determine the re-
            lated state-of-the-art knowledge.

Appendix F - USER'S MANUAL
            A simplified manual for Naval personnel
            using the numerical model described in Sec-
            tion 5.0 of this report.

Appendix G - CONVERSION FACTORS

Conversion Factors, Customary to SI Units of

Measurements

2.0 Conclusions and Recommendations

2.0 CONCLUSIONS & RECOMMENDATIONS

2.1 CONCLUSIONS

As a result of an intense investigation of the circulating cooling system fouling problems of Naval aircraft carriers during berthing and light off operations at port...the primary causal factor was identified as the sea-chest discharge jet.

Hydraulic model experimentation with underkeel clearances of 5, 13, and 21 ft indicated that a strong "jet" persisted throughout the entire jet path. The impingement of the jet on the berthing floor was found to cause dislodgement of bottom material. When the resuspended materials approached the suction sea chests, fouling was found to be likely to occur.

An in-depth study of the flow field was then conducted to characterize the velocity and pressure field of the jets. Data were compared to the results from other investigators, and good correlations resulted.

> In order to control the condenser fouling, it became obvious that structural modifications to the ship would be required.

Onboard solutions were subsequently developed to minimize marine organism fouling of the circulating cooling system of aircraft carriers. Solutions were provided in the form of HRS-optimized sea-chest diffuser designs for the Service Generator (SG) cooling system. The optimized sea-chest designs acted to reduce the strength of the discharge jet, reducing jet-produced disturbance of the berthing floor, and subsequent ingestion of the suspended materials into the suction sea chest.

The existing 5-foot keel clearance, corresponding to an average existing slip depth of 44 ft, was found to pose fouling problems. It was found that: (1) marine organisms,

usually "remain" up to 6 ft from the sea floor,* and (2) inadequate dispersions of the jet flow result from such "very confined" underkeel spaces. It was therefore concluded that the existing 5-foot underkeel clearance is inadequate to prevent fouling of aircraft-carrier circulatory cooling systems in the current Norfolk port environment. A recommended 13-foot underkeel clearance, corresponding to a dredged depth of 50 plus 2 ft, together with the onboard discharge diffusers, will provide a more promising alternative.

In summary, the following conclusions resulted from this study:

- The jet discharge from the sea chest causes the marine life to be suspended and catapulted into the zone of influence of suction chest.

- The 5-foot underkeel clearance results in extreme jet strength and extensive resuspension and insufflation of material. (Figure 2-1 shows the suspension of the bottom material resulting from the strong discharge jet).

- The 13-foot underkeel clearance would be beneficial, but would not cure the problem. A combination of onboard and offboard measures should provide the optimal means of reducing the problem.

- The main circulation cooling system does not have to be operated at full capacity during light off operations and, therefore, was further investigated at reduced flow rates of 20,000 gpm and 8,750 gpm. Test results indicated that under low flow rate, the disturbance of the sea floor was reduced.

---

*Conversation with Dr. Robert Diaz, VIMS.
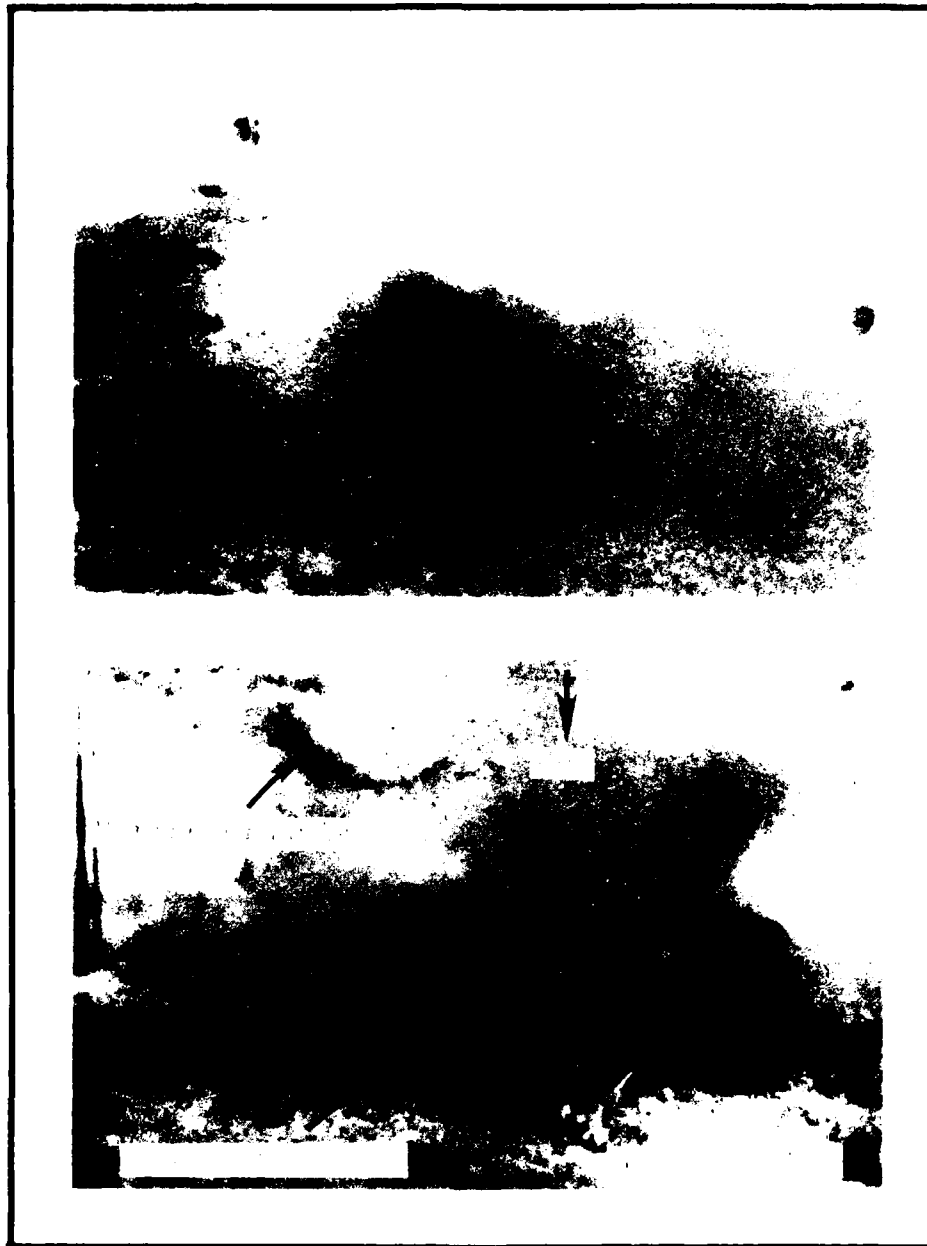
Figure 2-1

Suspension of Bottom Material
Resulting From Strong Jet Forces

- The diffuser designed for the service generator will
  reduce the strength of the discharge. Similar dif-
  fusers could be designed for other discharge open-
  ings. If desired by the Navy, the diffuser could
  be designed for even smaller exit velocities. How-
  ever, the louvered exit area would have to be
  expanded.

- Installation of the service generator diffuser must
  be considered a partial solution. It is anticipated
  that the suction fouling problem can be solved by
  implementing the following:

  - Deepening the berthing area by dredging to
    50 plus 2 ft

  - HRS follow-on study to investigate the pos-
    sibility of additional measures.

2.2 THE RESULTING RECOMMENDATIONS

Our recommendations for solving the suction fouling problems
are:

- Deepening the berthing area to achieve a 13-foot
  underkeel clearance.

- Installing the single-barrel and double-barrel
  diffusers designed for the service generator cool-
  ing system to suit the ship hull application. With
  the installation of the diffuser, the service gen-
  erator discharge jet will be reduced in strength
  which will aid in alleviating sea-chest fouling.

- Utilizing other onboard remedial measures such as
  throttling back main circulation system pumps and
  modifying existing waterfront structures to minimize
  the displacement of organisms and sediments.

It is further recommended that a much larger scale sea-chest model be studied (model-to-prototype scale ratio of 1:4) to provide additional detailed information on flow patterns, back pressures, velocities, and localized phenomena which was not clearly revealed by the current 1:10 hydraulic-model study.

3.0 The Problem

3.0 THE PROBLEM

3.1 OVERVIEW

The operational readiness of aircraft carriers has for years been reduced by what would seem to be a minor problem -- the fouling of sea chests and condensers due to the ingestion of bottom sediment and marine organisms at pier side and when entering and leaving the berthing areas of certain Naval harbors.

According to one source, "the pattern is that marine organisms become lodged against the intake screens of the auxiliary and main condenser intakes...causing the cooling water temperatures to rise to such a point that the generating plants are rendered inoperative." [1]

Serious consequences occur as a result of such interruptions in the operability of CVN-class vessel seawater circulating water systems. Problems have been reported [1] to include:

- Inability to conduct inport testing of the steam plant or catapult.

- Delays of flight operations for up to 12 hours following underway time, as the catapults cannot be warmed at the pier.

- Pre-underway electrical and electronic testing is complicated because turbine generators are not available for ship's power...requiring operation with the limited power available from the ship's emergency diesel generators.

- Underway evolutions cannot be conducted at pier-side using the main engines, and tug assistance to temporary remote anchorage is therefore required.

- Frequent malfunctions of the turbine generator and distilling plant occur, in addition to excessive wear of the ship's machinery and pump components.

In most cases an aircraft carrier experiencing such sea-chest fouling problems has to proceed to anchorage and have the clogged screens cleaned by divers. In other cases the divers have had to clean the screens with the carrier in the berth. Such a cleaning operation is often very difficult in Norfolk Harbor, where the underkeel clearance is 5 ft or less for CVN-class vessels. Additionally, such cleaning operations take 6 or more hours to perform and are complicated by "the inability of divers to maintain a given position under the ship because of tidal flow, and loss of vision due to the "fluid" mud condition that exists up to a height of 6 ft from the slip bottom." [1]

> The remainder of this section of the report summarizes the particulars of the fouling problem in terms of the available "pre-study" information and data.

3.2 NORFOLK HARBOR

The following pages discuss the harbor itself, including: (a) the geographic location, (b) the overall configuration of the harbor, (c) current and proposed dredge depths, and (d) berthing facilities for CVN-class vessels.

3.2.1 Geographic Location. The Norfolk Harbor is located in the vicinity of the confluence of the James and Elizabeth Rivers, as illustrated in Figure 3-1, Norfolk Harbor Orientation. Naval vessels enter the Hampton Roads via the entrance reach from Chesapeake Bay, the Newport News Channel, or the Norfolk Harbor Reach.

3.2.2 Overall Configuration. The Norfolk Naval Station is located at Sewells Point. It includes all piers and slips on Sewells Point or approaches to the Point between Pier 12 and
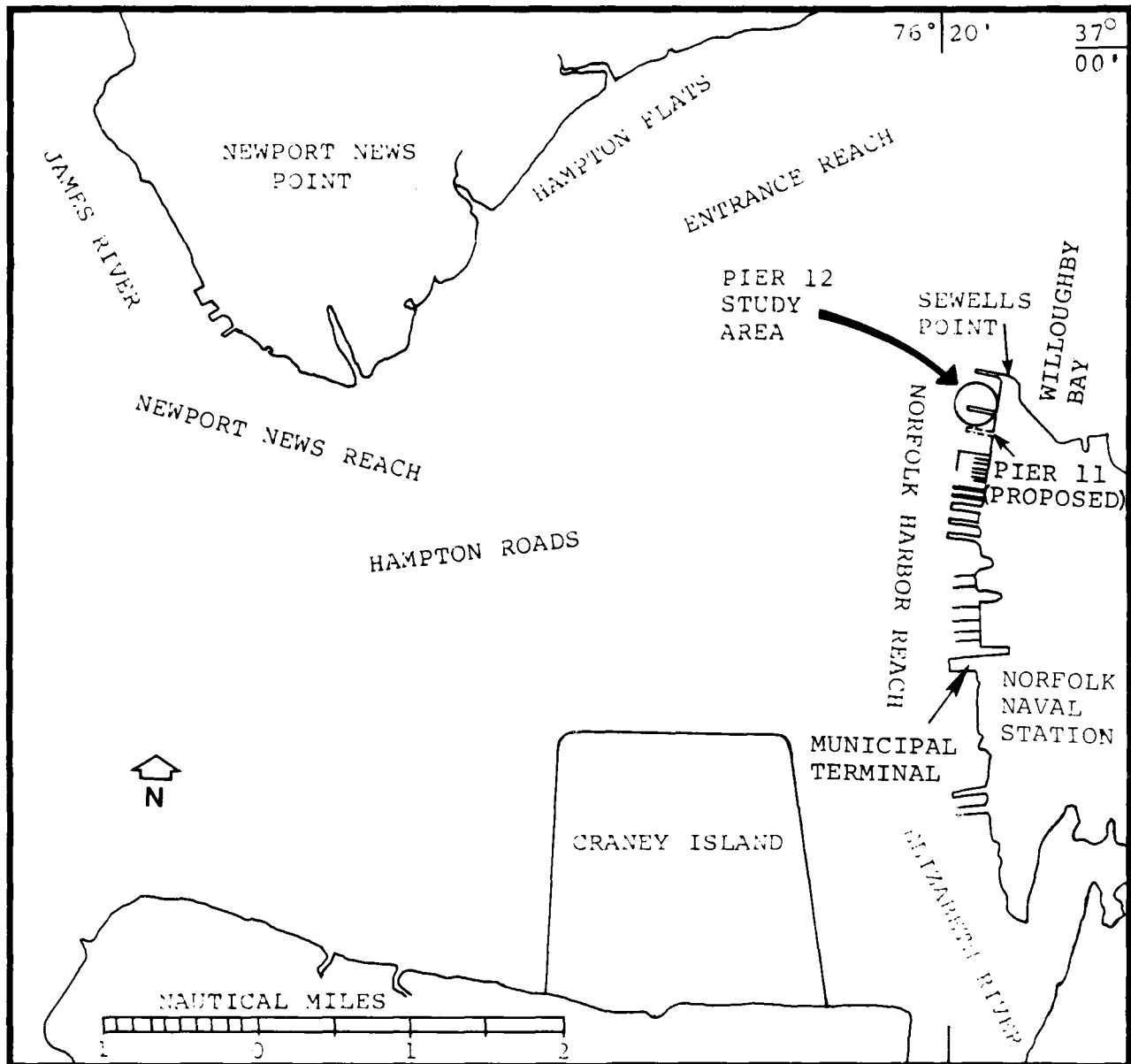
Figure 3-1

Norfolk Harbor Orientation

the Municipal Terminal to the west, and a small craft basin in Willoughby Bay. The study area for this project is within the Pier 12 berthing area.

3.2.3 Current and Proposed Dredge Depths. The Hampton Roads Entrance Reach, Norfolk Harbor Reach, and Newport News Channels are currently maintained at a depth of 45 ft below Mean Low Water (MLW). A plan to improve these channels by deepening the 45-foot channels to a depth of 55 ft below MLW, has been submitted by the Army Corps of Engineers. [8]

In the proposed Pier 11 and existing Pier 12 berthing areas, the Norfolk Naval Base is preparing a project for dredging the berthing depth of carrier berths to 50 ft.

3.2.4 CVN Berthing Facilities. The present berthing facilities for CV and CVN vessels (aircraft carriers) at Norfolk Harbor consists of slips at Pier 12...with occasional berthing at Pier 7. [4] Additional carrier berthing will be provided by Pier 11, proposed for construction adjacent to Pier 12 during 1982-1983.

3.3 HYDROLOGIC CONDITIONS

The hydrological conditions at the Chesapeake Bay/James River Estuary for the present study were divided into two categories: the average condition, and the extreme condition.

3.3.1 The Average Condition. The average hydrological conditions of the Chesapeake Bay/James River have been reported by previous investigators. [3] [9] The reported hydrological data include water depth, tidal current, wind, water temperature, and salinity for various locations throughout the James River Estuary. These existing data comprised the basic hydrologic information used in the physical model study.

3.3.2 The Extreme Condition. The extreme hydrologic condi-
tions of the Chesapeake Bay/James River occur when a hurricane
sweeps through the area. Existing reports describe various
extreme conditions. [10] [11] [12] [13] Hurricane Connie,
for example, precipitated from 5 to 6 inches of rainfall in
1955, causing up to 4.5-foot storm surges near Hampton Roads.

> Selected typical extreme conditions of the
> proposed Pier 11 and existing Pier 12 berthing
> sites are treated in detail in another related
> HRS study which concentrates on offboard solu-
> tions to the fouling problem.

3.4 HYDRAULIC CONDITIONS

The two key parameters of estuarine hydraulics are: (a)
the velocity of tidal currents, and (b) the tidal circulation
patterns.

3.4.1 Current Velocity. Preliminary information on Norfolk
Harbor surface and bottom currents is scarce. However, one
field study [14] reported a current velocity of more than
1 knot near the bottom off Sewells Point, and less than 0.5
knots in the access channel off Pier 12.

As for the Newport News Channel, the report stated that
the currents do not always follow the channel, and the average
velocity in mid-channel at strength of flood or ebb is about
1.5 knots. Information on the velocity near Pier 12 (the
north side) indicated that the bottom and surface currents
rarely exceed 0.2 knots.

Because of the nominal current within the berthing area,
zero current velocity was assumed for the underkeel clearance
study.

3.4.2 Circulation Patterns. The circulation in Hampton Roads
is not identical for flood and ebb tides. According to Neilson
and Boule, [15] the flood tide predominates over Hampton
Flats. The flow up the James River turns sharply around New-
port News Point. The flow toward the Elizabeth River divides
into two streams -- some of the flow moves to the west just
north of Craney Island, and the remainder moves into the Eliz-
abeth River proper. Eddies are believed to form in the lee of
both Sewells Point and Craney Island during flood tide.

Neilson and Boule [15] also reported that during ebb
tide, the flow down the James River is directed toward the
shoreline south of Sewells Point. The early flood in the
Elizabeth River and late ebb in the James River occur at the
same time. The flow towards Sewells Point, therefore,
branches into two streams: The first stream entering the
Elizabeth, and the second stream moving out of the river
mouth.

3.5 BOTTOM SOIL CONDITIONS

Sediments dredged from within Pier 12 berths range from
silt to coarse clay, and are probably the result of the floc-
culating* of suspended sediment and the bedload sediment move-
ment from the rivers flowing into Hampton Roads. [4] The
sediment characteristics in the study area and other harbors
are reported elsewhere. [16] [17] [18] [19] [20] These sedi-
ments are further discussed in the following paragraphs.

3.5.1 Soil Classification. The predominant sediment type
within Pier 12 consists of silts and clays (mud). Four sedi-
ment samples collected in Pier 12 had median particle sizes
of 5.5, 6.2, 6.3, and 7.0 microns -- therefore comprising a
medium- to fine-silt sediment.

---

* Flocculating -- The collection or uniting of
  suspended sediment to form a mass.

3.5.2 Sediment Composition. A survey of the sediment at both
slips of Pier 12 [6] revealed four basic sediment compositions
at the site:

- **Black homogeneous mud**, smooth when rubbed between
  the fingers, and of the consistency of pudding.
  From 30 to 35% solid by weight.

- **Coarse medium-brown sand**, containing shell frag-
  ments. Comprised 76% solid by weight.

- **Black clay and sand mixture**, containing shell frag-
  ments. Comprised 56% solid by weight.

- **Gray mud**, containing fine sand grains. Comprised
  44% solid by weight.

3.6 THE "FOULING" MARINE ORGANISMS

The bottom-sediment cumulation at the Norfolk Naval Sta-
tion poses a problem, for it is expensive to dredge. However,
the clogging of aircraft-carrier circulating cooling systems
by marine organisms poses an even greater problem.

The following paragraphs summarize the characteristics of
the marine organisms. More complete information has been in-
cluded in Appendix A of this report.

3.6.1 Species Involved in Fouling Problems. The specific sea-
chest fouling organisms identified in the Norfolk Harbor include
the hydroid Sertularia argentea and the bryozoan Alcyonidium
verrilli. Photographs of actual samples of each from Norfolk
Harbor appear as Figures 3-2 and 3-3. At Pier 12 the hydroid
is believed to contribute from 90 to 95 percent of sea-chest
fouling problems. The remaining 5 to 10 percent of the foul-
ing problems involve the bryozoan. [2] [10] Both the hy-
droids and the bryozoans move in the lower portion of the water
column and have densities ranging from 1.03 to 1.15.
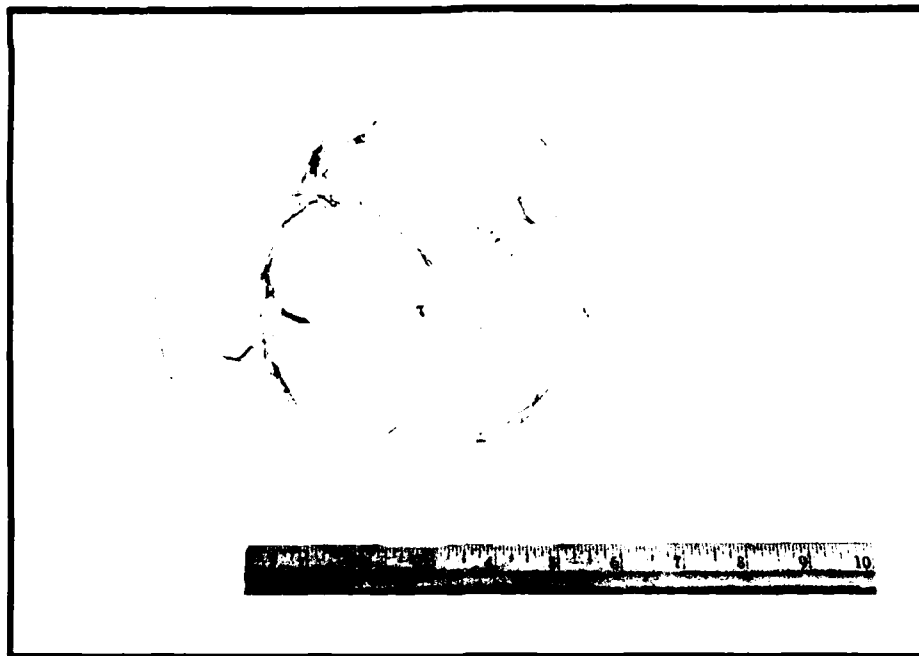
Figure 3-2

Photo of Hydroids from Norfolk Harbor

Figure 3-3

Photo of Bryozoans from Norfolk Harbor

3.6.2 Seasonal Growth Patterns. The hydroid is composed of colonies ranging from 10 to 12 inches high, with multiple branches. It is a "winter species" which achieves peak growth from November to February. Branches and side branches tend to break off during winter storms and are carried away by the current. Such branches continue to grow after separation from the parent colony. [2]

3.7 VESSEL-RELATED PARAMETERS

The remainder of this section of the report is concerned with the vessel-related parameters critical to understanding the reported CVN sea-chest fouling problems.

3.7.1 Vessel Circulating Water Systems. The current study concentrated on fouling problems associated with the two primary CVN-class seawater circulating water systems: (1) the Main Circulating Water system, and (2) the Service Generator (SG) system.

3.7.2 Sea-Chest Discharge Flow Rates. The pumping capacity of the circulating cooling systems of the subject aircraft carrier* ranges from 3,450 to 25,000 gallons per minute (gpm). Within the scope of the present study, the 25,000-gpm flow rate of the main circulating system and the 5,890 gpm of the service generator system, comprised the variables under investigation.

3.7.3 "Assumed" Operating Ranges. For the purposes of this study, the operating ranges of the circulating cooling systems were divided into three pumping rates. These "assumed" operating ranges consisted of 100, 80, and 35 percent of full-operating capacity.

---

* The Naval aircraft carrier used as the "model"
for this study was the USS Dwight D. Eisenhower
(CVN 69).

3.7.4 Light Off Operations. During "light off" operations,
the service generators pump at full capacity. The main circu-
lating system may, however, be operated at lower rates such as
10 or 20 percent of full capacity.

3.8 BERTHING-RELATED PARAMETERS

The following pages summarize the primary berthing-related
parameters associated with the sea-chest fouling problems of
CVN vessels in Norfolk Harbor.

3.8.1 General Orientation of a Berthed Vessel. To provide a
basic point of reference, the orientation of a capital ship
at berth is illustrated in Figure 3-4, Sectional Orientation
of a Capital Ship at Berth.

3.8.2 Operating Load Drafts. The maximum operating load
drafts of Naval aircraft carriers is reported to range from
37 to 40 ft. [4] The load draft, in turn, relates directly
to the underkeel clearance for a given berthing location.

3.8.3 Underkeel Clearance. The circulating cooling system
sea chests of Naval aircraft carriers are located on the under-
side of the vessel. In the case of an operating load, draft
of from 37 to 40 ft in a berthing position or channel with a
45-foot depth (the current condition)...only 5 to 8 ft of
underkeel clearance exists at low tide.

The suction and discharge openings of the sea chest
must, in turn, operate within the current 5- to 8-foot
underkeel clearance.

LEGEND

1 Draft
2 Underkeel Clearance
3 Typical Zone of Withdrawal
4 Suction Sea Chest
5 Discharge Sea Chest
6 Typical Discharge Action
7 Deformable Material Berthing Bottom
8 Marine Organisms
9
10 ⟩ Peripheral Confinement
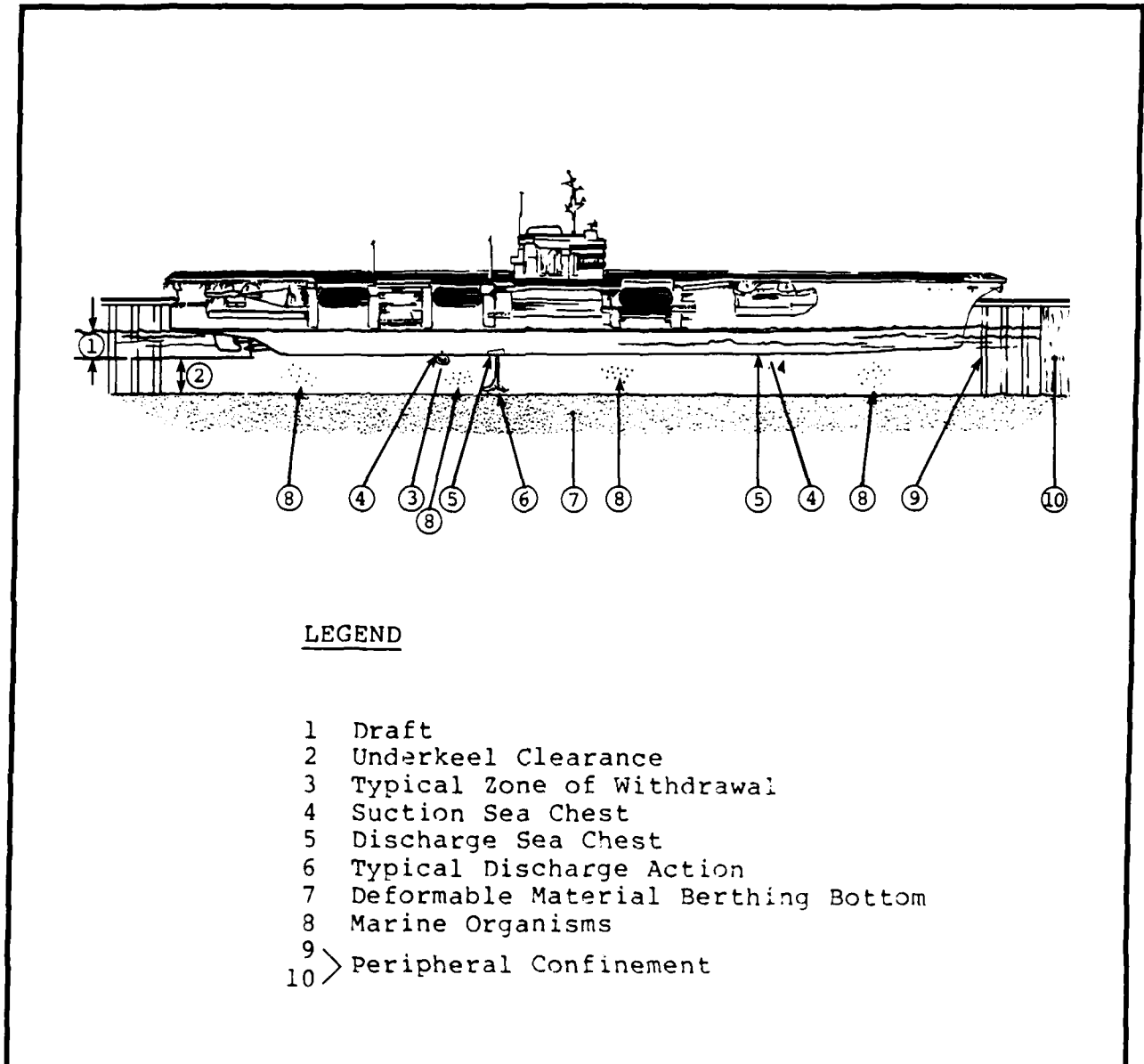
Figure 3-4

Sectional Variation of a Capital Ship at Berth

This study investigated several underkeel clearances using an assumed average draft of 39 ft, including: (a) a 5-foot clearance corresponding to the existing average Pier 12 CVN berthing depth of 44 ft, (b) a 13-foot underkeel clearance corresponding to the proposed dredged depth of 50 plus 2-foot overdredge, and (c) a 21-foot underkeel clearance corresponding to a hypothetical lower depth limit of 60 ft for experimental purposes.

4.0 The Analysis

4.0 THE ANALYSIS

Extensive state-of-the-art physical modeling procedures were utilized to analyze the sea-chest fouling problem. This section of the report consists of a "less technical" summary of the modeling procedures utilized to analyze the problem and then identify and refine the most promising onboard solutions.

> More detailed information on this aspect of the study has been included in Appendix B of this report.

4.1 THE PHYSICAL MODEL

4.1.1 The Berthing Tank. A platform was constructed and installed in the permanent HRS Berthing Tank. To aid the reader, a photo of the Berthing Tank appears as Figure 4-1.

Precision-constructed scale models* of the selected CVN-class service generator (SG) and main circulating (MC) cooling system were then placed in the tank and fully instrumented for experimental purposes. The tank bottom was filled with sized walnut-shell grains to simulate mud and algae to simulate marine organisms, and a dye probe was installed in the recirculating system to enable observation of the flow patterns.

4.1.2 The Sea Chest Models. Two pairs of SG cooling system intake and discharge openings and one pair of the main circulating system openings were modeled. The underkeel clearance for preliminary tests was first set at 21 ft and later set at 5 and 13 ft. A schematic layout of the modeled sea chests is detailed in Figure 4-2. A photo of the sea chest model appears as Figure 4-3.

---

* Models were constructed per the dimensions of CVN 69, the "model" for this study.
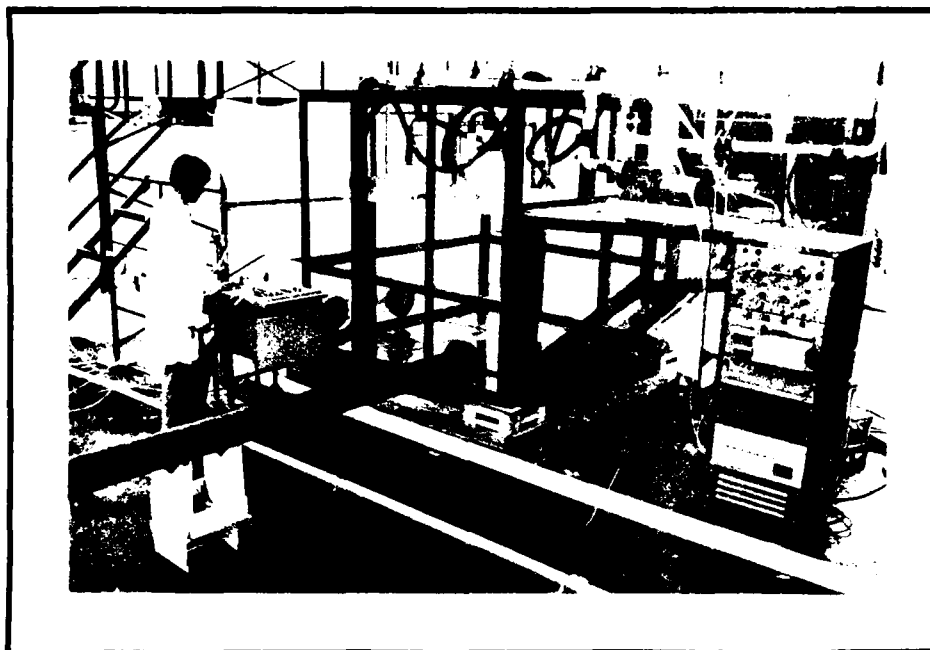
Figure 4-1
HRS Berthing Tank

Center-
line

Base Line — Main Deck Line —

BOTTOM VIEW
OF CVN 69

AFT LOCATION

FORWARD LOCATION

Approximate
Model !
Platform

DIMENSIONS OF MODELED AFT OPENINGS
OF CVN 69 VESSEL

Number	Service Description	Dimension (Inches)
41	#4 Main Circ. (MC) Suction	42+13/16 x 28+13/16
43	#4 SG/CG Sea-water Suction	38+5/8 x 31+7/8
45	#4 SG/CG Sea-water Discharge	16 DIA
46	#4 Main Circ. Discharge	69+13/16 x 46+13/16
53	#3 SG Seawater Suction	37+1/8 x 30+3/8
57	#3 SG Seawater Discharge	16 DIA

41

46

43

45   57

53

Keel Centerline

Base Line

DETAIL VIEW OF MODELED PLATFORM

Note: Forward and aft opening
       locations are symmetrical

Figure 4-2

Layout of Modeled Sea Chests
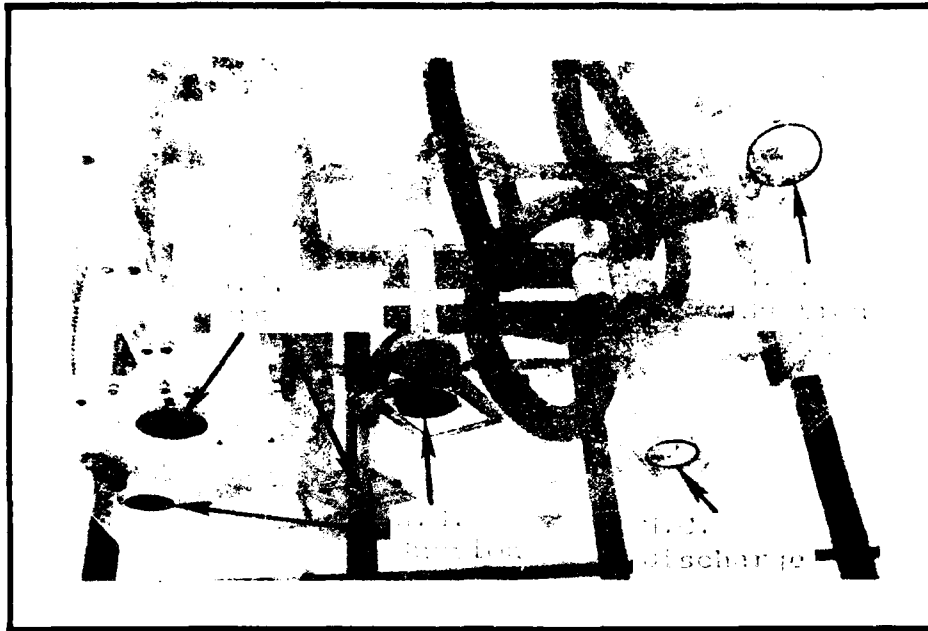
Figure 4-3

Sea Chest Model

4.2 THE PRELIMINARY ANALYSIS

Prior to conducting an extensive physical-model experimentation, a problem-oriented preliminary analysis was performed. The results are summarized on the following pages.

4.2.1 Suction Operations. Preliminary tests of the SG condenser unit suction were conducted with a flow rate of 5,890 gpm. Very little activity was observed near the suction sea chest. The influence zone was limited to the vicinity of the suction sea chests.

The velocity at the immediate area (within 1 foot) surrounding the suction opening was found to be 1.2 ft/sec. The decrease of velocity with distance was very noticable. Within a 4-foot radius, the velocity dropped to 0.2 ft/sec.

The tests indicated that suction action alone was not the major cause of the sea-chest organism fouling. A typical velocity distribution at the suction sea chest is shown in Figure 4-4.

37.83" Dia. Modeled
suction opening

EL 13.0'

EL 10.0'

0.0-ft/sec
Approx. zone of
withdrawal limit

EL 5.0'

EL 0'

SERVICE GENERATOR SUCTION OPENING #53

Q = 5890 gpm   Velocity profiles are
plotted from point
velocity recordings.
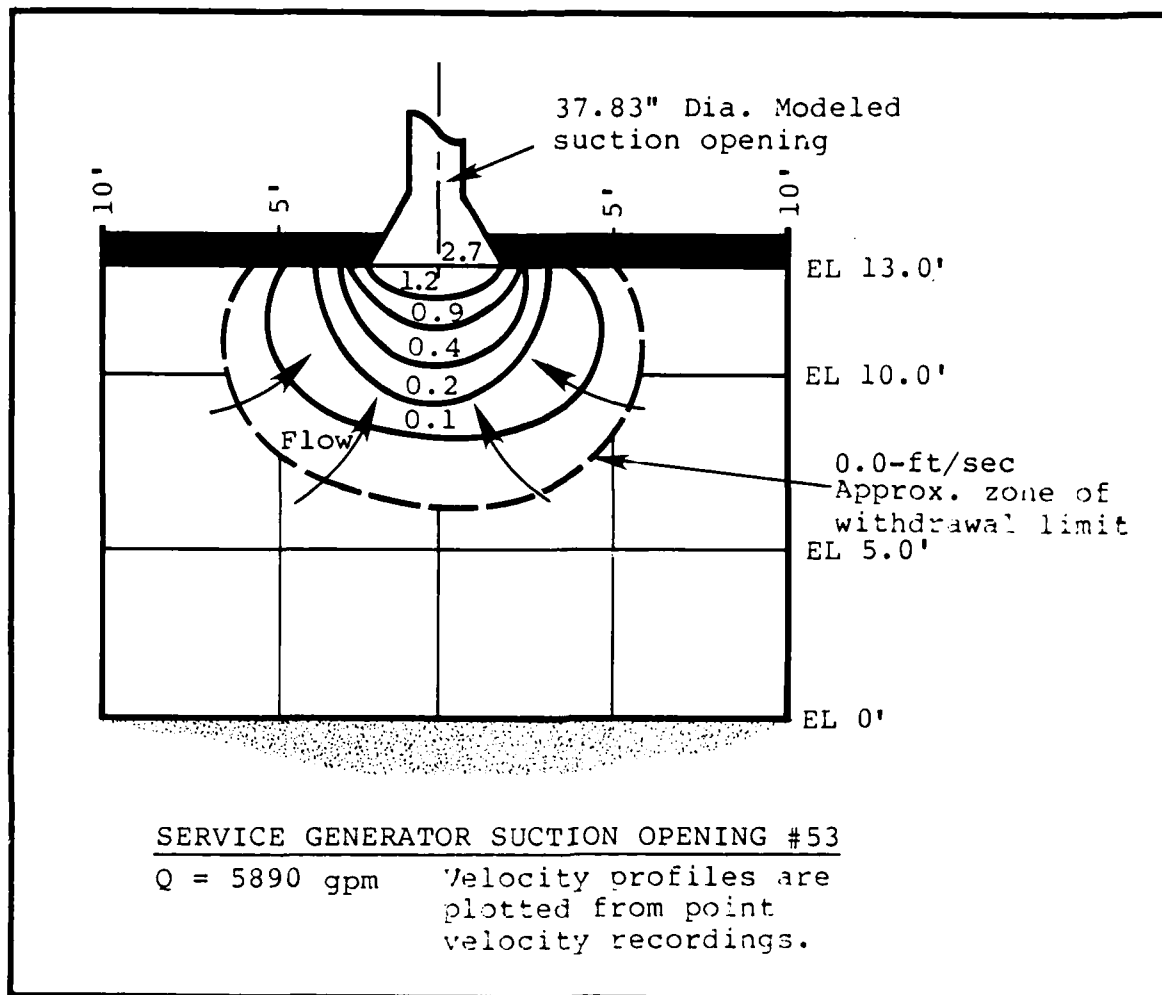
Figure 4-4

Typical Velocity Distribution at the Suction Sea Chest

Observations were also made at the main circulating sys-
tem suction sea chest. Similar phenomena were observed, lead-
ing to the conclusion that the suction action, by itself, did
not pose a serious sea-chest fouling problem.

4.2.2 Discharge Operations. Observations of the discharge
sea-chest operations were made on a pair of service-generator
condenser units (suction and discharge) with a flow rate of

5,890 gpm. Test results revealed that a very strong jet flow,
shooting downward from the sea chest, penetrated deep into the
surrounding water, impinged on the sea floor, and caused sub-
stantial disturbance to the bottom material.

This jet action resuspended the bottom particles, dispers-
ing them into the surrounding environment. Part of the sus-
pended material floated upward and was carried by the circula-
tion current. As such floatages approached the suction in-
fluence zone, the suction action pulled the particles into the
sea chest inlets. It was therefore concluded that:

<u>The jet is the primary causal factor
behind organism-fouling of sea chests.</u>

In order to ensure clear understanding of these jet and
scour processes, the following pages detail the HRS analyses
of: (1) the jet impinging on a solid boundary, and (2) the
jet impinging on a movable boundary.

4.3   ANALYSIS OF JET IMPINGING ON A SOLID BOUNDARY

Experiments were conducted on both the SG cooling system
and the main circulating system. The following pages detail
the experimental results.

4.3.1   <u>The Service Generator (SG) Discharge</u>. The SG discharge
sea chest has circular cross sections. The SG jet velocity
profile, therefore, tends to be axisymmetric about the center-
line of the circular pipe, and results in a symmetric flow
field under the sea chest.

A photograph of the circular jet patterns created by the
SG system appears as Figure 4-5. The SG discharge velocity
distribution measurements for a flow rate of 5,890 gpm indi-
cated that the maximum exit velocity V_o at an elevation of
13 ft above the solid bottom was 10.5 ft/sec. The maximum

velocity at an elevation of 5 ft was determined to be 7 ft/sec. At 2 ft from the jet centerline near the solid boundary, the radial velocity was 4.5 ft/sec -- which can move 1/2-inch-size medium gravel on a noncohesive sand bed.
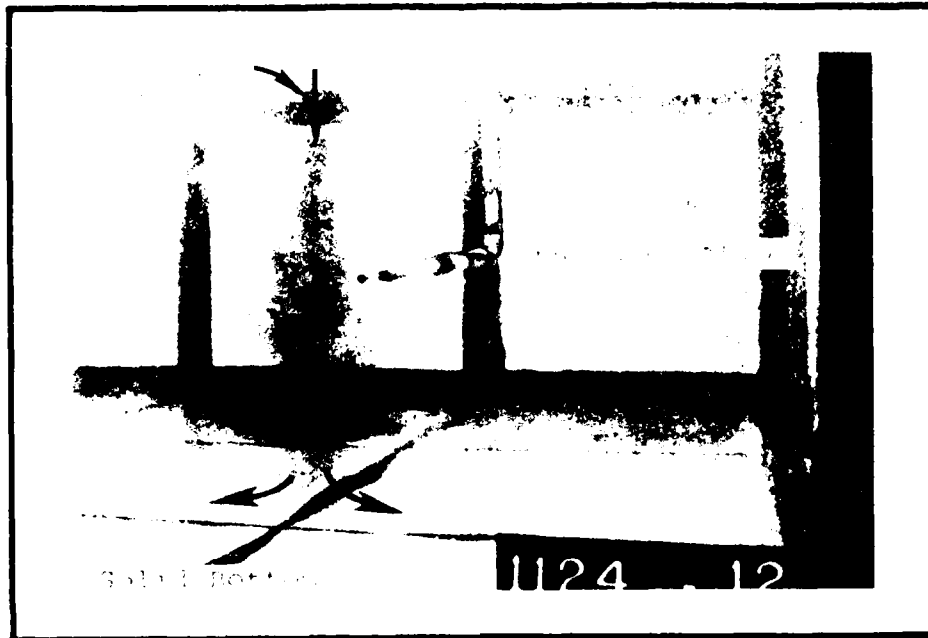
Figure 4-5
SG Circular-Jet Patterns

4.3.2 The Main Circulating System Discharge. The main circulating system discharge creates an elliptical jet pattern. For the main circulating system discharge sea chest at full capacity of 25,000 gpm, the maximum exit velocity V_o was 6.6 ft/sec at an elevation of 13 ft above the solid bottom. The maximum axial velocity was 4.7 ft/sec at an elevation of 5 ft above the solid bottom. At 7.5 aft of the vessel, the radial velocity near the solid bottom was approximately 2.5 ft/sec, which can move fine gravel of a size up to 0.2 inch on a non-cohesive sand bed.

A photograph of the elliptical jet patterns produced by the main circulating system appears as Figure 4-6.

The main circulating system discharge sea chest was also tested with a reduced flow rate of 20,000 gpm (80%) and 8,750 gpm (35%). The maximum exit velocities were 4.70 ft/sec and 2.32 ft/sec, respectively, and the maximum bottom radial velocities were 2.15 ft/sec and 1.01 ft/sec.
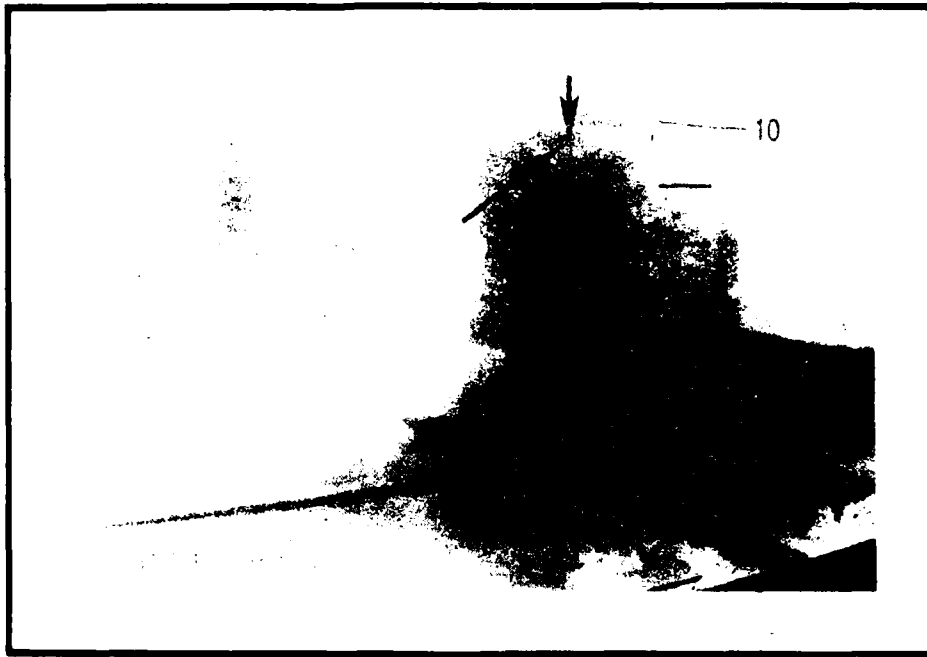
Figure 4-6

Main Circulating System Jet Patterns

Detailed velocity distributions for both SG and Main Circulating Systems are included in Appendix B of this report.

4.4 ANALYSIS OF JET IMPINGING ON A MOVABLE BOUNDARY

To date, there has not been a clear understanding of jet erosion mechanisms on movable boundaries. Few investigations of jet erosion have been conducted. [22] [23] [24] [25] None of the studies reported conclusive findings on jet erosion mechanisms, nor did they report velocity distributions. To

gain an understanding of the erosion mechanism and the flow
field in the vicinity of the scoured area, a test program of
jet impingement onto a movable boundary was conducted.

4.4.1 Movable Boundary Test Variables. This test program was
conducted to observe the effects of circular jet impingement
on the sea bottom. Materials used in the study included sand
(to simulate sand) and walnut shell grains (to simulate mud).
The underkeel clearance was set at 13 ft, with a flow rate
of 5,890 gpm.

4.4.2 Jet Impinging on Sand Bottom. Tests of the jet imping-
ing on sand showed that the jet eroded the bottom sand outward,
resulting in a scour hole with the bottom about 15.5 ft below
the discharge opening. The velocity at 11 ft below the dis-
charge opening was found to have a magnitude of 52% of its
original strength. At 15 ft below the discharge opening, the
velocity still maintained 32% of its original strength. The
radial velocity at 13 ft below had a magnitude of about 3 ft/
sec, which is capable of moving 0.4-inch gravel.

A photograph of the effect of the jet impingement on a
sand bottom appears as Figure 4-7, Typical Sand Bottom Scour
Effects.

4.4.3 Jet Impinging on Mud Bottom. The jet impinging on mud
is a dynamic process. Tests showed that the jet dug down into
the bottom layer, resulting in a scour hole about 16 ft below
the discharge opening. The mechanism of jet impinging on mud
bottom is discussed in Appendix B, Paragraph B.5.2.4. The
velocity measurement revealed that at 11 ft below the discharge
opening, the jet still possessed 54% of its original strength.
However, a measurement at 14 ft below showed the velocity to
be only 20% of the original strength. Figure 4-8 shows the
typical mud bottom scour effects.

Figure 4-7
Typical Sand Bottom Scour Effects
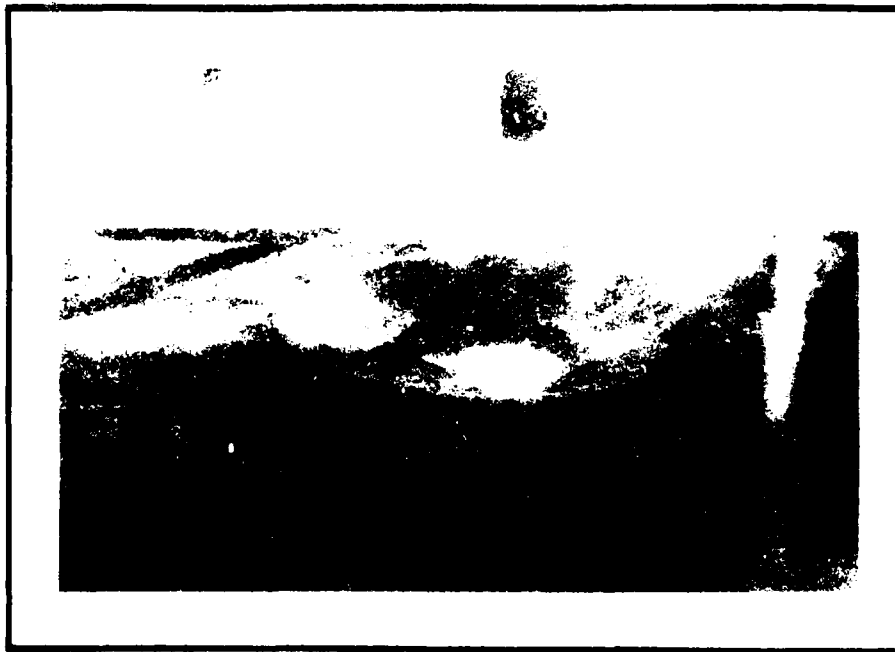
Figure 4-8
Typical Mud Bottom Scour Effects

4.5 MOVABLE BOUNDARY WITH MARINE ORGANISMS

4.5.1 Hydrodynamic Properties of the Organisms. To ensure
that the hydrodynamic properties of the marine organisms were
properly treated in the physical-model study, HRS contracted
with Virginia Institute of Marine Sciences (VIMS) to study
selected properties of each of the species. Performed by Dr.
Robert Diaz, the study produced the key results as summarized
in the following paragraphs:

- The initiation of motion for live hydroids requires
  a velocity of about 0.05 to 0.11 feet per second
  (fps). For live bryozoans, a velocity of 0.34 to
  0.41 fps will move the species. As to the mixture
  of live and dead colonies, the required velocities
  are 0.15 fps for hydroids, and 0.30 fps for bryo-
  zoans.

- The fall velocity of hydroids ranges from 0.02 to
  0.12 fps for live colonies, and 0.09 to 0.39 fps
  for dead colonies. The fall velocities are from
  0.21 to 0.29 fps for live bryozoans, and from 0.09
  to 0.21 fps for dead bryozoans.

4.5.2 The Marine Organism Test Variables. Green algae were
used to simulate the transport properties of the hydroids
for visual perception and qualitative assessment. The algae
were arranged in the test setup so that a portion was im-
planted into the bottom walnut-shell layer, and a portion
was suspended in the water, simulating the sea-bottom environ-
ment. A collection device for the algae was placed at the
middle section of the simulated suction pipeline. This col-
lection device consisted of a circular conduit section, with
several layers of screen baffle spaced inside the conduit
as interception mesh.

A test of the service generator discharge jet was conducted using a 13-foot underkeel clearance. In the test the jet flow dug into the bottom layer, disturbing the buried algae. The algae were then lifted and carried by the flow. Those carried into the region of influence of the suction sea chest subsequently disappeared into the suction pipelines.

Test results revealed that: (a) at 5,890 gpm, 12.5% of the algae was insufflated, (b) at a pumping rate of 4,800 gpm, about 9% of the algae was ingested, and (c) at the much lower pumping rate of 2,100 gpm, only 2% of the algae was ingested. A photograph of the marine organism movable boundary test appears as Figure 4-9.
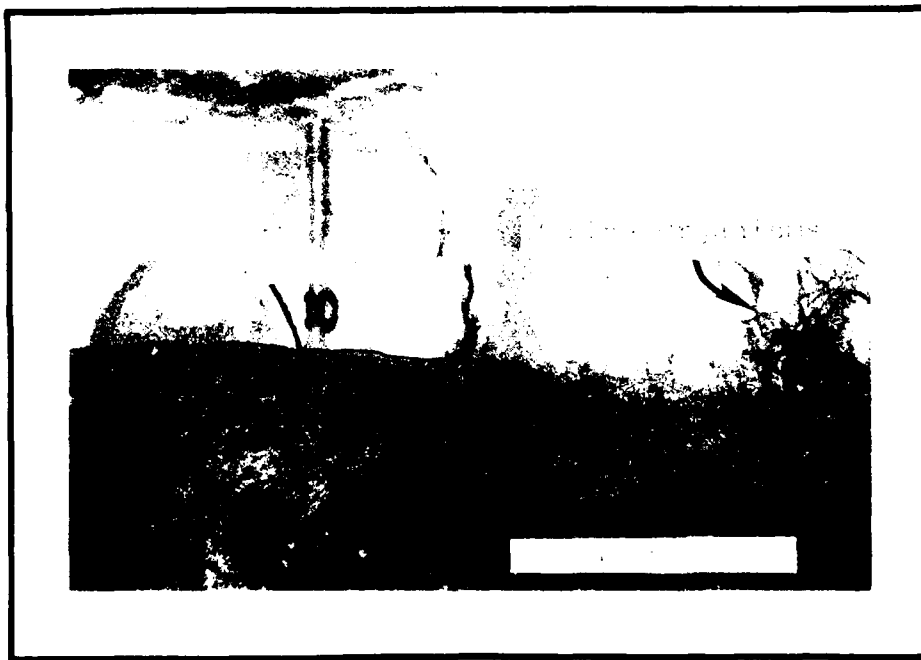
Figure 4-9

Resulting Scour Patterns from
One Pair of SG Cooling System Openings

A test was also conducted for the operation using two pairs of service generator openings (intake and discharge) and one pair of main circulating system openings with a 13-foot underkeel clearance. The results revealed an ingestion of about 11% of the algae into one of the service generator suction lines.

It was therefore concluded that even with the berthing area dredged to 50 ft, the fouling problem will still occur.

4.6 CONCLUSIONS FROM MOVABLE-BOUNDARY TESTS

The following conclusions were drawn from the results of the previously-cited movable-boundary tests:

- The discharge jet impinging on a movable boundary is a dynamic process which results in scouring of the bottom material.

- This scouring action only exists locally, and reaches an equilibrium condition such that the perpetuating eddie flow is contained within the scoured area.

- The disturbance of the bottom layer caused by the discharge jet scouring results in the sea-chest fouling problem.

5.0 The Numerical Model

5.0 THE NUMERICAL MODEL

The objective of this phase of the study was to develop a state-of-the-art numerical model relating the underkeel clearance of an aircraft carrier to the dynamics of sea-chest flow fields and the related berthing floor behavior.

5.1 OVERVIEW

The scope of this phase of the study encompassed:

- Conducting a general compilation and analysis of: (a) the physical model results, and (b) the mathematical formulations for the relevant fluid mechanics phenomena (suction and discharge flow patterns within various fields of confinement).

- Developing the algorithm for the numerical model and coding the computer program intended to satisfy the study objectives.

- Performing validation tests of the numerical model.

- Documenting the numerical model study and developing a User's Manual.

5.2 THE DATA COMPILATION

Physical-model data on both suction and discharge jet were compiled. The data on velocity, pressure, and shear stress were then tabulated and compared with other investigator's findings [26] [27] [28] [29]. Major attention was focused on the discharge jet data, as the jet was identified as the main driving force behind the fouling problem.

5.3 THE ALGORITHMS

The algorithms used to develop the working numerical model included both suction and discharge jet simulations. These algorithms are discussed in the following paragraphs.

5.3.1 <u>Suction Simulations</u>. A finite difference model was developed to predict the suction flow field. The fluid was assumed to be inviscid, incompressible, and irrotational. After defining the governing equations and boundary conditions, a finite difference form with the successive over-relaxation (S.O.R.) method was developed to calculate the velocities at any point confined under the keel.

> Detailed information related to the development of the formulation and its associated boundary conditions is included in Appendix C of this report.

5.3.2 <u>Discharge Simulations</u>. The flow field resulting from the jet discharge posed a very complicated problem. There are no existing, related general mathematical formulations. The present simulation of the jet discharge based upon HRS physical-model results is, however, in good agreement with the results of previous investigations. [26] [29]

Two very different bottom-boundary conditions were studied: (a) fixed (flat) boundary, and (b) movable boundary. The fixed-boundary numerical model of the discharge jet simulated the flow field velocities, the bottom pressure, and the bottom shear stress. The movable-boundary numerical model simulated the flow field velocities related to the underkeel clearances.

5.4 <u>NUMERICAL VS PHYSICAL MODEL RESULTS</u>

Figures 5-1 through 5-4 compare numerical-model versus physical-model results related to: jet discharge velocities, suction velocities, bottom pressure, and the bottom stress for fixed boundary.
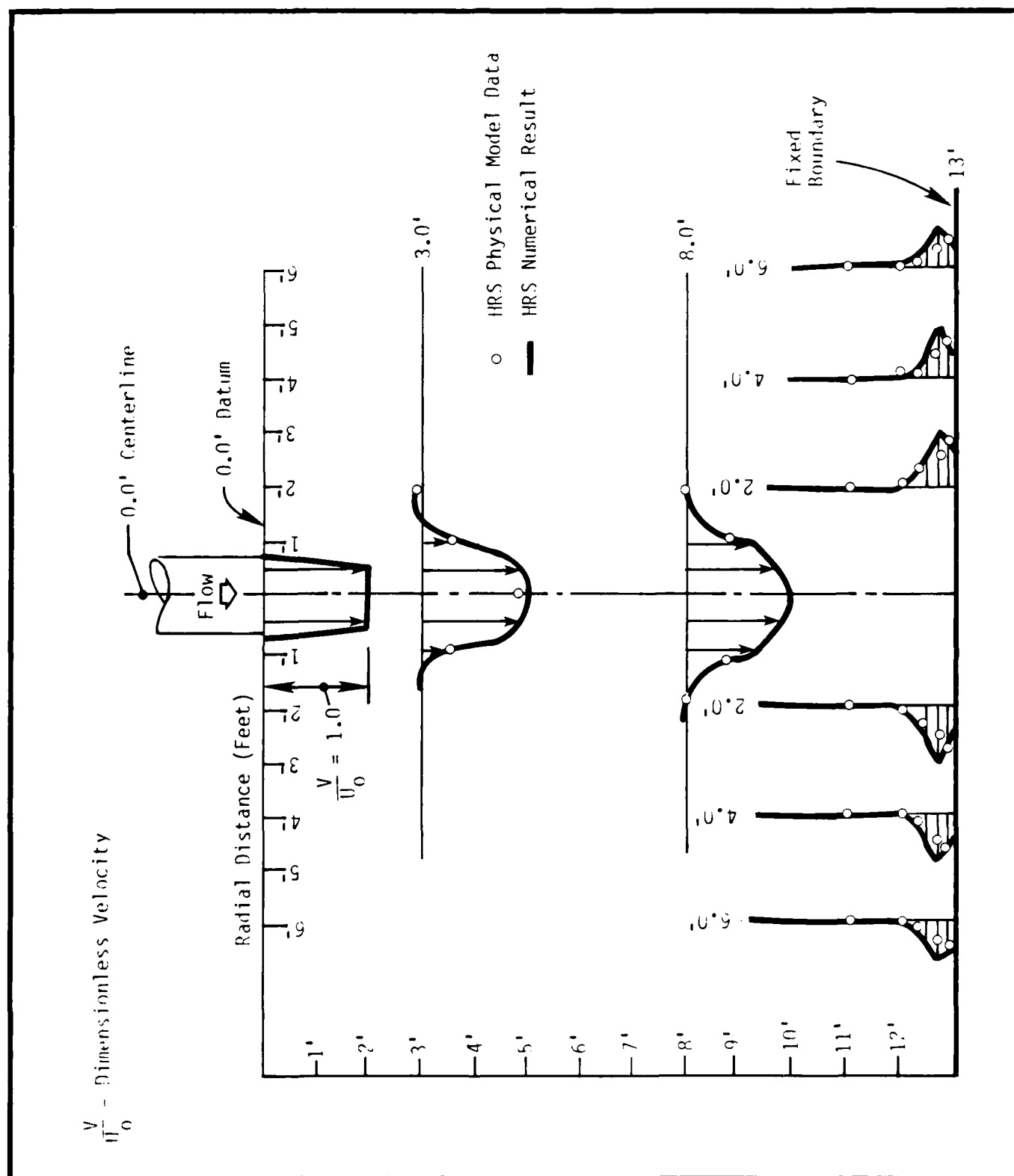
Figure 5-1

Flow Field for the Impingement of a Jet on Fixed Boundary

(Comparison of numerical results with physical model results)
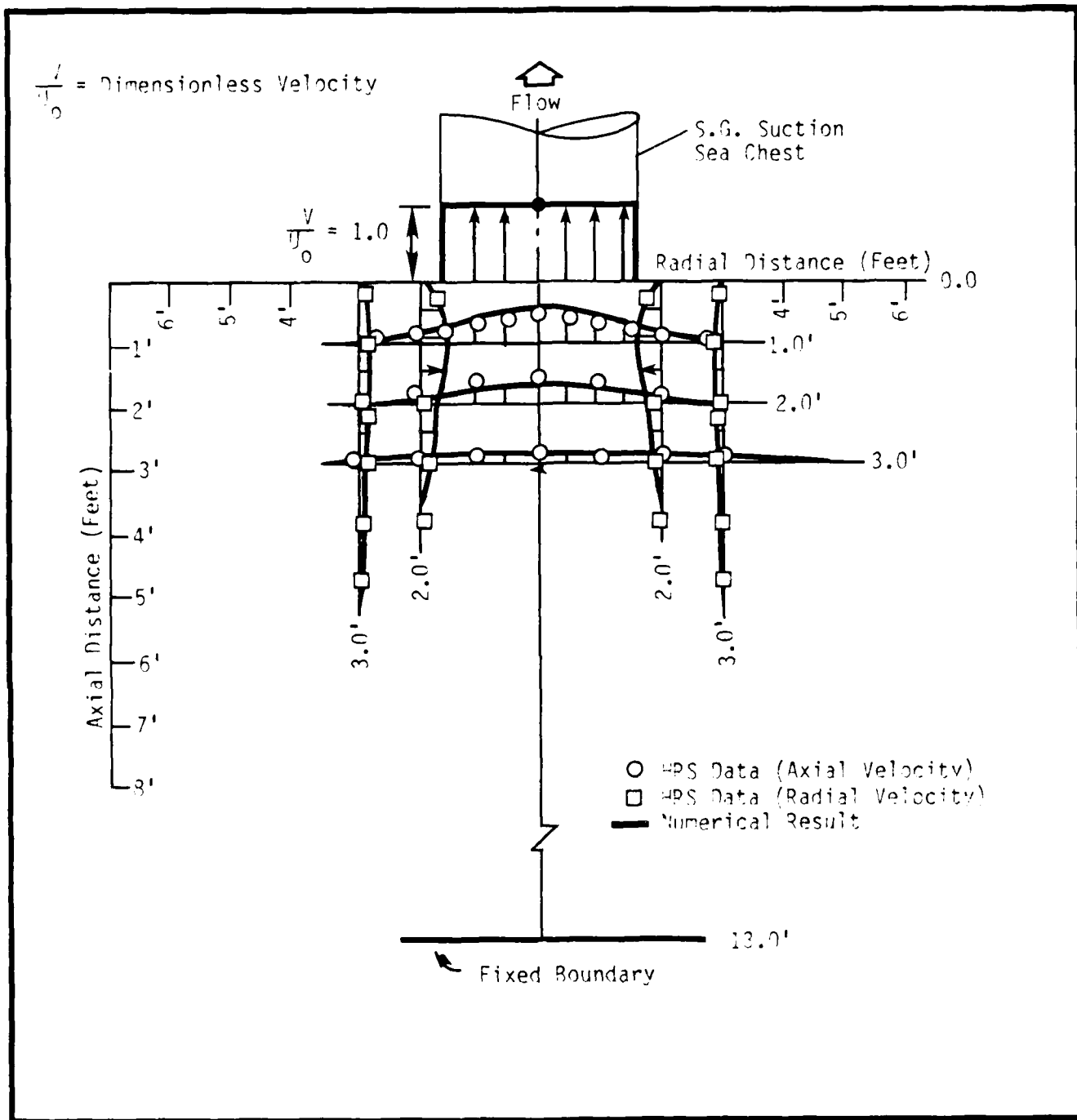
Figure 5-2

Suction Flow Field on Fixed Boundary

(Comparison of numerical results with physical model results)
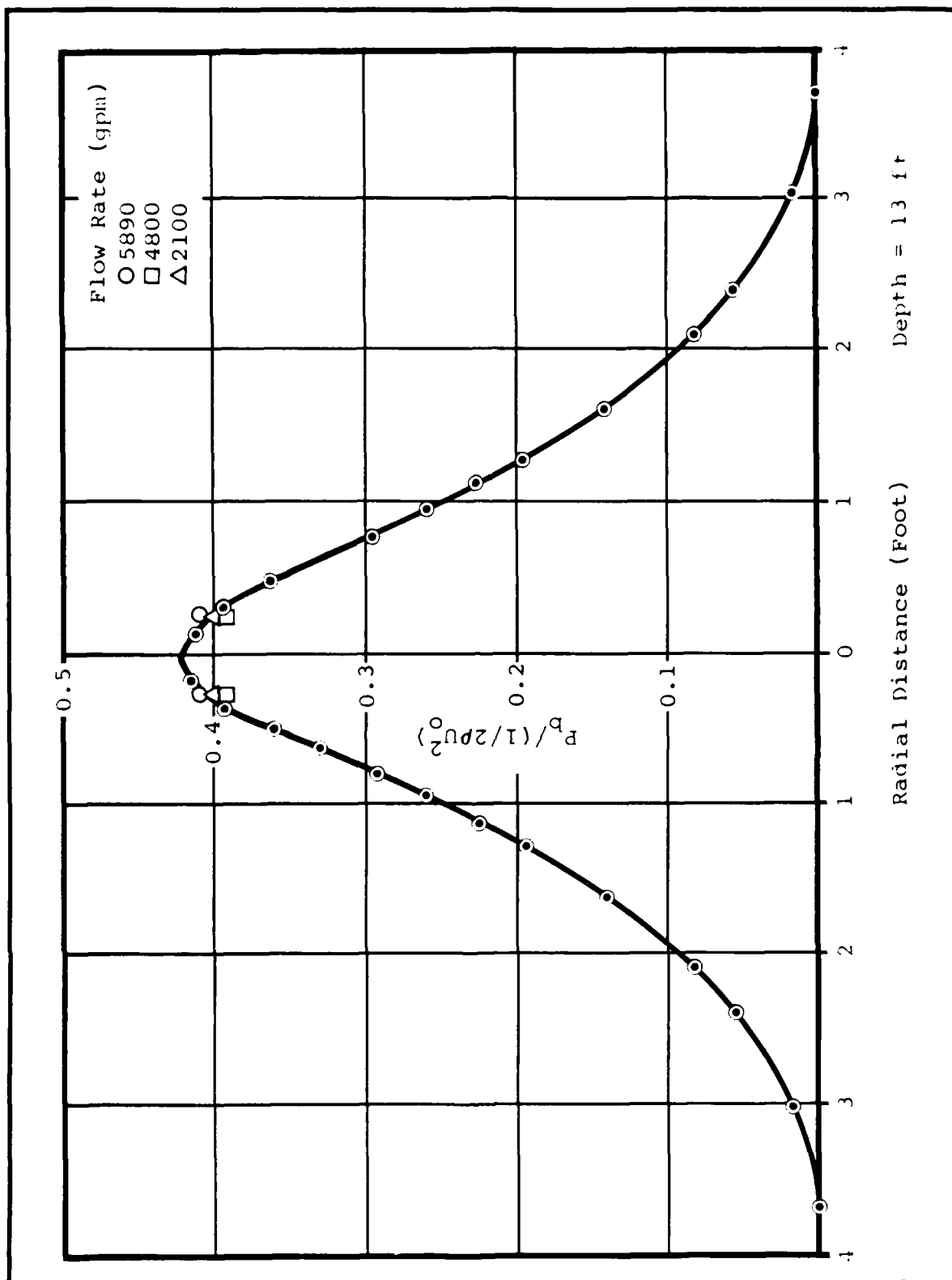
Figure 5-3

Bottom Pressure Distribution for the Impingement of a Jet
on Fixed Boundary

(Comparison of numerical results with physical model results)
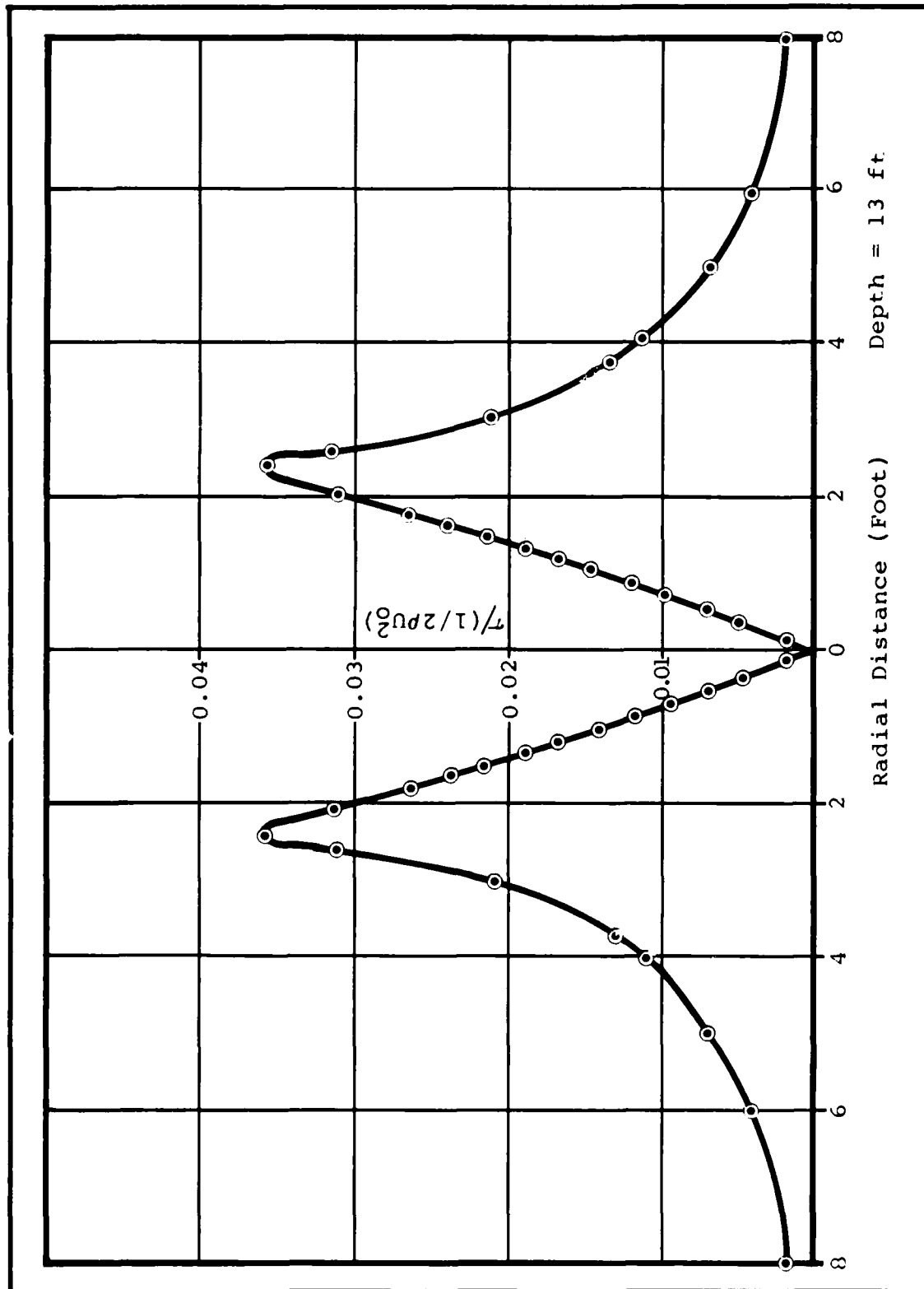
Figure 5-4

Bottom Shear Stress Distribution for the Impingement of a Jet
on Fixed Boundary

Figures 5-5 and 5-6 summarize the numerical model for the jet discharge flow field on a movable bottom. Two different simulated bottom materials are represented: (a) mud, and (b) sand. The numerical model results yielded a significant agreement with the physical model results.

Figure 5-5

Flow Field on Movable Bottom (Mud)
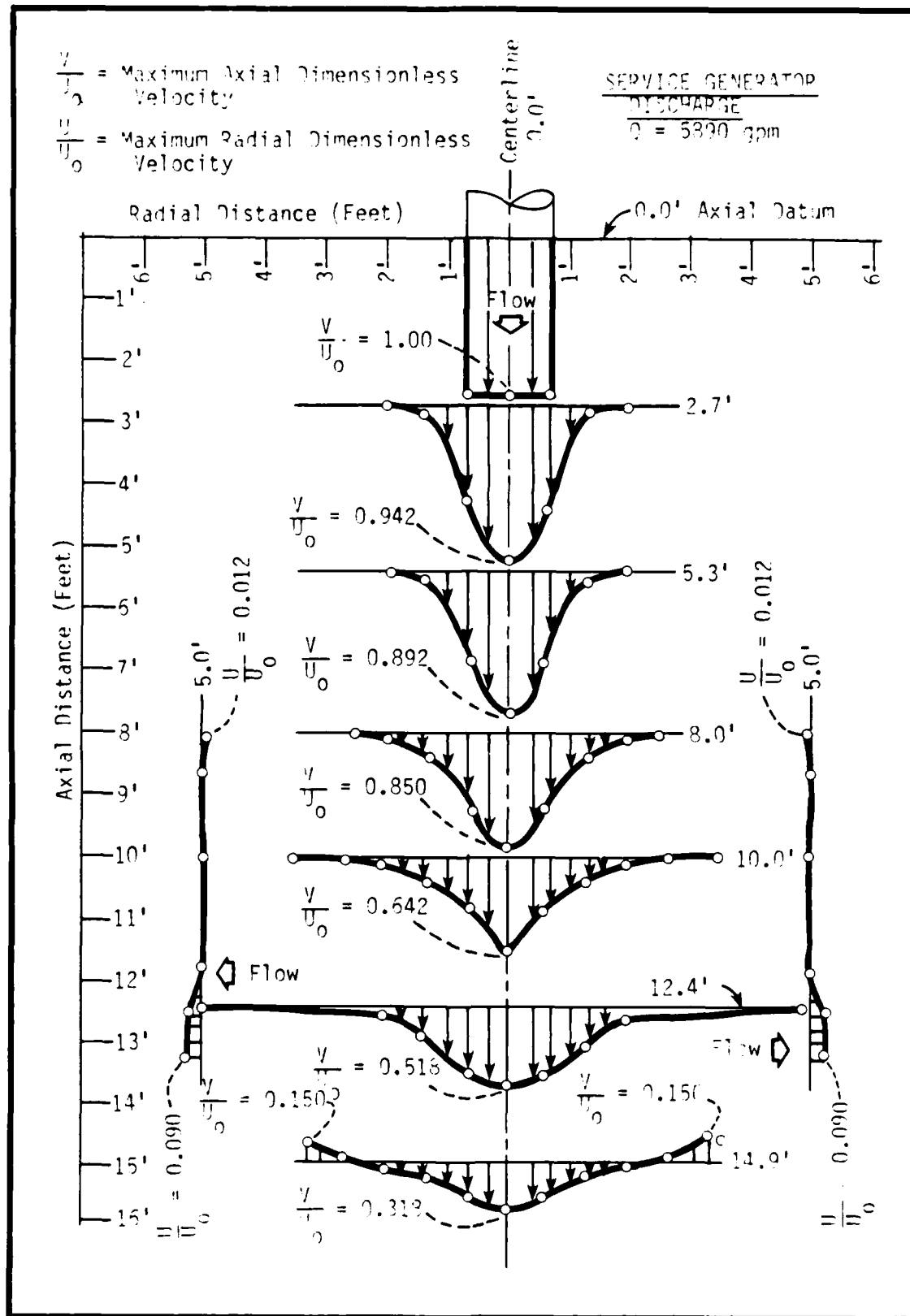
Figure 5-6

Flow Field of Jet on Movable Bottom (Sand)

5.5 APPLICATIONS AND LIMITATIONS OF THE MODEL

For a fixed (flat) boundary, the numerical model provides a means of predicting the jet impingement on: the flow velocities, bottom pressure, and shear stress for jet impingement and suction. The model was developed for the following purposes:

- Judging the stability of the bottom material by comparing the shear stress with the critical shear stress from Shields curve.

- Understanding the influence of underkeel clearance (water depth) as it relates to the impingement of a jet.

- Estimating the volume of bottom material or marine organisms which could be ingested given a specified concentration and distribution of the organisms.

- Determining the jet-center-to-suction-center distance required to reduce the volume of ingested materials.

For the impingement of a jet on a movable boundary the present model is not a general model because of the lack of formulation for mud environment and state-of-the-art difficulties faced in defining a mathematical approach to the problem.

6.0 The Solutions

6.0   THE SOLUTIONS

The analysis of the results of the fouling tests and scour studies indicated that with the original sea-chest configuration, fouling phenomena will occur with each of the three under-keel clearances of 5, 13, and 21 ft. Since sediment buildup can also be expected to create dredging problems, it was concluded that the design of additional control mechanisms would be required to minimize organism fouling and prevent sediment buildup problems. Various solutions can be applied to the aircraft carrier or to the estuary environment to control sediment and organism foulings.

6.1   PRACTICAL SOLUTIONS TO FOULING PROBLEMS

Practical solutions to the fouling problem fall into two categories: (a) onboard solutions and (b) offboard solutions. The onboard solutions include fouling control devices installed on the carrier itself.

Offboard solutions can further be subdivided into onsite solutions and peripheral solutions. Onsite solutions include those provided at the berthing area; peripheral solutions are those provided within the harbor for sediment control.

6.1.1 Onboard Solutions. Although various concepts could be applied to develop onboard solutions, this study concentrated on the use of diffusers.

The criteria provided to HRS for diffuser velocity reduction designs was a space of 4 x 3.5 x 4 ft for the single-barrel diffuser, and a space of 8 x 3.5 x 4 ft for the two-barrel diffuser. An exit velocity of 2.5 ft/sec was agreed by both NAVSEASYSCOM and NAVFACENGCOM to be acceptable, although HRS was prepared to further reduce the exit velocity.

6.1.2 <u>Onsite Solutions</u>. Various onsite solution techniques could be applied to the ship berthing area, including: (a) fencing pier slips with a barrier curtain, (b) providing jet arrays to sweep out bottom sediments, (c) using a crater-sink sediment bypassing system to pump sediment out, or (d) solidifying the sea floor to prevent deep digging of the sea bottom by jets. Only the "solidification of sea floor" option has been included in this study. The remaining onsite solutions will be investigated in a separate HRS research project of Piers 11 and 12.

6.1.3 <u>Peripheral Solutions</u>. Potential peripheral area sediment control techniques include: flushing, exclusion, trapping, and circulation. These techniques and methodologies will be further discussed in the above-cited Piers 11 and 12 study report.

6.2 <u>DIFFUSER DESIGN CONCEPT</u>

The concept of the diffuser design is to spread the flow through various physical arrangements such that the flow velocity will be reduced and a uniform exit velocity obtained. Such a dissipation of energy could be accomplished in three basic ways: (a) via direct impact, (b) via implantation of roughness elements, and (c) via geometric considerations. Each of these basic techniques is discussed in the following paragraphs.

6.2.1 <u>Impact Considerations</u>. Direct impact of the flow on a physical structure provides the most effective method of dissipating energy. Usually an impact chamber or an impact baffle plate is used for such a purpose. Caution must be used during design stages, however, to ensure that the structure can withstand the impact pressure.

6.2.2 <u>Implantation of Roughness Elements</u>. Utilizing rough-
ness elements to slow down a flow is also a common method of
dissipating energy. However, ease of construction is usually
a critical consideration.

6.2.3 <u>Change of Geometry</u>. Changing the structural geometry
of a structure to better guide the flow through, comprises
another effective method of adjusting flow velocity distribu-
tions [30].

6.3 <u>THE PRELIMINARY DIFFUSER DESIGN</u>

The optimal design criteria for the diffuser design in-
cluded:

- Compact diffuser space

- Capability of withstanding ship motions

- Optimal diffuser head loss

- Ease of design, construction, and installation.

Based on the cited design criteria, a series of diffuser
designs was developed, tested, and evaluated. Figure 6-1 il-
lustrates the conceptual design of the diffuser and its compo-
nents. Twenty-four different configurations of the diffuser
design were tested. Figure 6-2 is a photograph of the various
diffuser designs tested by HRS. The experimental evaluation
of the design indicated that the perforated impact plate and
louver arrangement was an effective design.
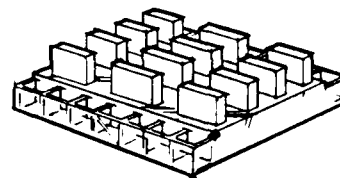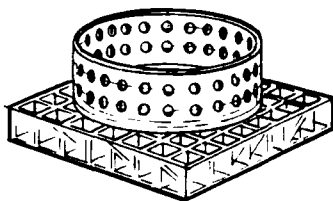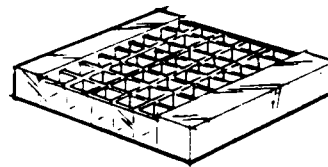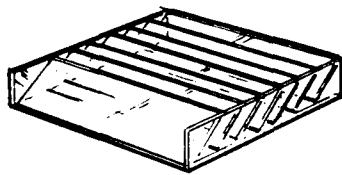
EXAMPLES OF VARIOUS CONCEPTS TESTED

DISCHARGE CONDUIT

LEVEL 1
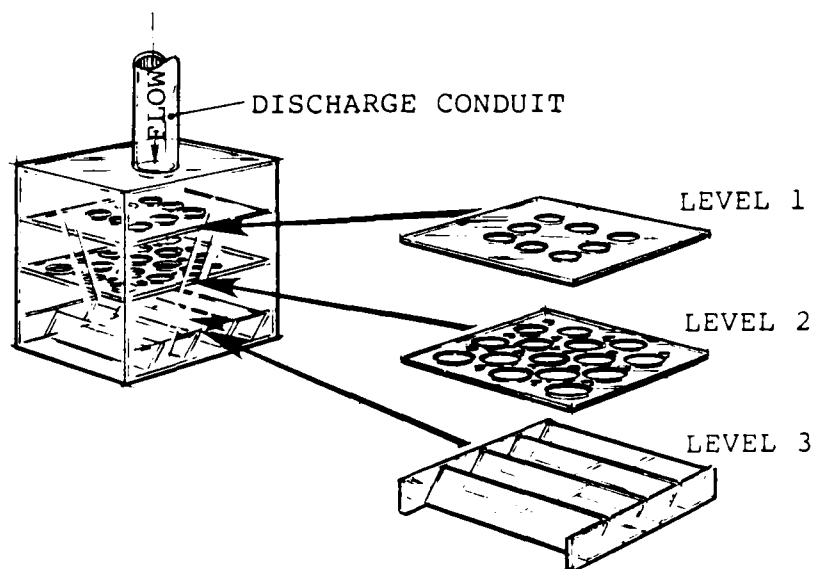
LEVEL 2

LEVEL 3

ARTIST'S CONCEPT OF DIFFUSER MODEL SHOWING
THREE LEVELS OF INSERTS

Figure 6-1

Conceptual Design of the Diffuser and Components
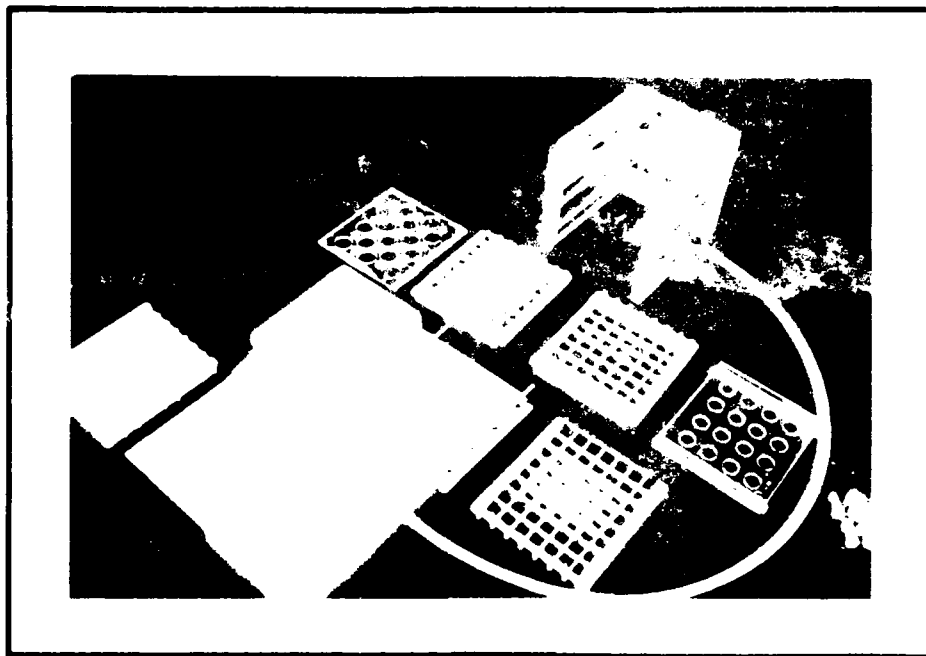
Figure 6-2

Diffuser Designs Tested by HRS

6.4 THE SINGLE-BARREL DIFFUSER

The single-barrel diffuser is used in the SG condenser
unit. The dimension of the diffuser was limited to a box struc-
ture 4 ft long by 3-1/2 ft wide by 4 ft deep.

6.4.1 Preliminary NAVSEASYSCOM Designs. NAVSEASYSCOM provided
HRS with two preliminary sea-chest diffuser designs for evalu-
ation. As shown in Figure 6-3, the impact chamber consisted of
two semicircular cups concaved upward and located directly
under the discharge line. The guide vanes, located on the
sides, were designed to change flow direction.

Tests of the diffuser yielded rotational flow patterns,
with the discharge branching into two streams, due to the de-
sign of the two semicircular cups. It was evident that
further modification of the impact chamber was required to
achieve better flow distributions.
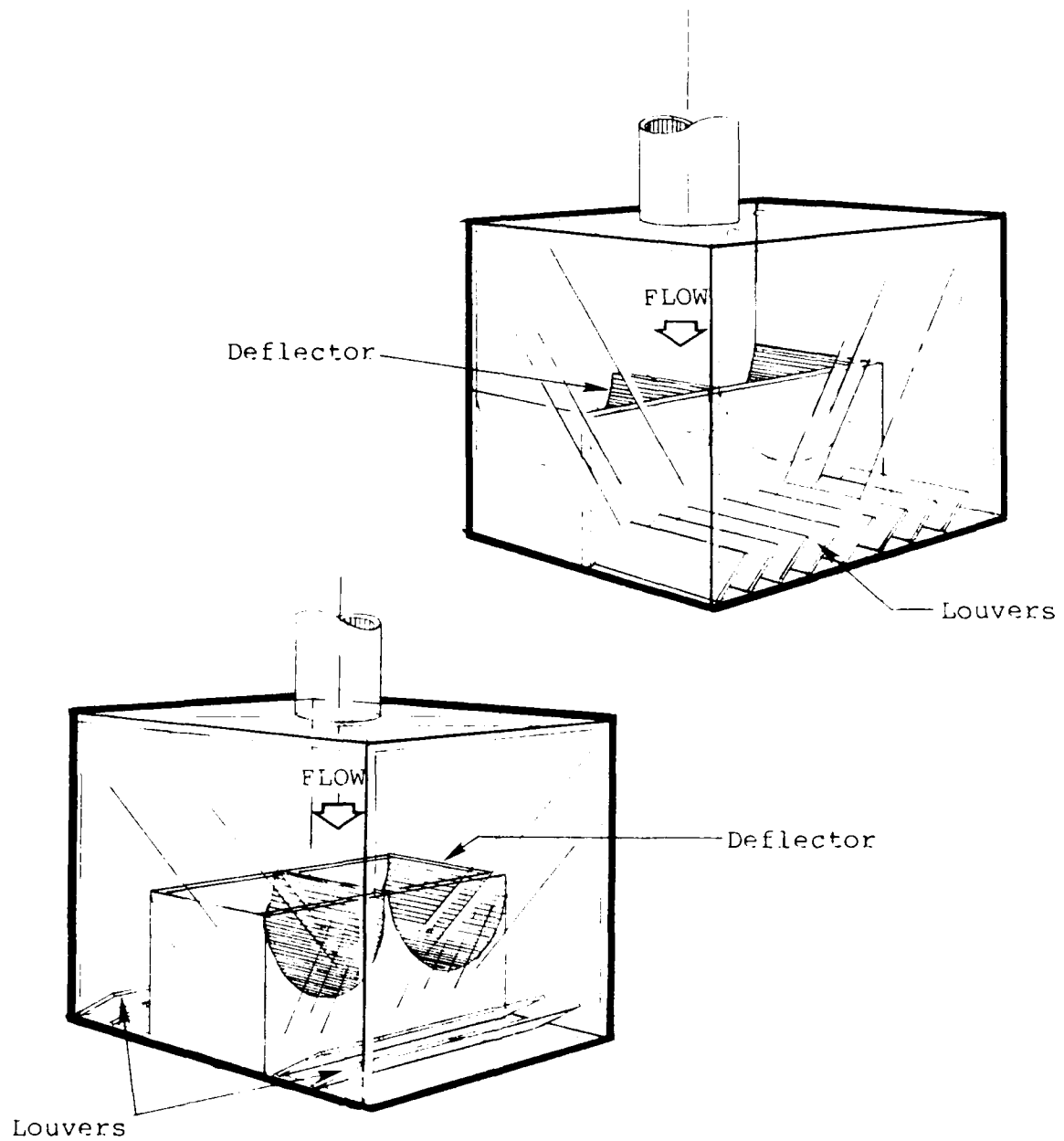
Figure 6-3

NAVSEASYSCOM Preliminary Diffuser Designs

6.4.2 <u>Single-Barrel Diffuser Development</u>. Various impact chamber arrangements were tested and compared with the original two NAVSEASYSCOM semicircular impact chamber diffusers. The configurations included an enclosed and a semi-enclosed rectangular chamber both with and without a roof structure, plus a circular impact chamber and impact plates. Figure 6-4 shows the different components tested.

The evaluation of these various arrangements revealed that the semi-enclosed rectangular chamber with rows of perforated 3-inch circular openings at the side walls, and with bottom slots, provided satisfactory velocity distributions at the louvered exit.
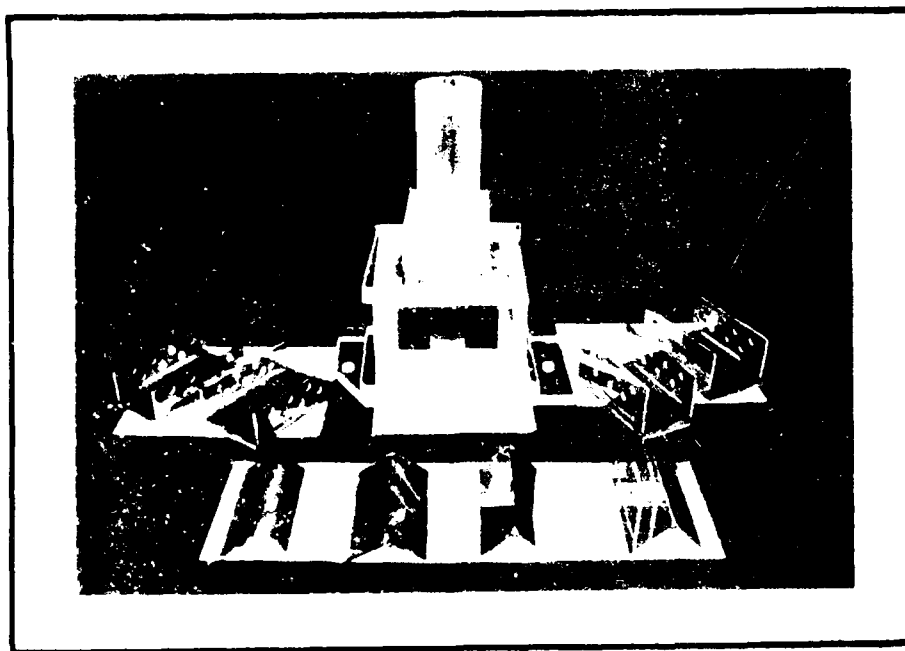
Figure 6-4

<u>Diffuser Test Components</u>

6.4.3 <u>Final Single-Barrel Design</u>. The final single-barrel diffuser design was obtained as the result of the optimization

tests. Figure 6-5 shows the final design of the single-barrel
diffuser. This design was tested at pumping conditions of
5,890, 4,800 and 2,100 gpm with keel clearance of 13 ft. The
results of these tests revealed a maximum velocity of 2.8
ft/sec at the exit. This velocity was reduced to 1.3 ft/sec
near the sea floor in the direction away from the suction sea
chest (see Figure 6-11). The back pressure to the discharge
pipe was equal to 10 inches of water head for a pumping rate
of 5,890 gpm. Figure 6-6 illustrates the dimensions of the
final recommended single-barrel diffuser.
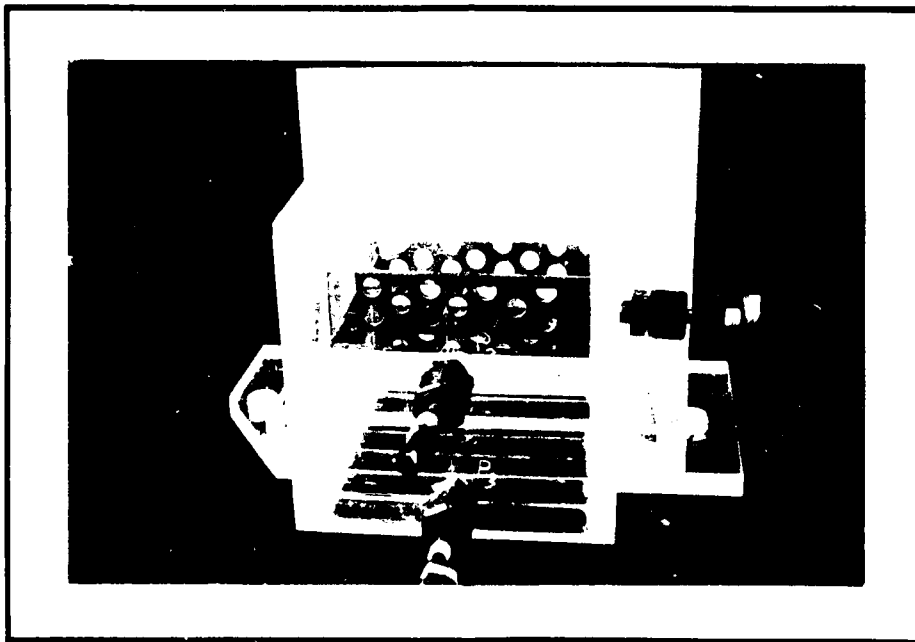
Figure 6-5

Final Design of the Single-Barrel Diffuser

16" Dia. Service
Generator Discharge
Opening

cell

Deflector

Louvers

ORIENTATION

16" DIA

FLOW

4"

3" DIA. VENTS

7° FILL

23"

3"
DIA.
HOLES

12"

48"

20"

30" SLOT
2" HIGH

50°

5.754"

42"

6.857"   48"

RECOMMENDED DIMENSIONS
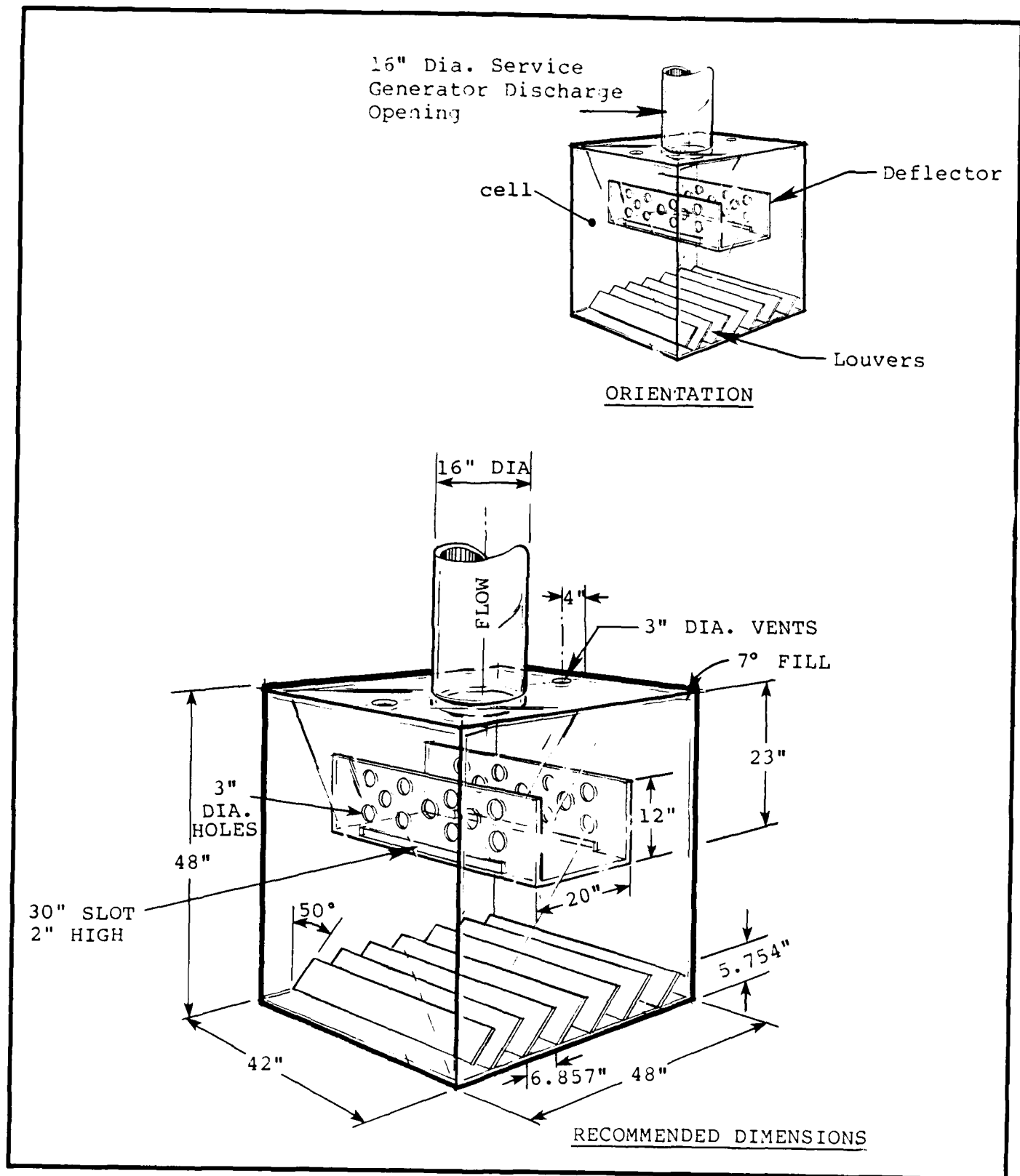
Figure 6-6

Final Recommended Single-Barrel Diffuser

6.5   THE DOUBLE-BARREL DIFFUSER

The preliminary design dimensions for the double-barrel discharge diffuser were 8 ft long by 3-1/2 ft wide by 4 ft deep. The inner barrel has an impact diverter with a roof design to divert the flow toward a 2-ft-diameter lightening hole on the separation wall between the inner and the outer barrels. In the other compartment, seven louvers located at the bottom guide the flow in the direction of the stern. Figure 6-7 illustrates the preliminary double-barrel diffuser design.
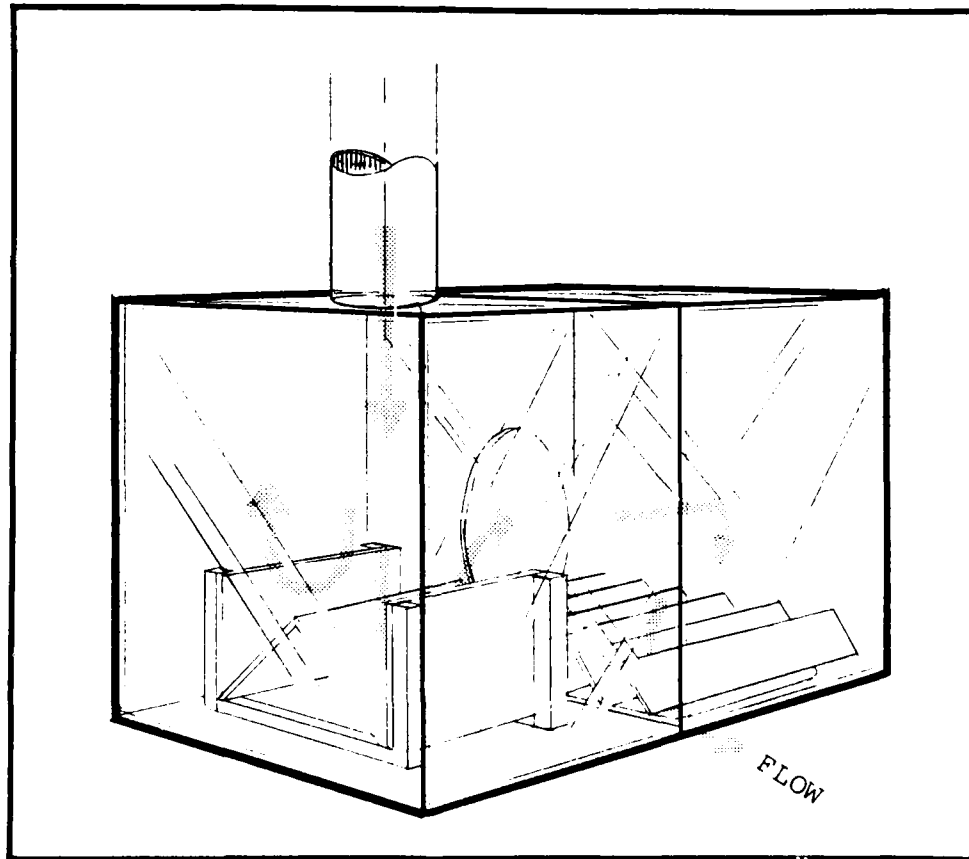
Figure 6-7

Preliminary Double-Barrel Diffuser Design

6.5.1 Double-Barrel Diffuser Development. The diffuser was
subjected to base tests to determine the effectiveness of the
velocity reduction. Observation of the flow patterns revealed
uneven-flow velocity distributions at the louver exit. These
distributions were found to result from the diversion of incom-
ing flow at the inner barrel through the lightening hole. When
the flow entered the outer compartment at high momentum, it im-
pacted on the outside wall, then deflected back with concentrated
jet flow patterns out of the louvers.

6.5.2 Final Double-Barrel Design. As with the single-barrel
discharge diffuser, several impact arrangements were tested.
These arrangements included rectangular and circular chambers
with perforated walls at the inner compartment to dissipate
energy, and a baffle beam design at the outer compartment to
redistribute the flow.

     Evaluations indicated that a design incorporating a semi-
enclosed rectangular impact chamber at the inner compartment,
and two parallel baffle beams with port-to-starboard orientation
at the outer compartment, provided a good exit velocity distri-
bution. This design is therefore recommended as an effective
onboard solution. The final recommended design is presented
in Figures 6-8, 6-9, and 6-10.
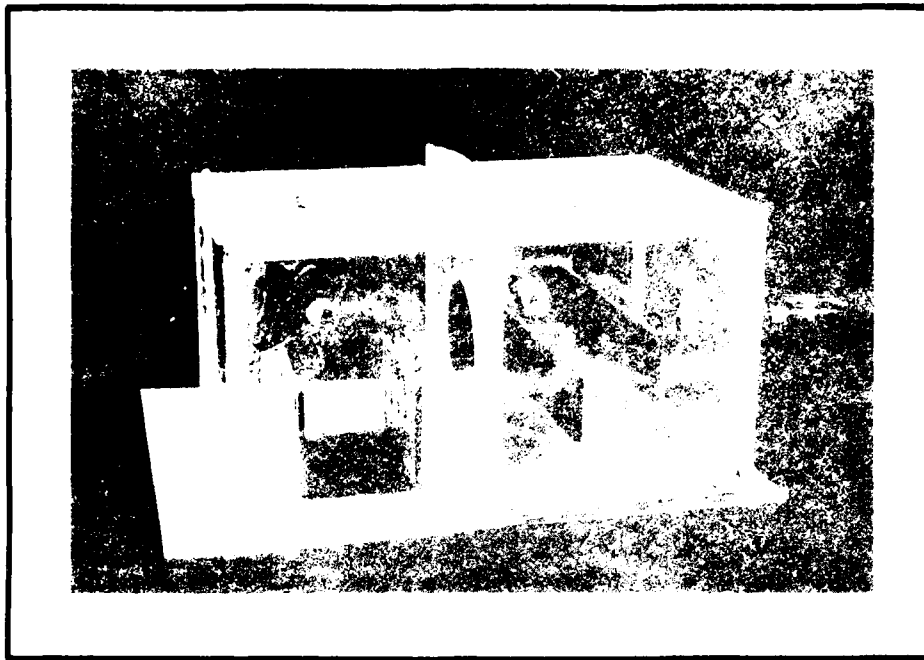
Figure 6-8

Final Design of the Double-Barrel Diffuser

Dia 16"
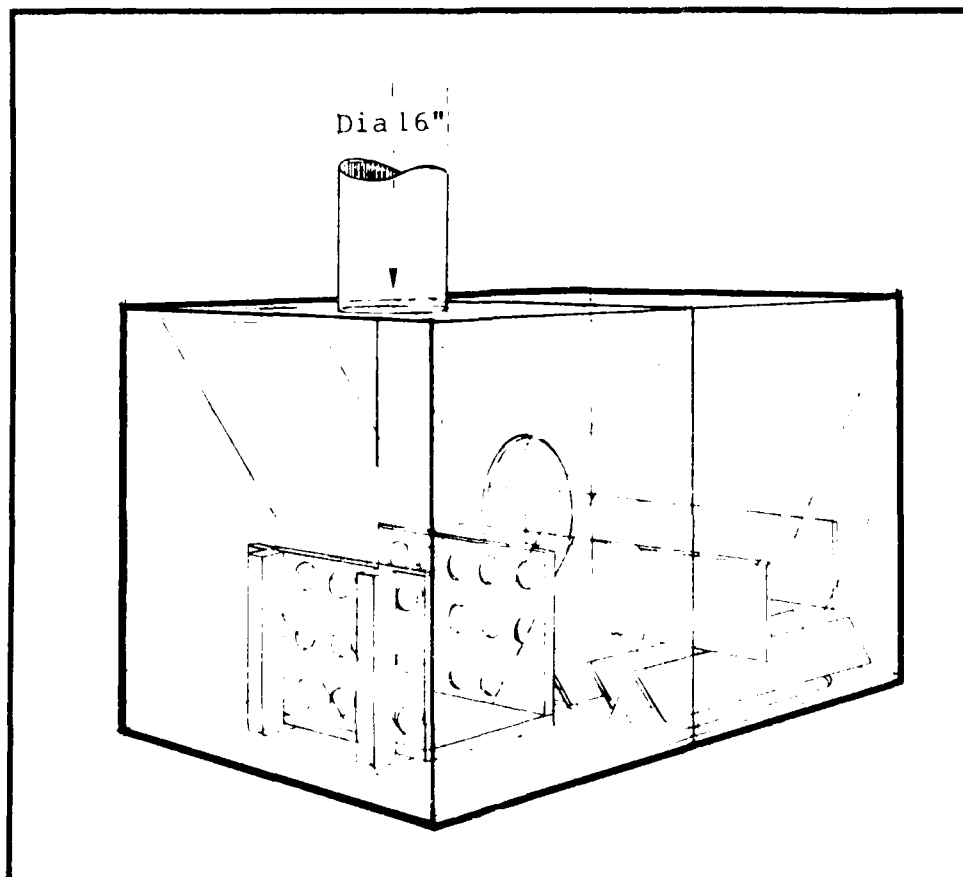
Figure 6-9

Final Recommended Double-Barrel Diffuser
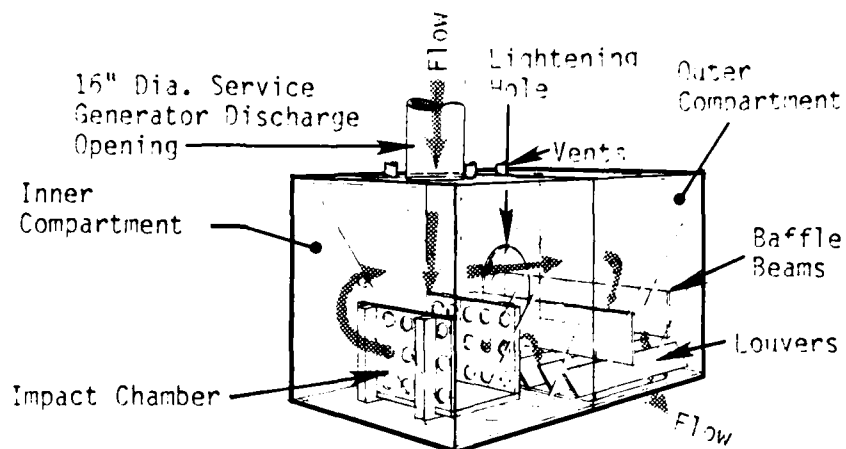
ORIENTATION

SECTION A-A

SECTION C-C

SECTION B-B

PLAN

Figure 6-10
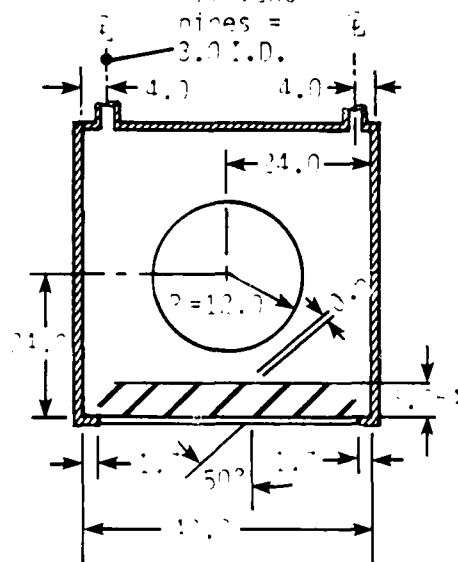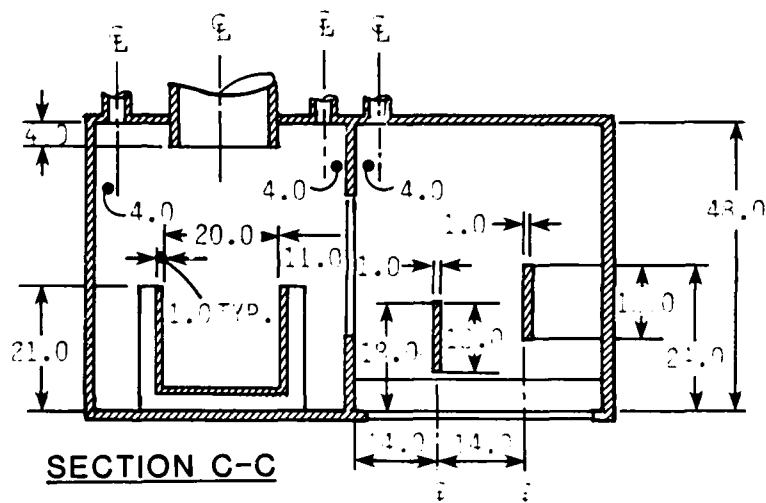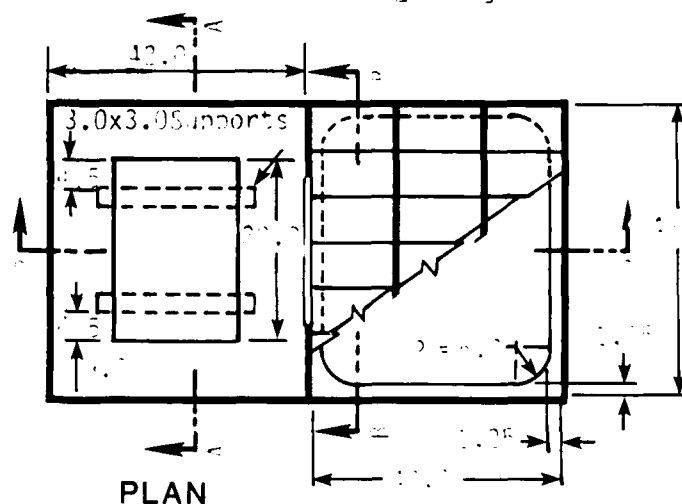
Final Recommended Double-Barrel Diffuser

6.6 VERIFICATION STUDIES

The final recommended diffuser designs were then subjected to various operational conditions to verify their operational characteristics.

6.6.1 Pier-Side Berthing Simulation. With the discharge diffusers in place, pumping rates of 5,890, 4,800 and 2,100 gpm were tested for the SG discharge sea chests. A dye probe was used to observe the exit flow patterns, and an electromagnetic velocity meter was used to measure the velocity distributions.

Excellent flow conditions were obtained. Figure 6-11 shows the flow patterns resulting from the two final diffusers. Figure 6-12 shows the flow patterns and velocity measurements obtained from these tests.

6.6.2 Ship-In-Motion Simulation. An alternative method of ship-in-motion simulation was adopted by moving the flow beneath the stationary platform to obtain the relative velocities. The flow patterns of a ship moving at speeds of 5 and 12 knots with a pumping rate of 5,890 gpm on the SG discharge were recorded, and are shown in Figure 6-13. The results indicated that with the diffuser as the onboard solution, problems will not be encountered during ship-moving operations.

Figure 6-11
Flow Patterns Resulting from Two Final Diffusers
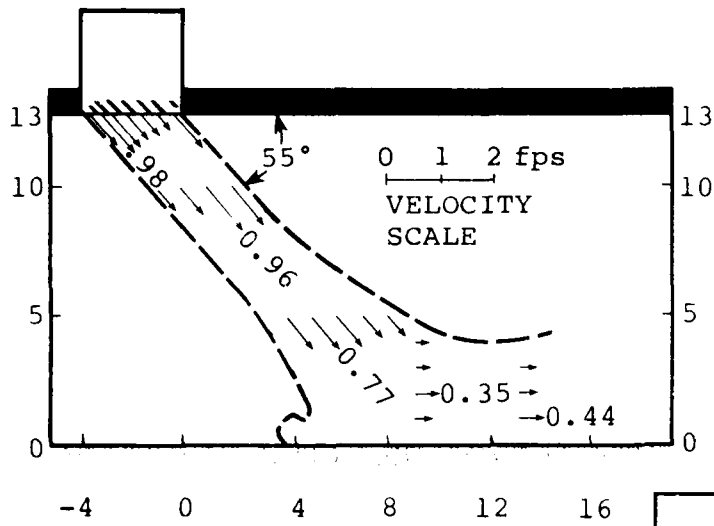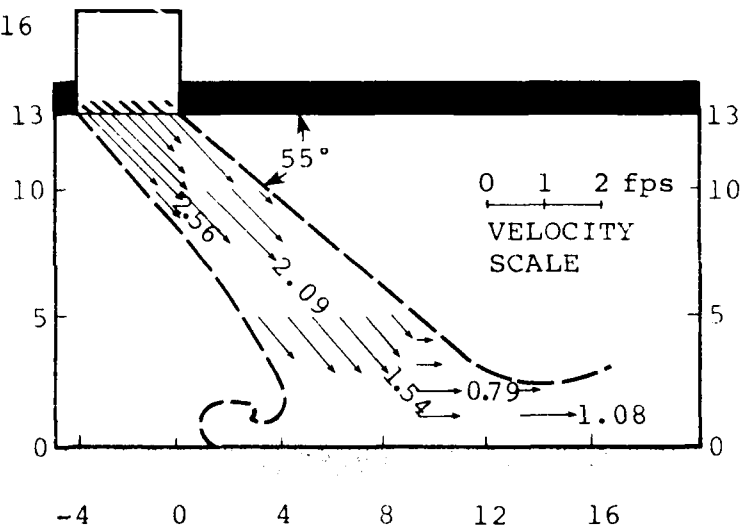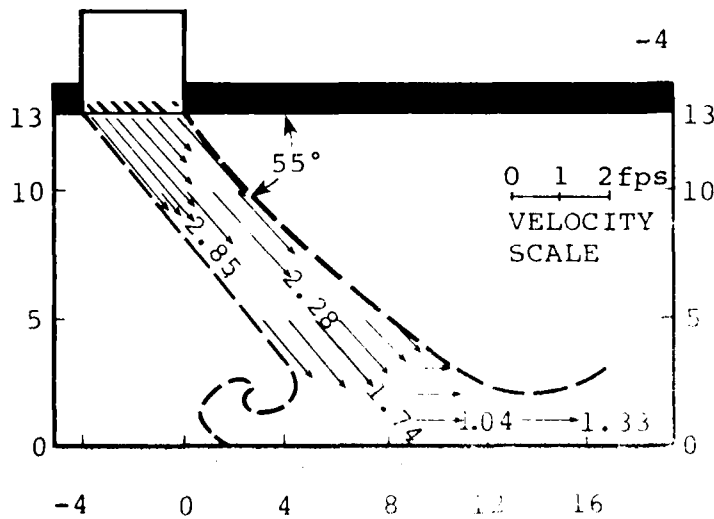
Figure 6-12

Pier-Side Diffuser Flow Patterns
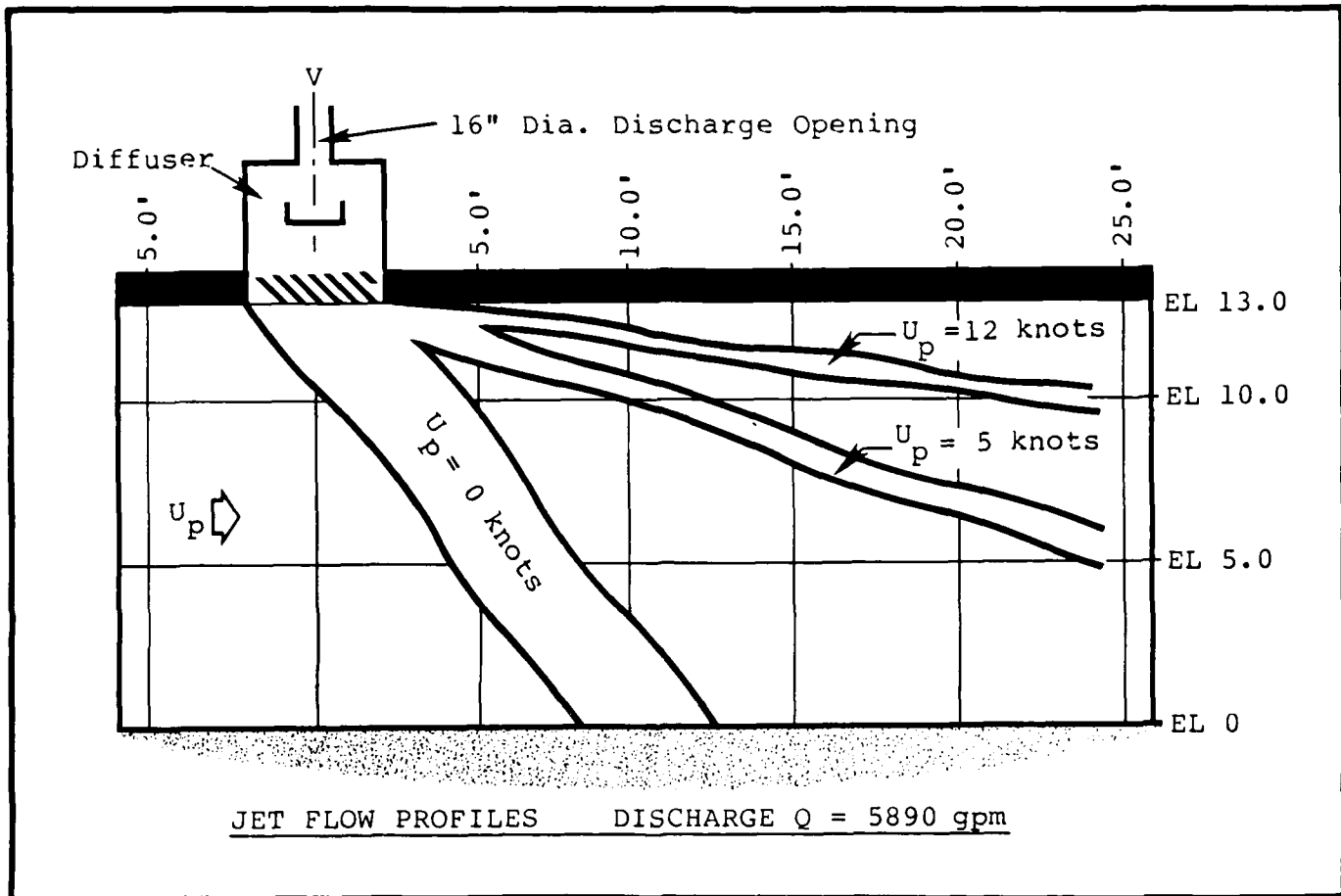
Figure 6-13

Flow Patterns from Moving-Ship Simulation

6.6.3 Sea Bottom Scouring and Fouling Tests. Both single-
and double-barrel discharge diffusers were tested using a
thick layer of mixed walnut-shell/green algae lying at the
bottom of the berthing tank. Flow rates of 5,890, 4,800, and
2,100 gpm were examined using a 13-foot underkeel clearance.
The primary purposes of this test were to qualitatively assess
the scouring of the bottom material, and to investigate the
insufflation of material into the suction sea chests.

Observation of the sea-bottom material scouring revealed that the bottom layer was only superficially disturbed, and a slight depression produced. Very small amounts of the floating material approached the suction sea chest as a result of this minor disturbance of the flow field.

6.7 CONCLUSIONS ON ONBOARD SOLUTIONS

The previously described test program concluded the study on the SG diffuser units. The problem of the main circulating cooling system had not yet been solved. However, according to the Navy personnel, the main circulating cooling system does not have to be operated at full capacity during berthing and light off operations. This provides a very promising fouling control measure by simply cutting down the pumping rate on the main circulating system sea chests.

It was concluded that with the diffuser as the on-board solution, and deepening of the berthing area to 50 ft, the fouling of the suction sea chest can be minimized.

6.8 CONCEPT OF SOLIDIFICATION OF SEA FLOOR

An alternative technique for controlling the fouling phenomena could utilize the previously discussed "jet on solid boundary" concept. This concept naturally falls into the category of onsite solutions.

6.8.1 Preliminary Test. A test was conducted to investigate whether a solid bottom underneath the discharge sea chest would improve sediment control. A thin layer of walnut shell was paved on top of a piece of acrylic Plexiglas platform to simulate a section of solid sea floor. With the main circulating cooling system in operation, the discharge pushed away the thin

layer of sediment without further digging down into the sea bottom. This reduced the chance of sea-chest clogging. Figure 6-14 shows the concept of sea-floor solidifications, and Figure 6-15 shows the resulting scour patterns.

PIER

SHIP

PLAN VIEW AT WATER SURFACE

Discharge Sea Chest.

PLAN VIEW AT BERTH BOTTOM

Solid Sea Floor
Test Pad
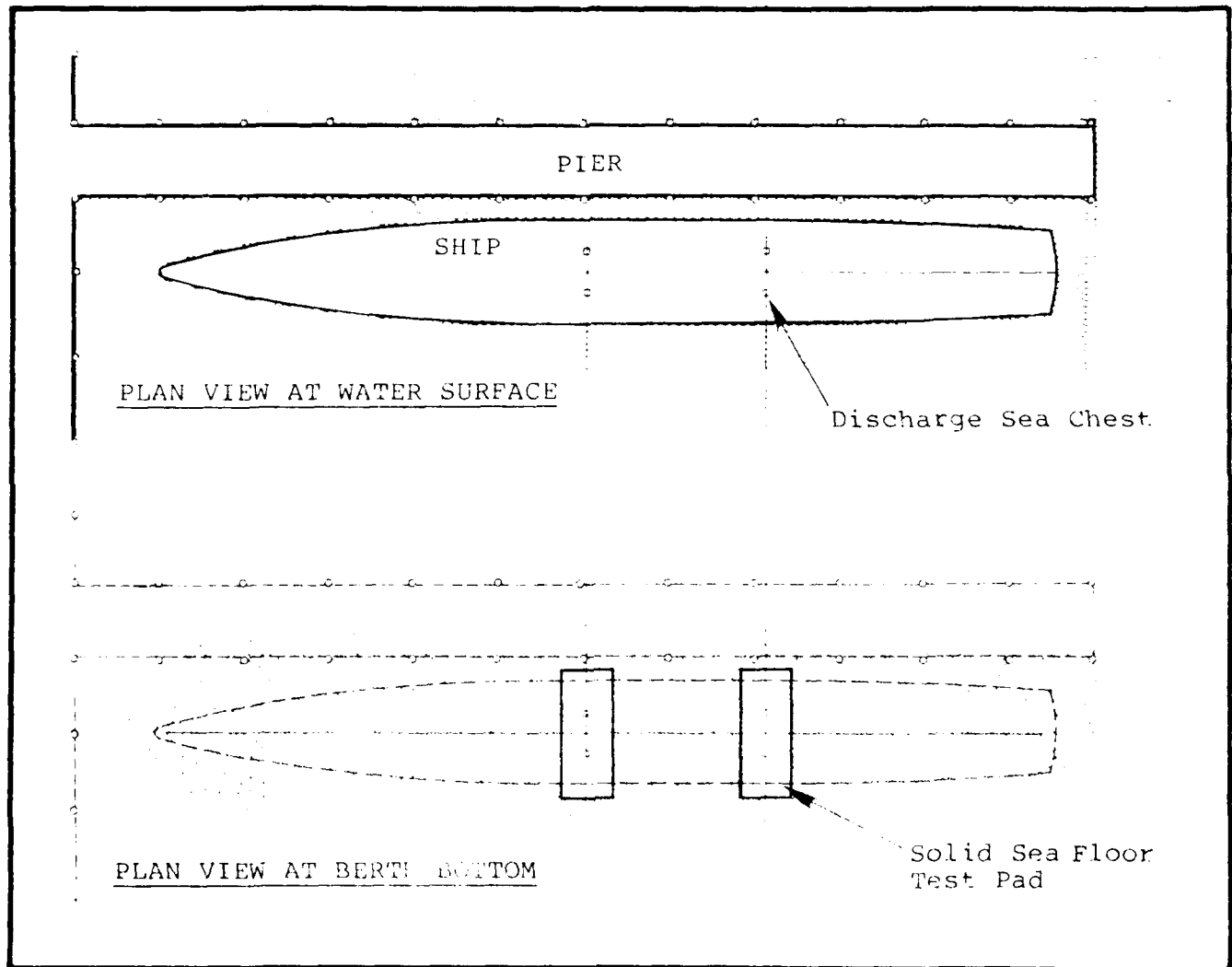
Figure 6-14

Concept of Sea Floor Solidifications

Figure 6-15
Resulting Scour Patterns

6.8.2 Recommendations. From the above-cited preliminary test, it is evident that further study of the sea floor solidifications is worth pursuing. This concept will be tested as part of the HRS study of Piers 11 and 12.

Appendix A,
Hydrodynamic Properties of Marine Organisms,
(By Dr. R.J. Diaz of VIMS)
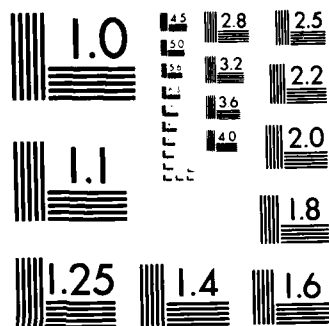
MICROCOPY RESOLUTION TEST CHART

NATIONAL BUREAU OF STANDARDS 1963 A

APPENDIX A

HYDRODYNAMIC PROPERTIES OF MARINE ORGANISMS

(By Dr. R. J. Diaz of VIMS)

Hydrodynamic properties of the fouling organisms were mea-
sured in the laboratory using the VIMS hydraulic flume [31] [32].
The flume has a 48-ft long by 3-ft by 3-ft test section with a
smooth level floor. Current velocities in the test section
were adjustable from 0 to 2.8-ft/sec. The overall uniformity
of velocity versus depth is within 2 to 3%.

A.1 DENSITY OF THE ORGANISMS

Density of the organisms was measured by a volume displace-
ment method. The volume of a given quantity of organisms was
estimated from the amount of water they displaced in a 1,000
ml graduated cylinder. The mass of the same quantity was then
estimated using a sartorius balance. The average density for
live hydroids was 1.026-g/cc; for live bryozoans 1.087-g/cc;
for dead and buried hydroids 1.128-g/cc; and for dead and
buried bryozoans 1.187-g/cc. The higher densities for dead
organisms resulted from the inclusion of sediment particles
within the skeletal remains of the organisms.

A.2 MOTION OF ORGANISMS IN FLOW

For this series of tests, organisms were placed on the
floor of the flume, and the flume velocity increased until the
organisms began to roll. Several parameters were measured, in-
cluding: critical flow velocity, and initiation of motion
velocity. Critical flow velocity was determined for indivi-
dual colonies and for a large cluster of colonies of various
sizes. Flume velocity was increased from zero to the point
where waving and saltation of colonies occurred. Results
are summarized in Table A-1.

TABLE A-1
Critical Flow Velocity

Individual Colony Hydroids	live	0.05 fps
Individual Colony Hydroids	dead	0.22 fps
Individual Colony Bryozoans	live	0.20 fps
Individual Colony Bryozoans	dead	0.22 fps
Mixed Colonies Hydroids		0.07 to 0.08 fps
Mixed Colonies Bryozoans		0.20 to 0.23 fps

Individual live colonies of hydroids have the lowest critical flow velocity, and are very easily moved along the flat floor of the flume. Dead hydroids that have been buried have mud incorporated into their hollow skeletons, and are harder to move. With bryozoans it makes little difference as to whether they are live or dead.

When a large amount of organisms was placed in the flume test section (about 20-lb) the intertwining of the colonies increased the resistance to movement, increasing the critical flow velocity. <u>This mix of colonies probably represents a more realistic picture of what occurs in the prototype system than the individual colony measurements.</u>

Initiation of motion velocities, defined as the flume velocity needed to cause sustained motion of colonies, were estimated similarly to critical flow velocities. Results are summarized in Tables A-2 and A-3.

TABLE A-2
Initiation of Motion Velocity (I)

Individual live colony			
Hydroids		Bryozoans	
wet weight (grams)	velocity (fps)	wet weight (grams)	velocity (fps)
0.6	0.05	16.8	0.34
1.7	0.07	27.1	0.37
4.1	0.09	73.0	0.40
7.8	0.11	89.1	0.41

TABLE A-3

Initiation of Motion Velocity (II)

Mixed live & dead colonies	
Hydroids velocity (fps)	Bryozoans velocity (fps)
0.14 to 0.17	0.28 to 0.32

For hydroids the size of the colony strongly affects the initiation of motion velocity. With bryozoans the effect of size on velocity is not as strong. Again as with the critical flow velocity, the initiation of motion velocity is higher for a mix of colonies, and probably represents a more realistic view of the prototype.

A.3 FALL VELOCITY OF ORGANISMS

Fall velocity was determined in a standing body of water about 3-ft deep. Organisms were placed below the water surface, released, and after achieving terminal velocity timed across a measured depth of water. Results are summarized in Tables A-4 and A-5.

The size of the hydroid colony, expressed as a wet weight, influenced the fall velocity. Larger live colonies sank faster. Dead colonies of equal size to live colonies had faster fall velocities, due to the higher density of the dead colonies. With the bryozoans there was no clear relationship to size of colony and fall velocity. That dead colonies of bryozoans had smaller fall velocities than live colonies is unexplainable, and may require further testing.

TABLE A-4

Fall Velocity of Organisms (Hydroids)

Live colonies -- Winter 1980 growth --		Dead colonies -- Winter 1979 growth --	
wet weight (grams)	fall velocity (fps)	wet weight (grams)	fall velocity (fps)
158.0	0.11	23.3	0.09
50.0	0.09	12.4	0.10
29.0	0.12	6.6	0.09
7.0	0.04	3.1	0.16
2.4	0.03	0.5	0.18
0.7	0.02	0.4	0.27
0.4	0.02	0.2	0.39

TABLE A-5

Fall Velocity of Organisms (Bryozoans)

Live colonies -- Winter 1980 growth --		Dead colonies -- Winter 1979 growth --	
wet weight (grams)	fall velocity (fps)	wet weight (grams)	fall velocity (fps)
278.0	0.22	77.2	0.09
130.0	0.21	42.4	0.11
94.0	0.29	20.5	0.13
45.0	0.27	18.2	0.16
28.0	0.25	9.1	0.13
22.0	0.26	8.2	0.12
17.0	0.22	3.7	0.16
		3.3	0.21

Appendix B,
Physical Model Test Results

APPENDIX B

PHYSICAL MODEL TESTS AND RESULTS

B.1 THE PHYSICAL MODEL SETUP

B.1.1 Key Elements of Model Setup

The model of the underkeel clearance study was constructed to an undistorted linear-scale ratio, model to prototype, of 1:10. The model was built to be flexible enough to make the components readily exchangeable if the need arose for the revisions to the model structure. The model consisted of four main components:

- The facility (the HRS berthing tank)

- The model proper (the sectional sea-chest model)

- Auxiliary equipment

- Instrumentation.

B.1.2 The Berthing Tank -- The Model Housing

The sectional sea-chest model was constructed and then installed in the HRS berthing tank. This tank is a permanent HRS facility 6.3 ft wide and 6 ft deep. The side walls and floor of the tank are made of clear acrylic plastic to enable easy observation of flow patterns.

B.1.3 The Model Proper

The model proper encompassed significant sections of the bottom hull of the CVN 69 aircraft carrier, shown in Figure 4-2, where assessment of sea-chest fouling was to be performed. These critical sections included:

- Suction sea chest with strainer plate for SG Units #43 and #53

- Discharge sea chest for SG Units #45 and #57

- Main circulating system suction sea chest with in-
  let strainer bars for Unit #41

- Main circulating system discharge sea chest for
  Unit #46.

B.1.4 The Auxiliary Equipment

The actual model components were augmented by auxiliary
equipment, including: sumps to store water, centrifugal pumps
to circulate the flow through the model, and a system of dis-
charge valves and butterfly valves to regulate the flow for
the simulation of the sea-chest pumping conditions.

B.1.5 The Instrumentation

The primary metering devices used to measure flow veloc-
ities and pressures included: Pitot tube, current meters, dye
probes, pressure transducers and piezometers, and orifice
meters to monitor the flow rates. Higher velocities were
measured using a conventional Pitot tube with a minimum read-
ing of 0.3 feet per second (fps) (prototype value) and an
electromagnetic water current meter with a minimum reading of
0.2 fps (prototype value).

The electromagnetic velocity meter was equipped with a
calibration check mechanism to monitor the magnetic drive sig-
nal and channel amplifiers to ensure that the calibration re-
mained the same as that preset at the factory. A calibration
check was performed every time an experiment was conducted.
The Pitot tube measurements were compared with the electromag-
netic meter simultaneously operated in the model.

Dye meters were used to observe and record flow patterns
and any other eddy formations. Subsurface patterns were deter-
mined by means of dye introduced into the model at the desired
depths. The differential pressure transducers used in the
pressure measurement study were equipped with replaceable dia-
phragms to measure pressure fluctuations from 0.1 to 25 psi.

The 2-channel oscillographic recorder recorded pressure-variation dispatches through the transducers at locations of the sea floor beneath the jet.

B.2 THE MODEL LAWS

The similitude relationships between the model and the prototype for flows in the study are based on the Froude Law. The resulting mathematical relationships between the basic hydraulic quantities of the model and the prototype are summarized in Table B-1. The scale relationships in this table can be used to transfer quantitatively the discharge, depth of flow, and the velocity of flow from the model to the prototype.

TABLE B-1

Similitude Relationships

Dimension	Ratio of model to prototype	Scale Relationships
Length	$L_r = \dfrac{L_m}{L_p}$	1:10
Area	$A_r = (L_r)^2$	1:100
Time	$T_r = (L_r)^{1/2}$	1:3.16
Velocity	$V_r = (L_r)^{1/2}$	1:3.16
Discharge	$Q_r = (L_r)^{5/2}$	1:316

B.3 THE STATISTICAL DESIGN DATA

B.3.1 Structural Design Data

Data pertinent to structural features of the original sea-chest design are summarized in Table B-2.

TABLE B-2

Sea-Chest Structural Features

Service Generator (SG) suction opening	37-1/8" x 30-3/8"
Service Generator discharge opening	16" circular
Main Circulation System suction opening	42-13/16" x 28-13/16"
Main Circulation System discharge opening	69-13/16" x 46-13/16"
Underkeel clearance	5', 13', and 21'

B.3.2 Hydraulic Design Data

The hydraulic design data related to the model investigations are summarized in Table B-3.

TABLE B-3

Hydraulic Design Data

SG circulation flow rate (Full Capacity)	5,890 gpm
Main Circulation System flow rate (Full Capacity)	25,000 gpm
Ship speed	0 to 15 knots

B.4 PHYSICAL MODEL LIMITATIONS

B.4.1 Similarity Limitations

Similarity between the model and the prototype was obtained in accordance with the Froude Law, which assumes

gravity as the dominant force. Since complete dynamic simil-
itude and accurate reproduction of some properties of the
prototype materials are not possible, some limitations must
be imposed on the model results.

B.4.2 Scour Interpretations

Data on scour are to be considered as qualitatively
reliable, since it has not yet been found practical to re-
produce quantitatively the resistance to erosion of a proto-
type bed material in a model. The observed scour data served
as a basis for determining the relative effectiveness of the
types and placement of the protective elements, as well as
indicating areas most vulnerable to erosive attacks.

B.4.3 Air-Entrainment Considerations

Air entrainment cannot be modeled by the Froude Law
alone. Air entrainment is a function of the flow velocity,
depth and distance traveled, or, in the case of a trajectory,
the flight path. At present there is no acceptable method to
correlate air entrainment between the model and the prototype.

B.4.4 Simulation of Turbomachinery

The sea chests were the terminal components of the model
proper, therefore, neither the prototype turbomachinery nor a
model scale relationship for this type of turbomachinery was
established. Instead, the properly-scaled discharge quantities
were used to simulate prototype turbomachinery discharges.
Therefore, the model should be considered as representative
only within the confines of the terminal sections of turbo-
machinery structures.

B.4.5 Limitations of the Sea-Chest Model

Within the scope of model interpretation and limitations,
the sea-chest model proper is only a partial model taken out

of context from a total functional system. It is thus some-
what limited in its predictive applicability.

B.5 MODEL TESTS AND RESULTS

B.5.1 Jet Impinging on a Solid Boundary

B.5.1.1 Jet Regions

Three distinct regions of flow can be recognized on a
circular jet impinging normally on a plate. The flow at the
immediate area surrounding the jet opening tends to discharge
freely, as it is not influenced by bottom boundary effects.
The flow characteristics in this region are therefore desig-
nated as "free jet".

Beyond the free-jet region the jet undergoes considerable
deflection. Close to the boundary, the flow becomes almost
parallel to the plane wall. The flow characteristics in
the vicinity of the plane-impact zone are therefore designated
as the "impingement" region and the "wall jet" region.
Figure B-1 illustrates a jet impinging on a solid boundary.

B.5.1.2 SG Discharge Velocity Measurements

As mentioned in Section B.1.5, the velocity distribution
of the SG discharge was recorded using an electromagnetic flow
meter. The observed conditions included three underkeel
clearances and three pumping rates.

Figure B-2 shows the SG discharge velocity distributions.

Service Generator Discharge Sea Chest

Free Jet Region I

Impingement Region II

Wall Jet Region III
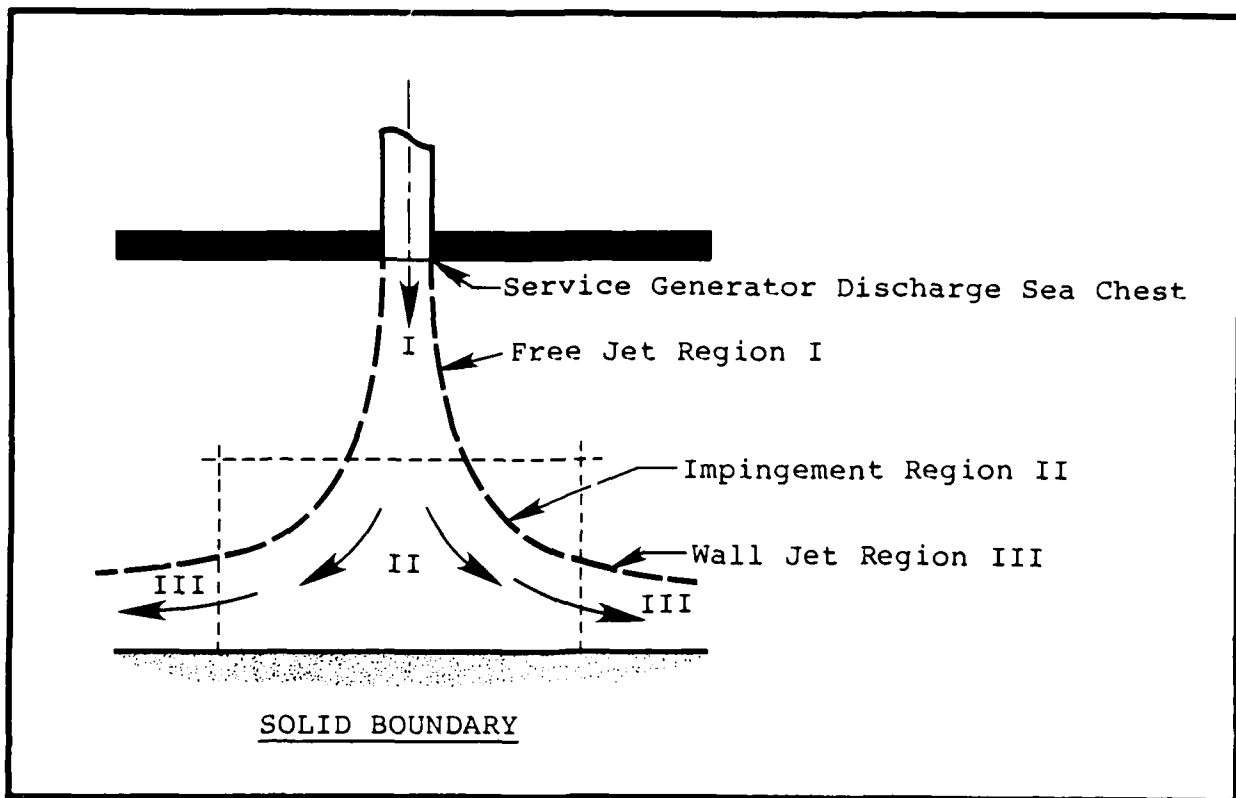
SOLID BOUNDARY

Figure B-1

Jet Impinging on a Solid Boundary

SERVICE GENERATOR DISCHARGE OPENING

Q = 5890 gpm   Velocity measurements are the
maximum recording for each
measured plane.
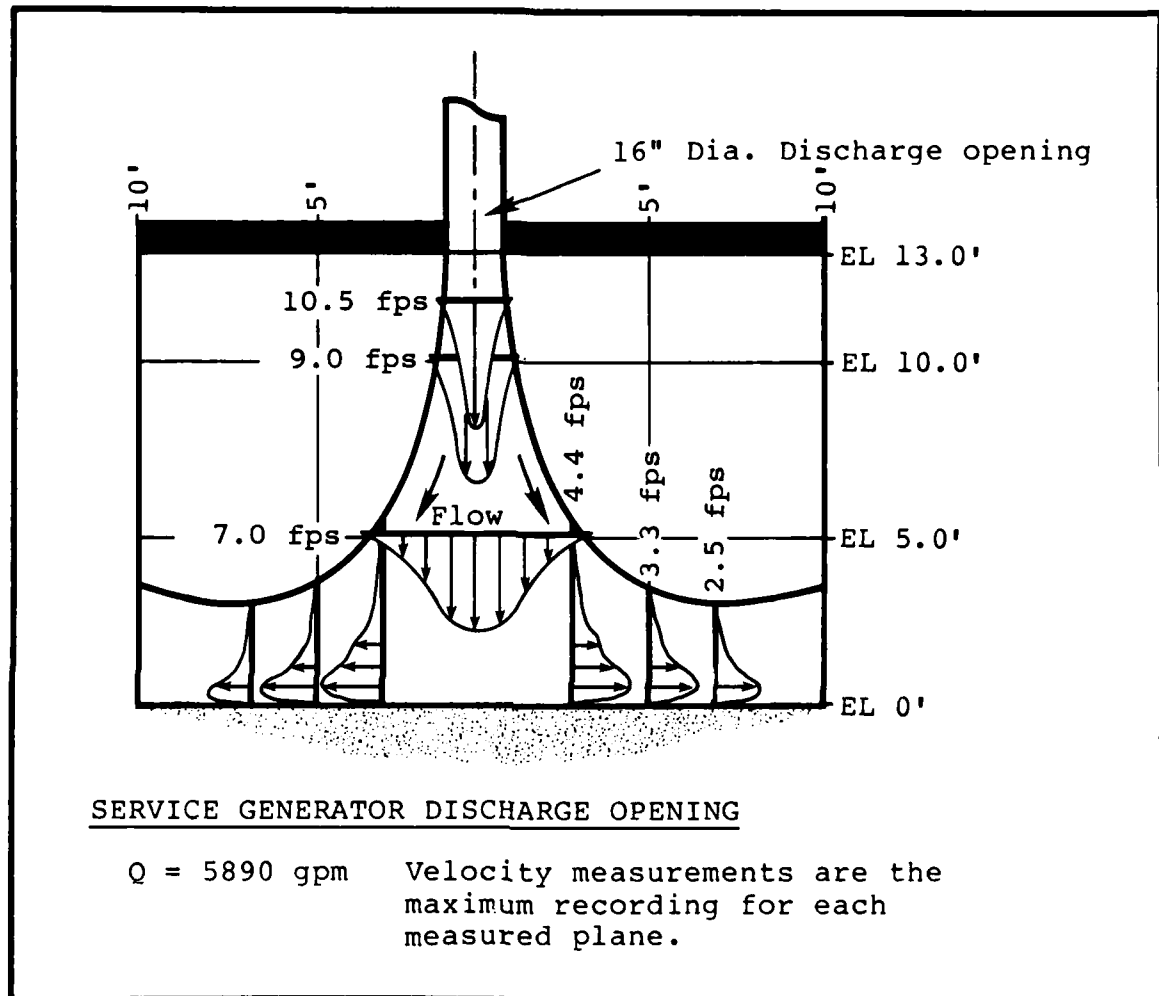
Figure B-2

SG Discharge Velocity Distributions

Table B-4 is an example of the velocity data obtained from
the observations.

TABLE B-4

Sample Circular Jet Velocity Data

Underkeel Clearance	$(V_n)_{5-ft}/V_o$ Ratio of normal velocity measured at EL. 5 ft to the maximum exit velocity		
	Q = 5890 gpm V_o = 10.5 fps	Q = 4800 gpm V_o = 9.5 fps	Q = 2100 gpm V_o = 4.5 fps
5 ft	0.9 - 0.95	0.9 - 0.95	0.9 - 0.95
13 ft	0.7 - 0.75	0.65	0.55
21 ft	0.55	--	--

The measurements from this study correlated with the available data of other experiments in terms of normal velocity V_n, radial velocity V_r, and bottom pressure Δp. Excellent correlations were found to exist between HRS findings and the data of other investigators.

The key variables of a jet include: the diameter of the jet nozzle D, the exit velocity V_o, the normal velocity V_n, the radial velocity V_r, the bottom pressure differential Δp, and the bottom shear stress τ.

B.5.1.3 Main Circulating System Discharge Sea-Chest Velocity Measurements

The main circulating system discharge sea chest has a circular-to-elliptical transitional cross section much like a boot. The exit velocity therefore has a skewed distribution in the direction of the stern as shown in Figure B-3.

MAIN CIRCULATING DISCHARGE OPENING

Q = 25,000 gpm   Velocity measurements
                  are the maximum re-
                  cording for each
                  measured plane.
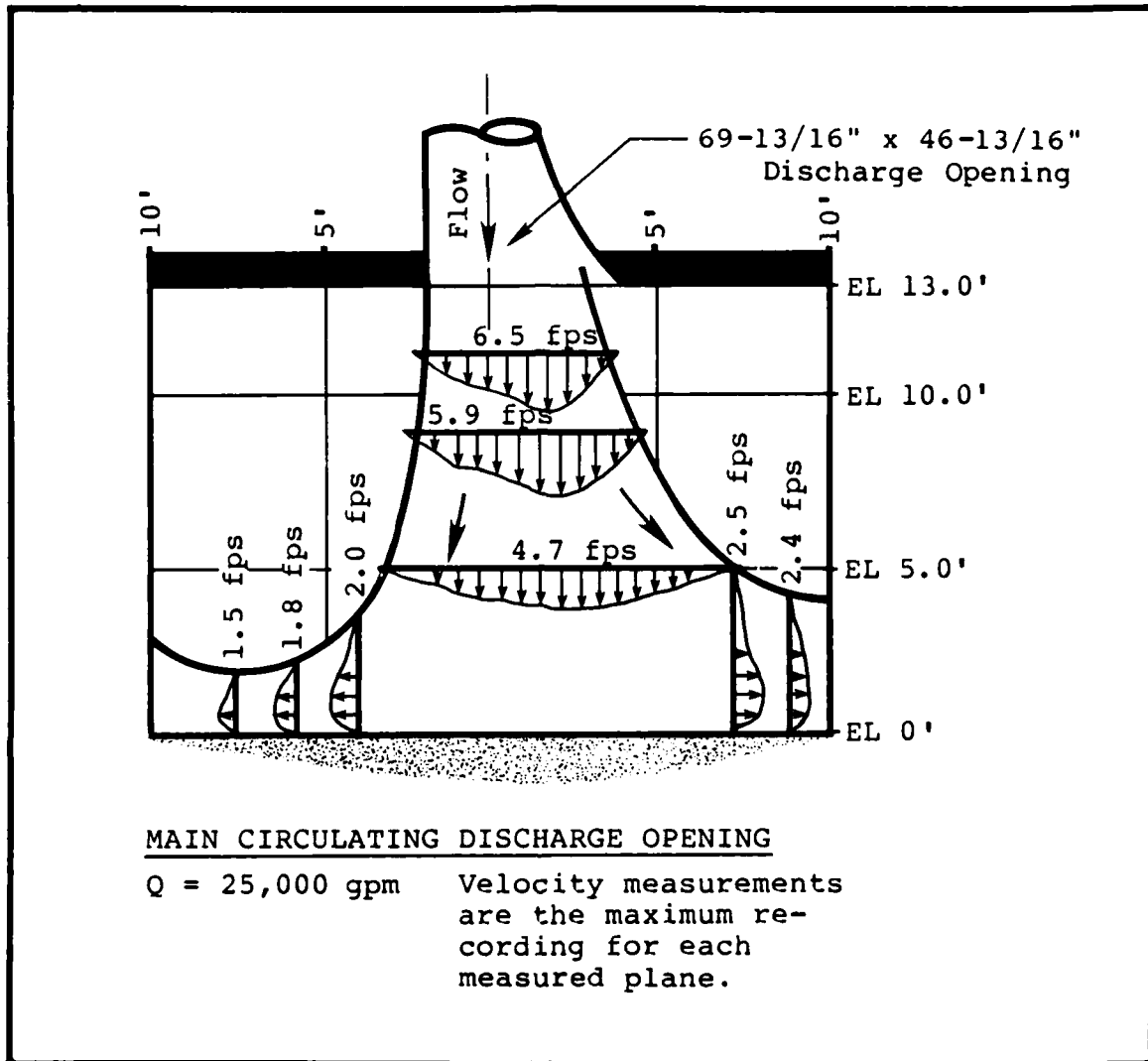
Figure B-3

Main Circulating System Discharge Sea Chest
Velocity Distributions

B.5.2 Jet Impinging on a Movable Boundary

B.5.2.1 Jet Regions

The jet regions for the movable boundary can be divided
into three regions: the free jet region, the impingement

region, and the boundary jet region. The jet impinging on a movable boundary is a dynamic process. It digs down to the bottom and forms a perpetuated eddy pattern, scouring the bottom materials. Figure B-4 illustrates the concept of a jet impinging on a movable boundary.

Service Generator Discharge Sea Chest

Free Jet Region I

Impingement Region II

Boundary Jet Region III
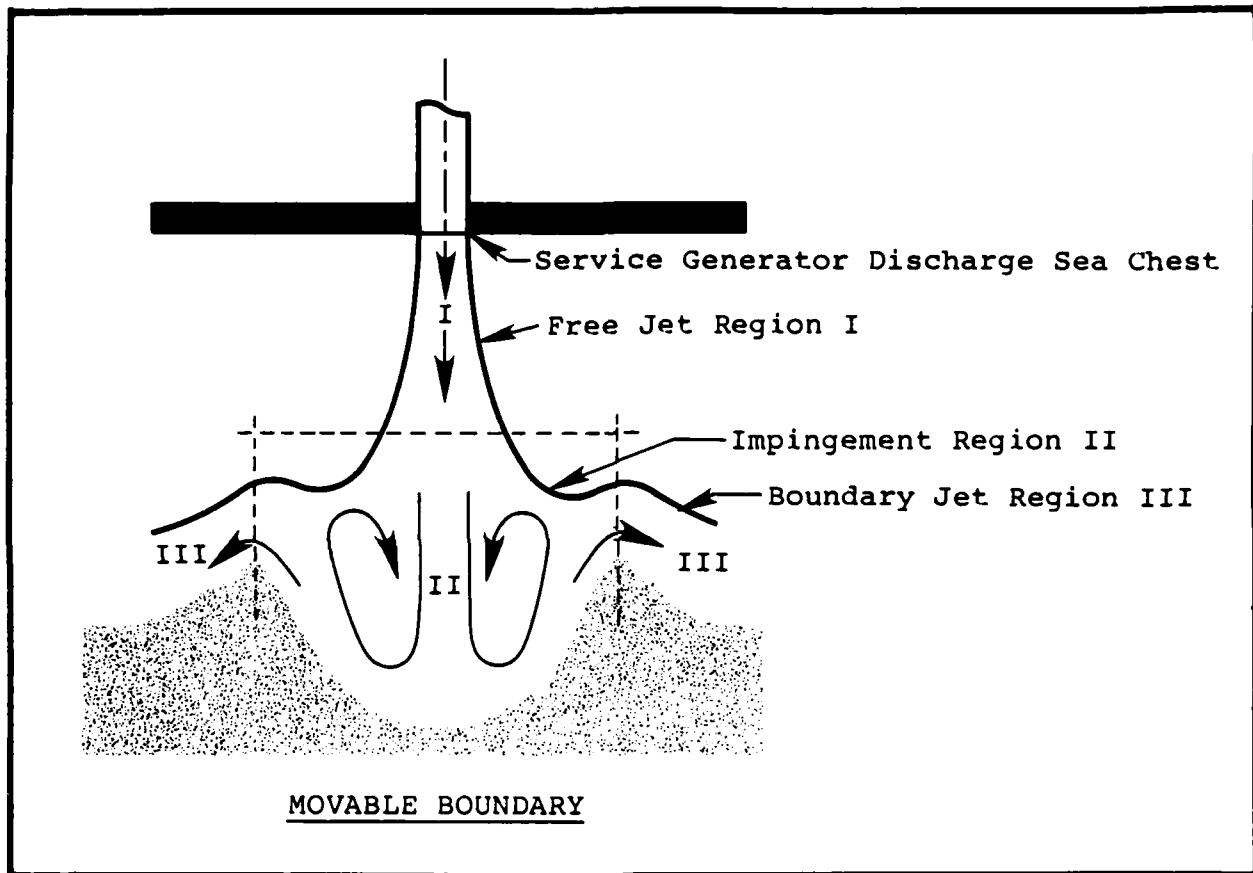
MOVABLE BOUNDARY

Figure B-4

Jet Impinging on a Movable Boundary

B.5.2.2 **SG Discharge Velocity Measurements**

The velocity distribution of the SG discharge jet impinging on a movable bottom was recorded. The model materials included sand (to simulate sand) and walnut shells (to simulate mud). The jet velocity distributions on sand and mud bottoms are presented in Figures B-5 and B-6, respectively.
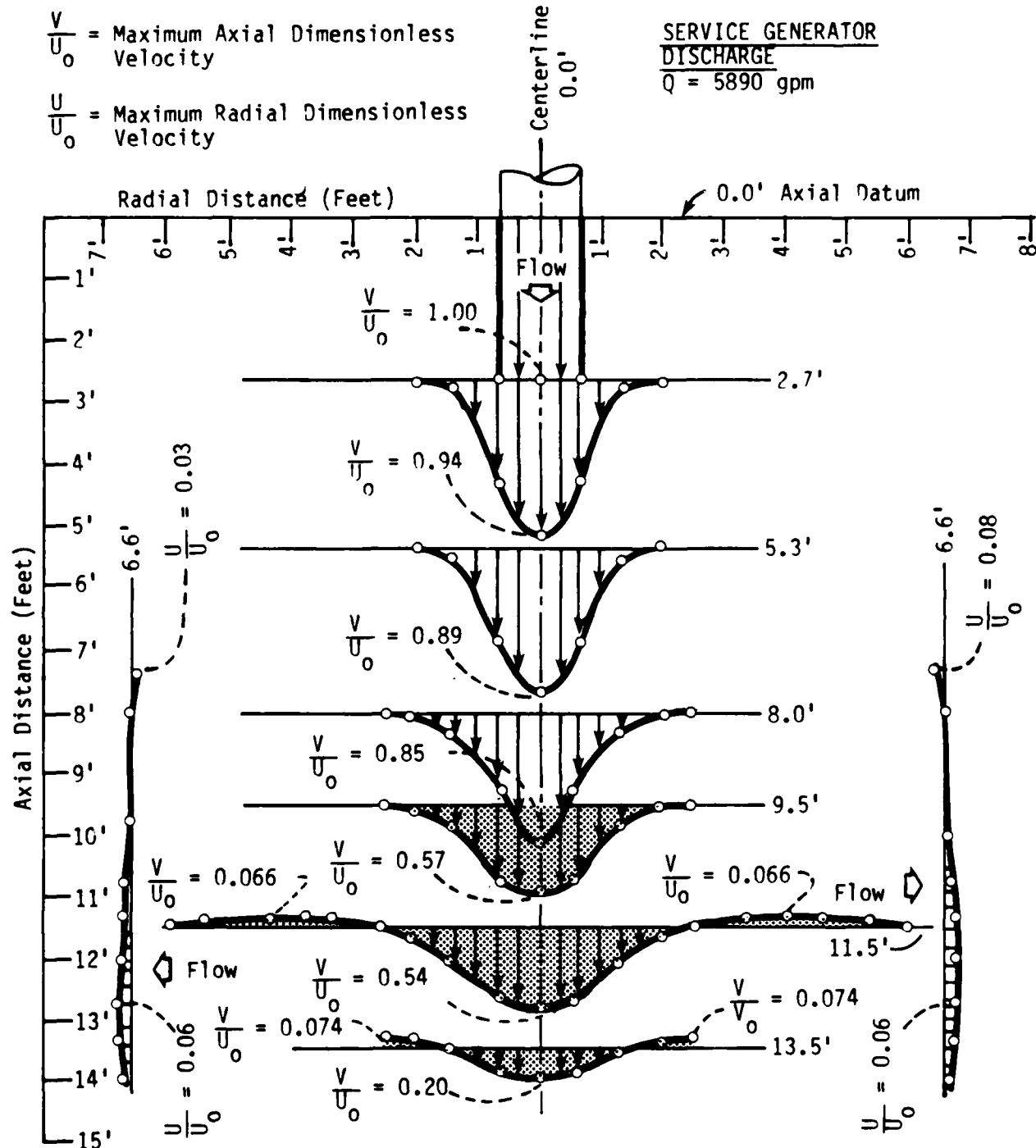
Figure B-5
Flow Field on Movable Boundary (Mud)
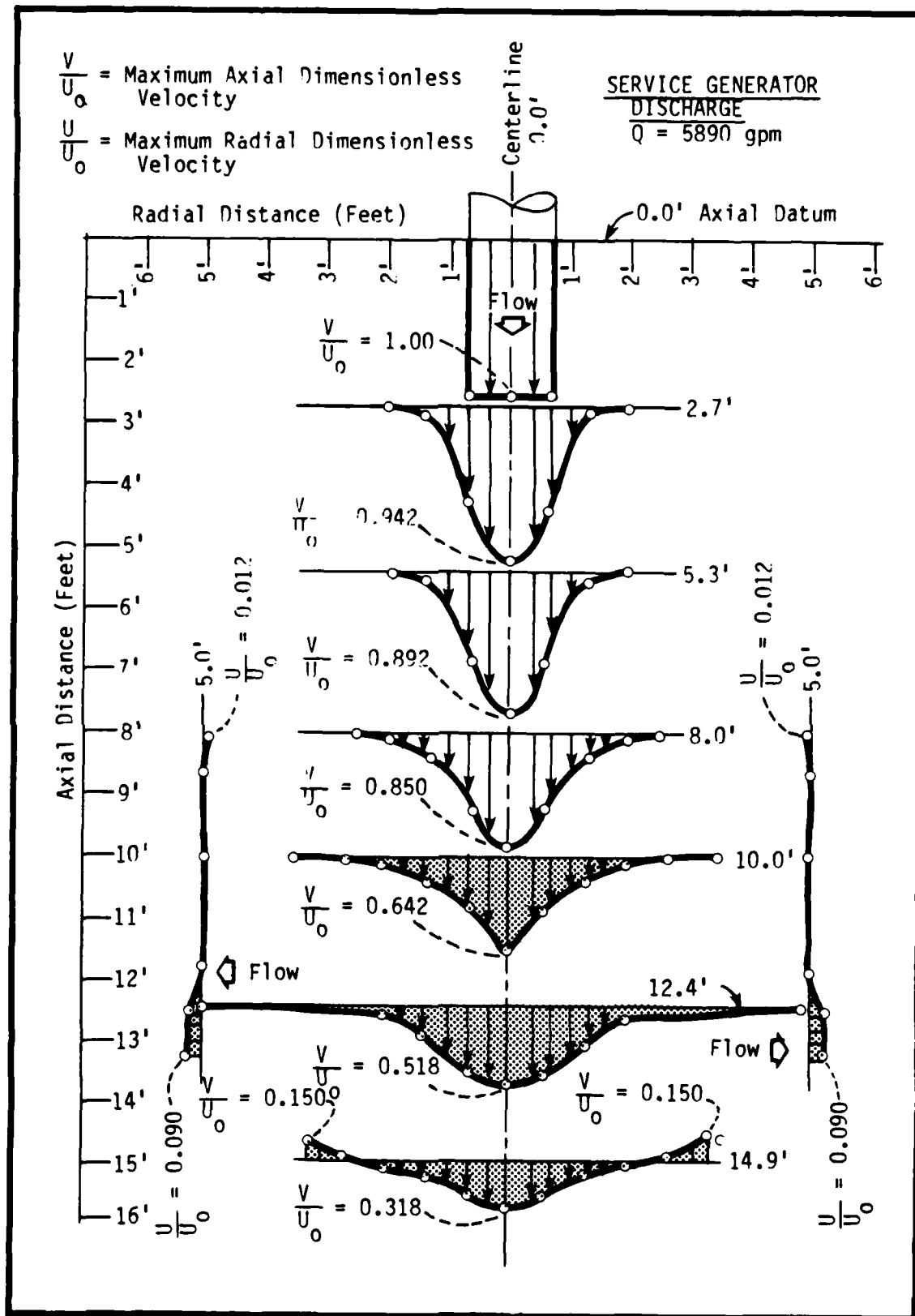
Figure B-6

Flow Field of Jet on Movable Boundary (Sand)

B.5.2.4 Scouring Mechanisms

From the jet on movable bottom tests, the following two
types of scouring mechanisms were hypothesized:

Noncohesive Material (sand): the flow impinged onto the
bottom layer, eroded the material, and created a scour hole in
the stagnation region. The movement of the particles began
when the bottom shear exceeded the critical shear. Away from
the stagnation region jet flow characteristics were found, and
the jet velocity decreased its strength in the radial direc-
tion. This dispersing led to deposition along the inner
flanks of the scour hole -- reaching a dynamic equilibrium
condition following an adequate period of time.

Cohesive Material (mud): the flow dug to the bottom and
resulted in circulatory eddy patterns. Above the scour hole
the boundary of the hole was bigger and deeper than the non-
cohesive material hole. In both cases bottom material was
moved upward and carried by the current drifting under the
ship, which increased the chance of sea-chest clogging.

The resulting scour holes for sand bed (to simulate sand)
and walnut shell bed (to simulate mud) are shown in Figure
B-7.
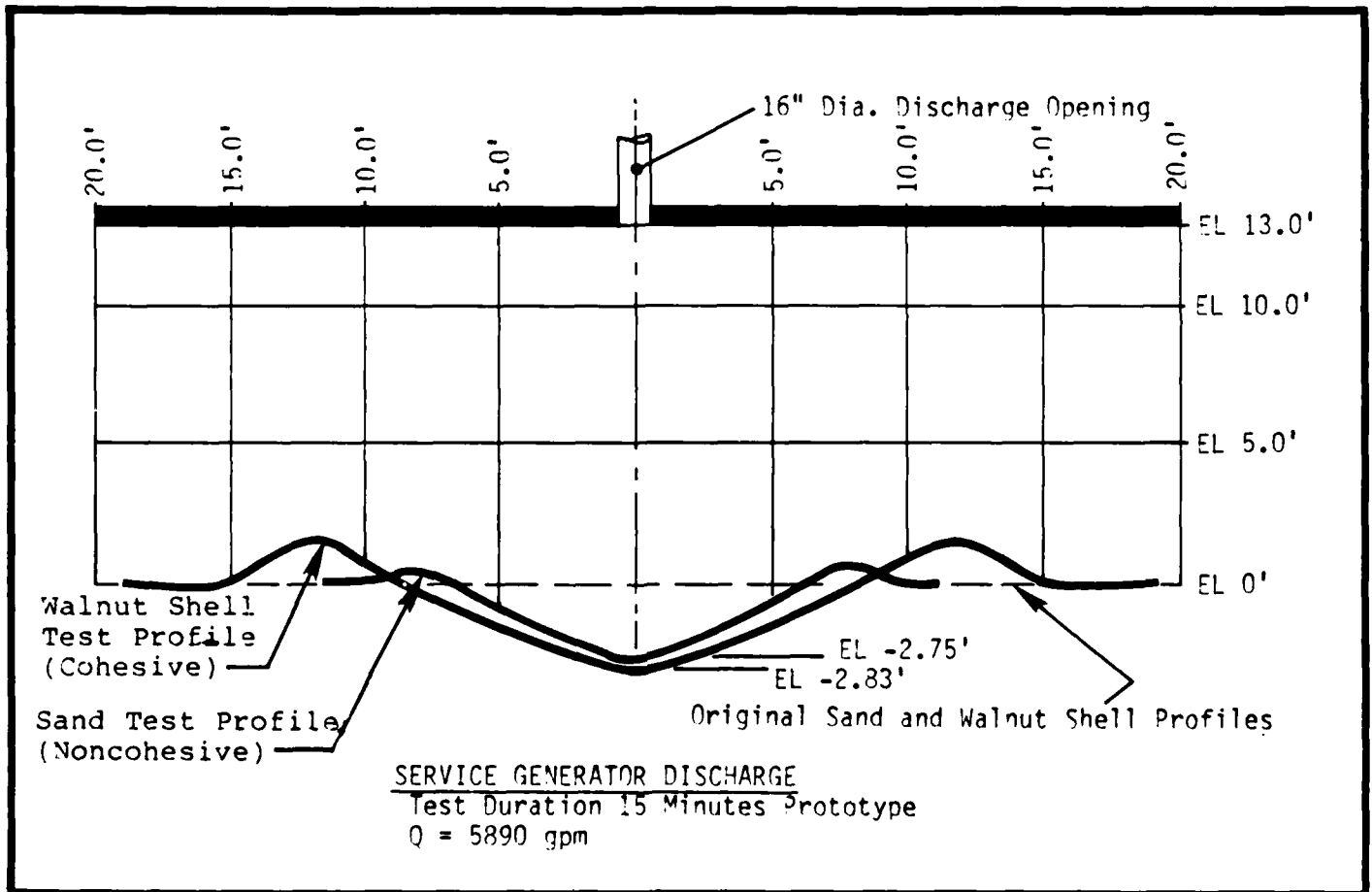
Figure B-7

Composite of Physical Model Scour Study

Appendix C,
Development of the Numerical Model

APPENDIX C
DEVELOPMENT OF THE NUMERICAL MODEL

C.1 THE ALGORITHM OF JET SIMULATION

The impingement of a jet on a flat or movable bottom has been observed by many investigators in the last two decades. [22] [24] [26] [29] The flow field of this problem has been defined in three regions: the free jet, impingement, and wall jet regions. Since laboratory data are available concerning jet impingement on a solid boundary, the present effort concerns the definition of a general equation for the problem based on the laboratory data, and the development of a numerical model to calculate the flow field under the impingement of a jet.

C.1.1 Free Jet Region

In the free jet region the flow characteristics are identical to those of the free jet. A dimensionless form of the axial velocity for a jet with diameter of the nozzle D may be obtained as follows:

$$\frac{V}{U_c} = e^{-0.0693\eta^2} \qquad \text{for } r \geq r_1 \qquad (1)$$

$$\frac{v}{U_c} = 1 \qquad \text{for } r < r_1 \qquad (2)$$

where $\eta = \dfrac{r - r_1}{b}$ and U_c is the axial velocity along the center-line, r is the radial distance from the center to the point of interest, and r_1 is the center core radius in the radial direction which can be expressed as:

$$r_1 = 0.39D - 0.065\ x \qquad \text{for } x \leq 6D \qquad (3)$$

$$r_1 = 0 \qquad \text{for } x > 6D \qquad (4)$$

where x is the axial distance from nozzle to the point of interest, and b = 0.115D + 0.087x.

C.1.2 Impingement Region

In the impingement region, the flow starts to change direction from the free jet to the wall jet. It was found that the axial velocity distributions along the radial direction for any given depth have the same form as the free jet region, that is:

$$\frac{V}{U_m} = e^{-0.0693\eta^2} \tag{5}$$

where U_m is the axial velocity at r_1 and given the following definitions:

$$\frac{U_m}{U_c} = 1, \quad \text{for } H \geq 6D \tag{6}$$

$$\frac{U_m}{U_c} = 1.15, \quad \text{for } H < 6D \text{ and } H-x \leq 0.7D \tag{7}$$

$$\frac{U_m}{U_c} = 1, \quad \text{for } H < 6D \text{ and } H-x > 0.7D \tag{8}$$

H is the total depth from the nozzle to the flat bottom. If r_1 is greater than zero, then the axial velocity between the center to r_1 has the following form:

$$U = U_c + (U_m - U_c) \; \lambda^2(2-\lambda^2) \tag{9}$$

where $\lambda = \frac{r}{r_1}$.

Tani and Komatsu [26] presented the jet centerline velocity
with axial distance for three different water depths: four,
eight, and twelve times the diameter of the nozzle. The solid
line in Figure C-1 summarizes the results of their experimental
data. There is difficulty in using these data to develop a
general model for any total depth of interest, because there
is no simple general form for the results. Based on Beltaos
and Rajaratnam's study [29], a general trend for the total
depth less than 5.17 nozzle diameters is presented in Figure
C-2.

A new parameter was defined to analyze Tani and Komatsu's
results for the total water depth equal to eight and twelve
times the nozzle diameter. This parameter is U_R, the reference
velocity, and is equal to the centerline velocity at the in-
tersection of the free jet and impingement region. This point
is located at a distance of about two nozzle diameters. Figure
C-3 presents the result of the new approach, and shows the
general form for the two different total depths.

A numerical model was developed to calculate the jet center-
line velocities based on the least square fitting of Figures C-2
and C-3. If the total depth is less than six nozzle diameters,
the jet centerline velocity was based on Figure C-2. Otherwise,
it was based on Figure C-3. The numerical results for the jet
centerline velocity is compared with the laboratory data in Fi-
gure C-1, and shows that the numerical results are in reasonable
agreement with the experimental data.

C.1.3 Wall Jet Region

In the wall jet region the flow spreads out radially over
the bottom. Figure C-4 illustrates the measured velocity re-
sulting from various depths. Again, there is a general trend
for the cases of the total depth of eight or twelve nozzle
diameters. A least square fitting for these two curves pre-
sents the general form for the case of a total depth greater
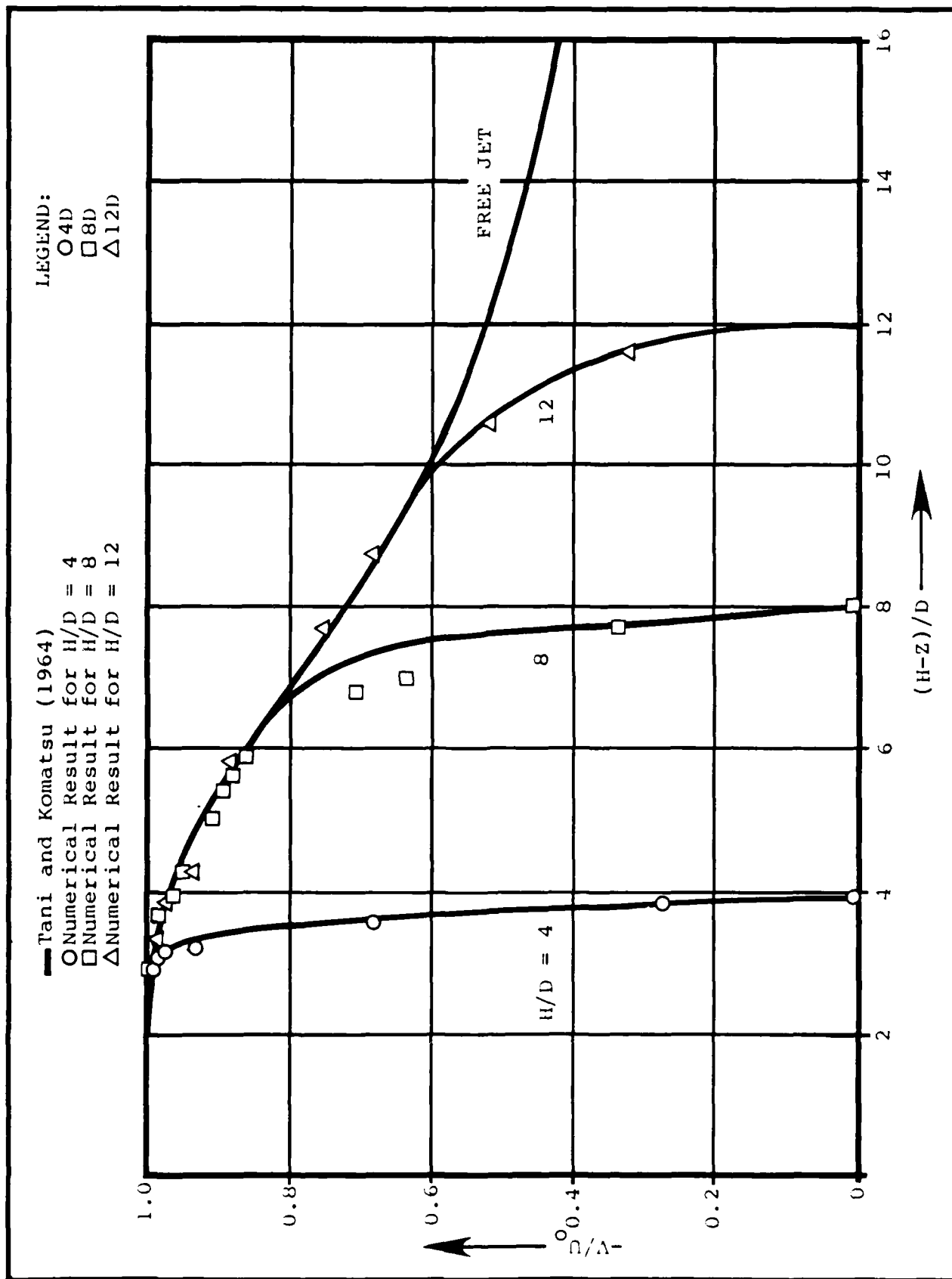
Figure C-1
Variation of Jet Centerline Velocity with Distance from Seachest Discharge
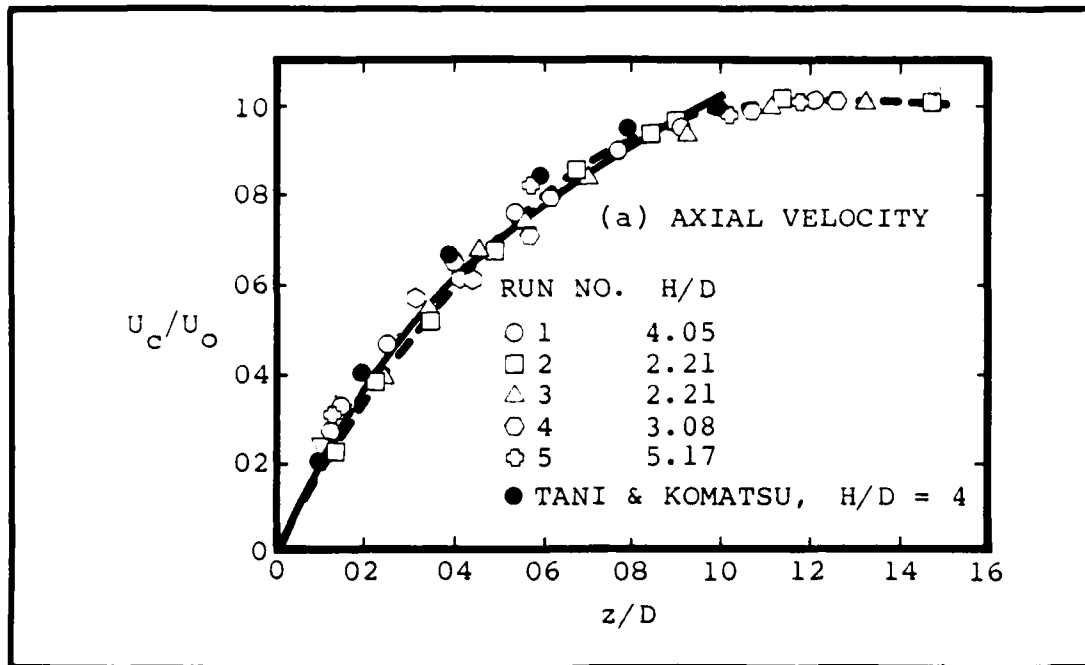
Figure C-2

Variation of Circular Jet Centerline Velocity
from the Bottom (Beltaos and Rajaratnam, 1977)

than six nozzle diameters. For the case of a total depth less
than six nozzle diameters, the calculation is based on the
four nozzle diameter measurements.

C.1.4 The Bottom Pressure and the Shear Stress

The bottom velocity distribution derived from the surface
pressure is presented in Figure C-5, and the bottom pressure
distribution is shown in Figure C-6. A comparison between the
numerical results and the laboratory data reveals reasonable
agreement.

LEGEND:
□ H/D = 8
△ H/D = 12
○ Average

$\frac{U_c}{U_R}$

Z/D
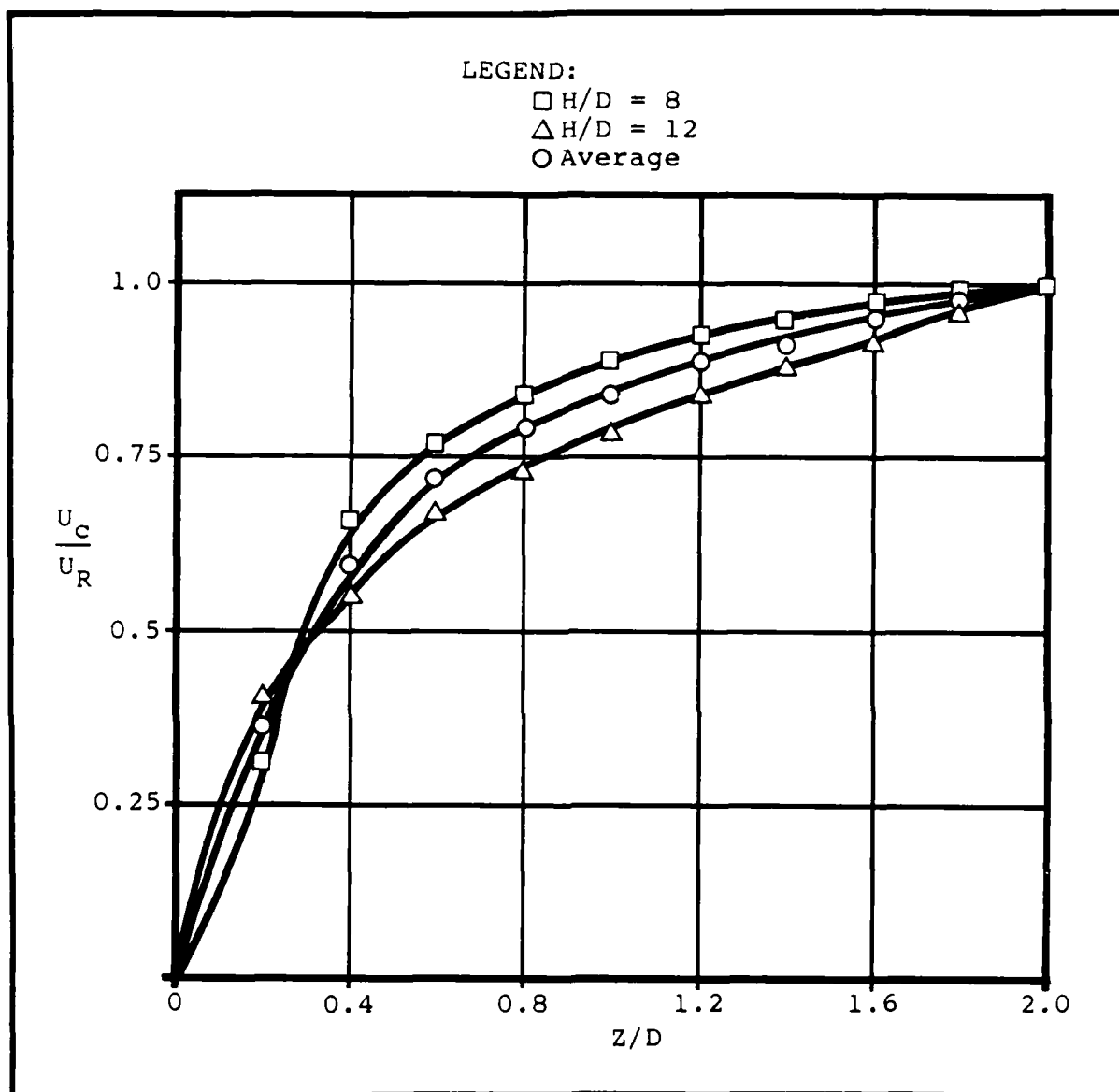
Figure C-3

Variation of Circular Jet Centerline Velocity from the Bottom
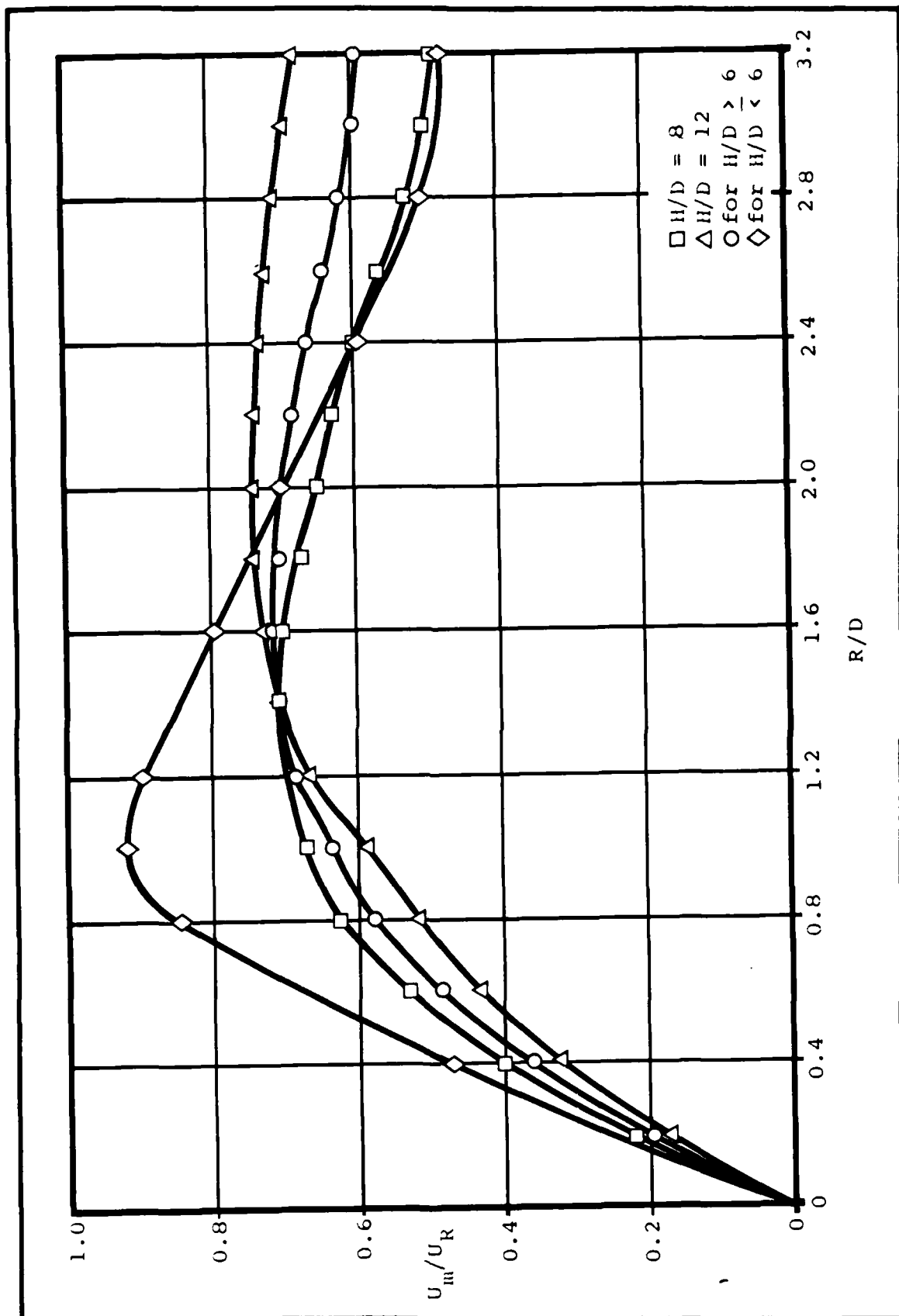
Figure C-4

Dimensionless Variation of the Radial Velocity (Peak Velocity)
with Radial Distance
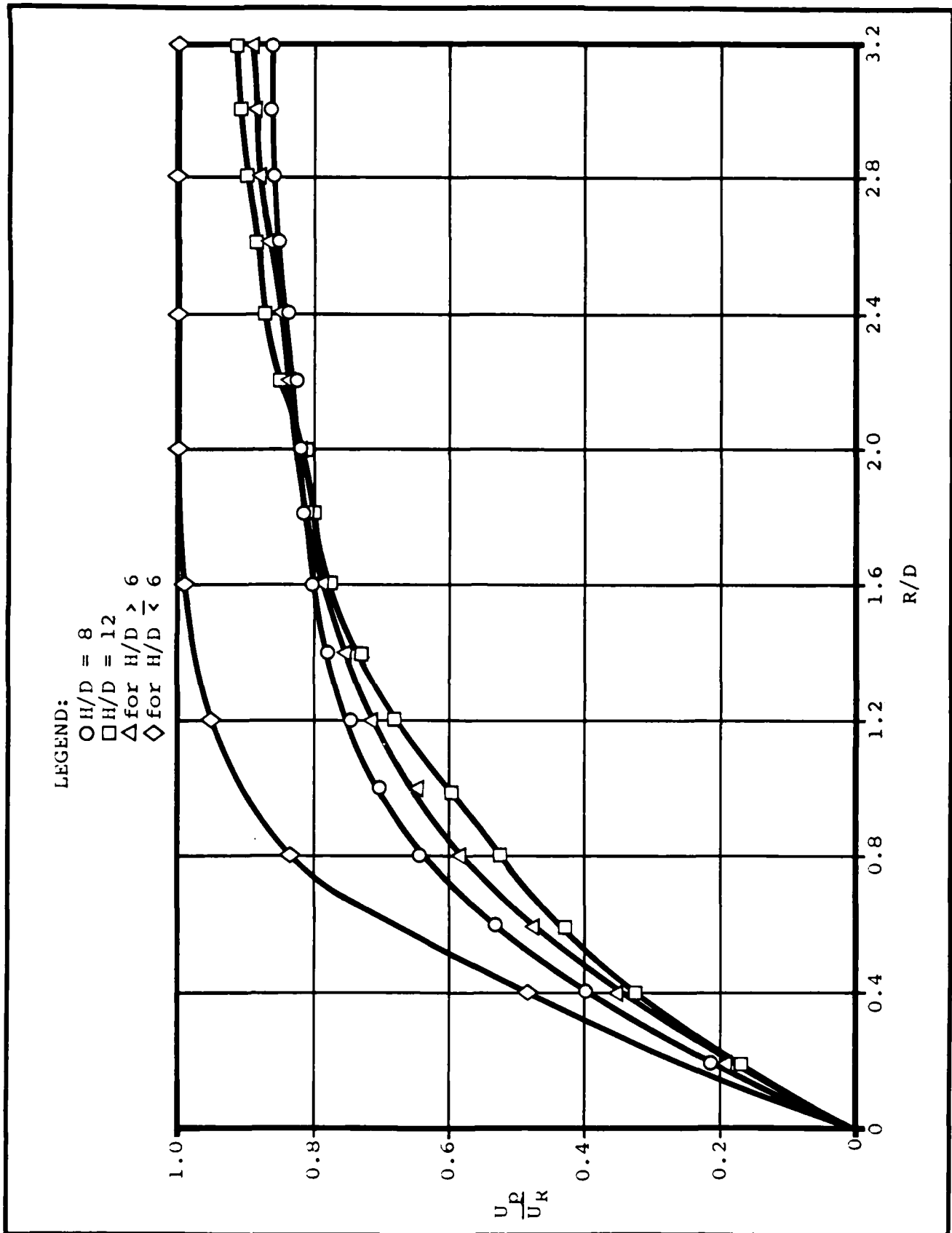
Figure C-5

Dimensionless Variation of the Radial Velocity
(Derived from Surface Pressure Distribution) with Radial Distance
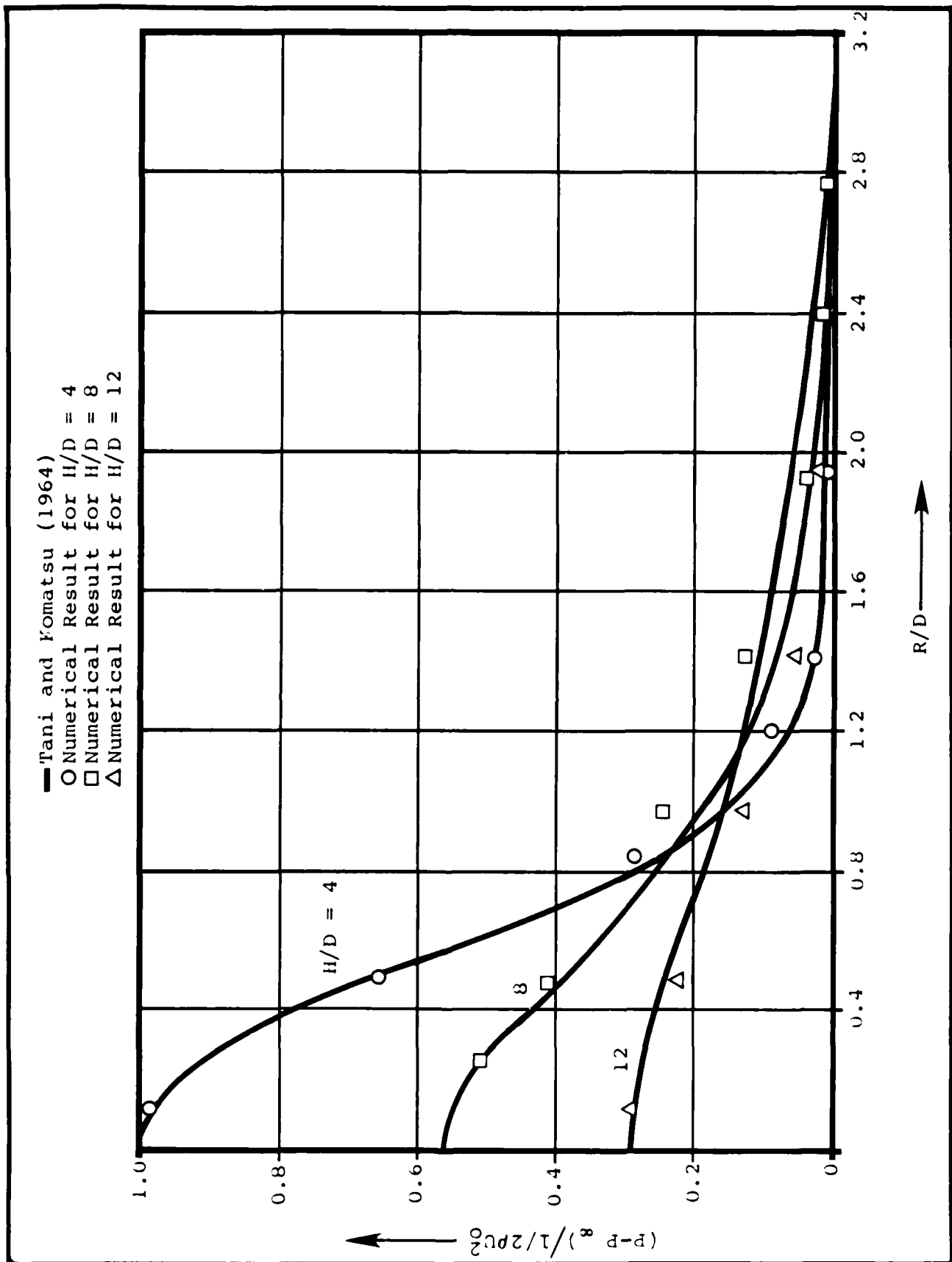
Figure C-6

Variation of Surface Pressure with Radial Distance

It was found that the shear stress can be derived from the following empirical results:

$$\tau = 1.270 \frac{\rho K}{H^2} \left(\frac{\sqrt{K}}{\nu}\right)^{-1/2} \frac{r}{H} \text{, for } \frac{r}{H} < 0.03 \qquad (10)$$

and

$$\tau = 0.3 \frac{\rho K}{H^2} \left(\frac{\sqrt{K}}{\nu}\right)^{-0.3} \left(\frac{r}{H}\right)^{-2.3} \text{, for } \frac{r}{H} > 0.3 \qquad (11)$$

where

ρ = the density of the fluid

$K = \dfrac{\pi U_o^2 d^2}{4}$

U_o = the average velocity at the jet nozzle

d = the diameter of the jet nozzle

H = the distance from the nozzle to the bottom

ν = the kinematic viscosity of the fluid

r = the radial distance from the centerline to the location of interest.

The numerical calculation for the shear stress was based on this relationship, and is shown in Figure C-7.
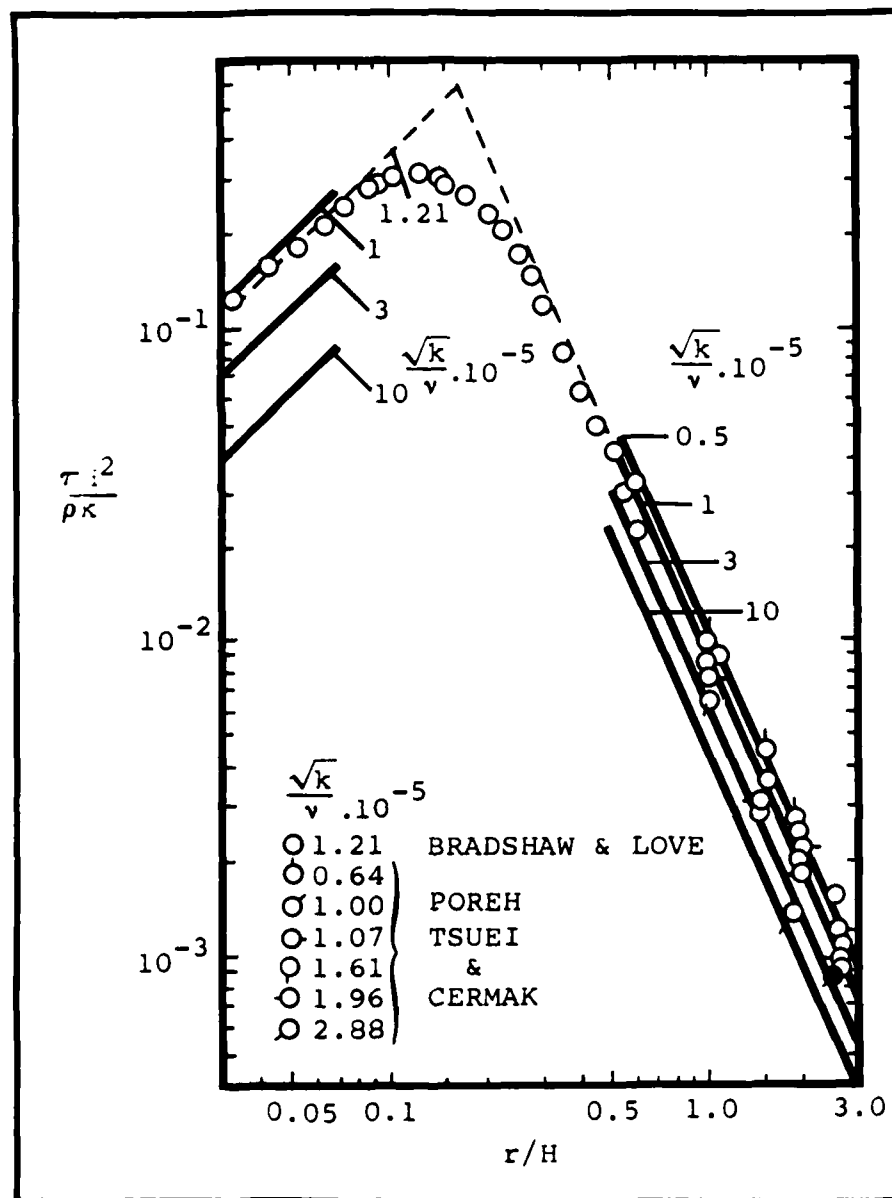
Figure C-7

Shear Stress Distribution

C.1.5 Movable Boundaries

There is little existing data on jet impingement on movable boundaries. The numerical model for the jet impingement on a movable bottom was developed in this study based on

laboratory data. The data were obtained from the tests of 5- and 13-foot underkeel clearances. The jet nozzle diameter was 16 in. Two different bottom materials were used for each depth: sand (to simulate sand), and walnut shells (to simulate mud).

C.2 THE ALGORITHM OF SINK SIMULATIONS

C.2.1 Governing Equations

In simulating the sink the flow is assumed to be inviscid, incompressible, and irrotational. The stream function, ψ, can be defined by:

$$U = \frac{1}{r} \frac{\partial \psi}{\partial z} \tag{11}$$

and

$$W = \frac{1}{r} \frac{\partial \psi}{\partial r} \tag{12}$$

where r is the radial coordinate, z is the axial coordinate, and U and W are the radial and axial components of fluid velocity, respectively. The equation of irrotationality in axisymmetric flow is:

$$\frac{\partial U}{\partial z} - \frac{\partial W}{\partial r} = 0 \tag{13}$$

Substituting Equations 11 and 12 into Equation 13 yields the following equation for the stream function:

$$\frac{\partial^2 \psi}{\partial r^2} + \frac{\partial^2 \psi}{\partial z^2} - \frac{1}{r} \frac{\partial \psi}{\partial r} = 0 \tag{14}$$

C.2.2 Boundary Conditions

The boundary conditions applied to the sink model are as follows: (1) the stream function ψ along the centerline and the surface at the bottom is a constant, and is set to zero,

(2) it is assumed that the fluid velocity U_o across the boundaries of the incoming flow is constant, therefore the stream function ψ at the sink opening is equal to $1/2 \, U_o r^2.$, (3) the stream function ψ on the free surface is constant and is equal to $1/2 \, U_o r_o^2$, where r_o is the radius of the sink opening, and (4) the downstream stream function ψ along the axial direction at $r = R$ is set equal to the stream function value at $r = R - \Delta r$, where R is the total radial distance in the calculation, and Δr is the grid increment in the radial direction.

C.2.3 Finite Difference Form

Let ψ_{ij}, U_{ij} and W_{ij} represent $\psi(r_i, z_j)$, $U(r_i, z_j)$ and $W(r_i, z_j)$, respectively. The notation (i, j) indicates the intersecting point of the axial grid line passing through r_i and the radial grid line through z_j. The increment of the radial grid is equal to Δr, and the increment of the axial grid is equal to Δz. The finite-difference approximations of the partial derivatives then becomes:

$$\frac{\partial \psi_{ij}}{\partial r} = \frac{\psi_{i+1,j} - \psi_{i-1,j}}{2\Delta r} , \tag{15}$$

$$\frac{\partial^2 \psi_{i,j}}{\partial r^2} = \frac{\psi_{i+1,j} - 2\psi_{i,j} + \psi_{i-1,j}}{(\Delta r)^2} \tag{16}$$

and

$$\frac{\partial^2 \psi_{i,j}}{\partial z^2} = \frac{\psi_{i,j+1} - 2\psi_{i,j} + \psi_{i,j-1}}{(\Delta z)^2} \tag{17}$$

Substituting Equations 15, 16, and 17 into Equation 14, one obtains:

$$\psi_{i,j} = \frac{1}{\left(\frac{2}{\Delta r^2} + \frac{2}{\Delta z^2}\right)} \left(\frac{\psi_{i+1,j} + \psi_{i-1,j}}{\Delta r^2} + \frac{\psi_{i,j+1} + \psi_{i,j-1}}{\Delta z^2} \right.$$
$$\left. - \frac{1}{r_{i,j}} \frac{\psi_{i+1,j} - \psi_{i-1,j}}{2\Delta r} \right) \tag{18}$$

When Equation 18 is applied to all the interior points, there are $(m-2)(n-2)$ algebraic equations that automatically include the boundary conditions, where m and n are the total number of increments in the axial and radial directions of the rectangular region. Theoretically, it is possible to solve these equations for values of ψ at the interior grid points; but this direct procedure is tedious and time-consuming, especially when the number of grid points is large. The present numerical model uses the successive over-relaxation (S.O.R.) method to solve the problem. This method used the following iteration scheme for a rectangular domain instead of Equation 18:

$$\psi_{i,j}^{(k+1)} = (1-w)\psi_{i,j}^{k} + \frac{w}{(\frac{2}{\Delta r^2} + \frac{2}{\Delta z^2})} \left(\frac{\psi_{i+1,j} + \psi_{i\,1,j}}{\Delta r^2} \right.$$

$$\left. + \frac{\psi_{i,j+1} + \psi_{i,j-1}}{\Delta z^2} - \frac{1}{r_{ij}} \frac{\psi_{i+1,j} - \psi_{i-1,j}}{2\Delta r} \right) \quad (19)$$

where k represents the kth iteration.

The values of ψ are computed for the next iteration by executing Equation 19 at every interior point based on the values of ψ at the current iteration. The sequence of computation starts from the upper left-most interior point, proceeds downward until reaching the bottom, and then moves to the top of the next axial line on the right.

This process is repeated until the next value of ψ at the last interior point at the lower right corner has been obtained. In this model, the values of ψ are first estimated at all interior points, in addition to those prescribed at the boundary. These values are:

$$\psi_{i,j}^{o} = \frac{1}{4} U_o r_o^2 \quad (20)$$

The value of w in Equation 19 is a constant, and

$$w = \frac{8 - 4\sqrt{4-a^2}}{a^2} \tag{21}$$

where

$$a = \cos(\frac{\pi}{m}) + \cos(\frac{\pi}{n}).$$

The error of the stream function values is defined as:

$$\xi = \sqrt{\sum_{i=2}^{m-1} \sum_{j=2}^{n-1} \left(\frac{\psi_{i,j}^{k+1} - \psi_{i,j}^{k}}{\psi_{i,j}^{k}}\right)^2 \cdot \frac{1}{(m-2)(n-2)}} \tag{22}$$

In the present model if the value of ξ is less than 0.01, the iteration will be stopped with the final value of the stream function given. The central finite-difference approximations for the axial and radial velocities are:

$$U_{ij} = \frac{1}{r_{ij}} \frac{\psi_{i,j+1} - \psi_{i,j-1}}{2\Delta z} \tag{23}$$

and

$$W_{ij} = \frac{1}{r_{ij}} \frac{\psi_{i+1,j} - \psi_{i-1,j}}{2\Delta r} \tag{24}$$

On the boundary, the forward or backward finite-difference approximations may be used for the axial and radial velocities. They are:

$$U_{ij} = \frac{1}{r_{ij}} \frac{\psi_{i,j+1} - \psi_{ij}}{\Delta z} \tag{25}$$

and

$$W_{ij} = \frac{1}{r_{ij}} \frac{\psi_{i+1,j} - \psi_{ij}}{\Delta r} \tag{26}$$

When i equals one, then r_{ij} is zero. The axial and radial velocities were then assumed to be equal the value at i equals two:

$$U_{1j} = U_{2j} \tag{27}$$

and

$$W_{1j} = W_{2j} \tag{28}$$

After the finite-difference form of the sink mode was constructed, the development of the numerical model for the sink problem proceeded.

Appendix D,
Key Words and Definition

APPENDIX D
KEY WORDS AND DEFINITIONS

Aircraft Carrier	A ship equipped with a takeoff and landing deck, and designed to serve as a base for aircraft operations.
Berthing Area	The port or harbor slips where vessels are anchored.
Critical Shear Stress	A threshold value of the shear stress, above which the particle starts to move from its resting position.
Diffuser	A structure which serves the function of spreading fluid flow through various arrangements to reduce the flow concentration or velocity intensity.
Discharge	Amount of fluid flow released from a storage or a fluid impelling system.
Draft	The vertical distance from the top of the keel plate of a vessel to the load waterline.
Fall Velocity	The average terminal settling velocity of a single particle in distilled water.
Flocculating	The collection or uniting of suspended sediment to form a mass.
fps	feet-per-second
gpm	gallons-per-minute

Keel Clearance	The clear space between a vessel's keel plate and the sea bottom.
Light off	The operation involved in preparation of a vessel's departure from a harbor.
Main Circulating Cooling System	A circulating water system that provides for cooling of a vessel's main circulating system.
Marine Organism	Biological species which exist in the marine environment.
MLW	Mean low water
Movable Boundary	A boundary that can be deformed by external pressures.
Sea Chest	A pipe between a ship's side and a flow control device for transporting water.
Sea Floor	The bottom of the ocean.
Service Generator Cooling System	A circulating water system that provides for cooling of a vessel's service generator.
SG	See Service Generator Cooling System.
Solid Boundary	A boundary that cannot be deformed by pressure force.
Solidification	A procedure which hardens a material into a solid state.

Appendix E,
Annotated Bibliography

APPENDIX E

ANNOTATED BIBLIOGRAPHY

[1]   Jones, S. H., Cdr., USN., <u>CVN 68 Class Condenser Fouling</u>.
        U.S. Navy, April, 1980, 9 figs.
              The condenser fouling problems of an aircraft
        carrier are described.

[2]   Brehmer, M. L., Nichols, M. M., and Calder, D. R. <u>Study</u>
        <u>and Control of Marine Fouling Organisms, Naval Base,</u>
        <u>Norfolk, Virginia</u>. Virginia Institute of Marine
        Science, Gloucester Point, Virginia, February, 1967,
        4 figs., 8 tables.
              The authors investigate the biology and distri-
        bution of marine organism, including current velocity
        and sediment characteristics, and identify the silver
        hydroid and the fleshy bryozoan as being primarily
        responsible for condenser fouling resulting in vessel
        operational difficulties.

[3]   Shidler, J. K. and MacIntyre, W. G., "Hydrographic Data
        Collection for 'Operation James River - 1964'."
        <u>Data Report No. 5</u>. Virginia Institute of Marine
        Science, Gloucester Point, Virginia, October, 1967,
        3 figs., 5 tables.
              This report presents collected hydrographic
        data on the James River estuary for verification of
        an hydraulic model and for calculation of circulation
        dynamics in the James River.

[4]   Hoffman, J. F., "Investigation into Deep-Draft Vessel
        Berthing Problems at Selected U. S. Naval Facilities."
        <u>Report No. 4914-801</u>. E G & G Washington Analytical
        Services Center, Inc., Rockville, Maryland, October,
        1980, 21 figs., 16 tables.
              This report provides a detailed investigation
        of shoaling and addresses sediment control problems,
        such as retardation of deposition of sediments or
        flushing of resuspended sediments, in the pier slips
        and associated waterways of six deep-draft harbors
        used by the U. S. Navy. Information on marine or-
        ganism fouling at Norfolk Naval Station is also pre-
        sented.

[5]   Nichols, M. M., "Sediments of the James River Estuary,
        Virginia." Memoir 133. The Geological Society of
        America, Inc., New York, 1972, pp. 169-212, 28 figs.,
        1 table.
            This article reports the distribution, composi-
        tion, chemistry and characteristics of the sediments
        in the James River Estuary, Virginia.

[6]   Van Dorn, W. G., et al., "The Evaluation of Sediment
        Management Procedures Phase II Final Report 1975-
        1976." SIO Reference 77-10. Scripps Institution of
        Oceanography, La Jolla, California, August, 1977,
        42 figs., 4 tables.
            This report summarizes a study of a number of
        sedimentation removal techniques and recommends the
        resuspension of sediments by submerged hydraulic jet
        method. Physical model of a berthing complex using
        a phased array of ten radial jets was built and
        tested. The report also includes the current and
        (mud) sediment information near Pier 12 area in Nor-
        folk Harbor.

[7]   Environmental Impact Assessment: Norfolk Naval Base
        Complex Long-Range Maintenance Dredging Program.
        Arthur D. Little, Inc., Massachusetts, February,
        1976, 22 figs., 19 tables.
            This report provides the environmental impact
        assessment on the maintenance dredging for the Nor-
        folk Naval Base Complex. Conclusions from the study
        indicate that the maintenance dredging will redis-
        tribute polluted sediments and adversely affect es-
        tuaraine biota.

[8]   U. S. Army Corps of Engineers. Norfolk Harbor and Chan-
        nels, Virginia, Deepening and Disposal, Feasibility
        Report and Appendices. U. S. Army Corps of Engi-
        neers, Norfolk District, July, 1980.
            This report addresses and evaluates possible
        solutions for two problems: first, the existing
        disposal needs facing Norfolk Harbor and adjacent
        waters, and second, the need for improved and ex-
        panded channels and anchorages.

[9]   Fang, C. S., et. al., "Physical and Geological Studies of
       the Proposed Bridge-Tunnel Crossing of Hampton Roads
       near Craney Island." Special Report in Applied Ma-
       rine Science and Ocean Engineering No. 24. Virginia
       Institute of Marine Science, Gloucester Point, Vir-
       ginia, August, 1972, 10 figs., 20 tables.
           This report is divided into four parts. Part
       1 presents the hydraulic model study of the effects
       of a proposed river crossing structure on the tides,
       currents and distribution of sea salts and sediments
       at Hampton Roads near Craney Island. Part 2 investi-
       gates the impact from the proposed bridge-tunnel
       model study on the shoreline, Hampton Flats and New-
       port News Point area. Part 3 reports the field survey
       of currents in the Newport News area using the drogued
       buoys. Part 4 presents the hydraulic model test re-
       sults of tidal currents.

[10] Chen, H. S., "A Storm Surge Model Study Volume II A Fi-
       nite Element Storm Surge Analysis and its Application
       to a Bay-Ocean System." Special Report No. 189 in
       Applied Science and Ocean Engineering. Virginia In-
       stitute of Marine Science, Gloucester Point, Virginia,
       September, 1978, 86 figs., 9 tables.
           This report describes the development of a two-
       dimensional storm surge model for calculation of
       water elevation and circulation subject to the ef-
       fect of a hurricane, in the James River estuary and
       Chesapeake Bay area. The storm surge model was
       first used to simulate tides in the Chesapeake Bay
       until tide simulation was satisfactory, then a storm
       surge hindcast was conducted in the Chesapeake Bay
       and its Virginia Atlantic nearshore area.

[11] Jacobson, J. P. and Fang, C. S., "Flood Wave-Tide Wave
       Interaction on the James River During the Agnes
       Flood." Studies of Certain Impacts of Tropical
       Storm Agnes on the Chesapeake Bay and its Tributaries.
       Virginia Institute of Marine Science, Gloucester
       Point, Virginia, August, 1974, pp. 119-130.
           This article summarizes the tidal height data
       and current measurement at the James River during
       the Agnes Flood. The authors concluded that the
       flood did significantly affect the water level in
       the upper portion of the tidal James. However, in
       the lower portion of the James River, no discernible
       rise was evident due to the passage of the flood
       wave.

[12] Namias, J. and Dunn, C. R., "The Weather and Circulation
      of August, 1955." Monthly Weather Review. Vol. 83,
      No. 8, August, 1955, pp. 163-170, 8 figs., 1 table.
          This article presents the characteristic atmo-
      spheric circulation during August 1955. The weather
      information over the Northeast United States, where
      flood-producing rains associated with hurricanes
      Connie and Diane, are also reported.

[13] Chapman, W. T., Jr., and Sloan, Y. T., "The Paths of
      Hurricanes Connie and Diane." Monthly Weather Re-
      view. Vol. 83, No. 8, August, 1955, pp. 171-180,
      13 figs.
          This article deals with two hurricanes, Connie
      and Diane, which crossed the North Carolina Coast
      near the middle of August 1955 and inflicted great
      damage over a large area of the eastern seaboard.
      The tracks and surface maps of these hurricanes are
      reported.

[14] Ruzecki, E. P. and Ayres, R., "Suspended Sediments Near
      Pier 12, Norfolk Navy Base, on 26 June and 15 Septem-
      ber, 1973." Data Report No. 11. Virginia Institute
      of Marine Science, Gloucester Point, Virginia, October,
      1974, 2 figs., 30 tables.
          This report summarizes the results of two sus-
      pended sediment studies near Norfolk Naval Base Pier
      12 area. Salinity, temperature and current velocity
      information are also provided in conjunction with
      suspended sediment samples at five stations.

[15] Neilson, B. and Boule, M. Oceanographic, Water Quality,
      and Modeling Studies for the Outfall from a Proposed
      Nansemond Waste Water Treatment Plant. Vol. 2 An
      Analysis of Currents and Circulation in Hampton Roads,
      Virginia. Virginia Institute of Marine Science,
      Gloucester Point, Virginia, January, 1975, 98 pp.,
      39 figs., 5 tables.
          The investigation of the water circulation in
      Hampton Roads concluded that it is dominated by tidal
      currents. Results of current measurements from the
      James River Hydraulic Model demonstrate all of the
      essential features of the tidal circulation in pro-
      totype.

[16] Malloy, R. J. U. S. Navy Harbor Maintenance Dredging
         Atlas (CONUS). (Preliminary Outline Copy) Foundation
         Engineering Division, Civil Engineering Laboratory,
         Port Hueneme, California, April, 1980, 21 figs.
             This article discusses dredging and alternative
      methods for Navy harbors. Sediment types and sedi-
      ment prevention systems are also reported.

[17] O'Connor, D. J. and Lung, W., "Suspended Solids Analysis
         of Estuarine Systems." ASCE Journal of the Environ-
         mental Engineering Division, Vol. 107, No. EEI,
         February, 1981, pp. 101-120, 12 figs.
             A two-layer salinity and suspended solids model
      for estuarine systems is reported. The model includes
      the considerations of a seaward advective flow in the
      surface layers, landward in the bottom layer, vertical
      advective flow, vertical dispersion across the layer
      interface, and the settling of suspended solids.
      Velocity, salinity and suspended solids distributions
      of the James River estuary are also reported.

[18] Krone, R. B., "A Study of Rheologic Properties of Es-
         tuarial Sediments." Technical Bulletin No. 7. U. S.
         Army Corps of Engineers, Committee on Tidal Hydraulics,
         September, 1963, 38 figs., 10 tables.
             The author provides information on rheological
      properties of sediments from a variety of estuaries
      including the stability of deposits and the charac-
      teristics of sediment during transport. Data on
      shear strength and relative differential viscosity
      of soil samples are also reported.

[19] Kranck, K., "Sediment Deposition from Flocculated Sus-
         pensions." Sedimentology, Vol. 22, No. 1, February,
         1975, pp. 111-123, 10 figs.
             This article reports the sediment deposition
      from flocculated suspensions in coastal environments
      which is part of the composition of mud. The nature
      and formation of flocculated sediments and their
      settling characteristics is discussed.

[20]   Shelley, P. E., "Sediment Measurement in Estuarine and
         Coastal Areas." NASA CR 2769, National Aeronautics
         and Space Administration, Washington, D. C., December,
         1976, 17 figs., 5 tables.
             This report discusses the direct and indirect
         methods of measuring and preserving sediments in
         estuarine and coastal areas. Sediment mechanics,
         including sediment sources, characteristics and
         transport, are also discussed.

[21]   Hancock, D. A., Drinnan, R. E., and Harris, W. N., "Notes
         on the Biology of Sertularia Argentea L." Journal,
         Marine Biological Association, Vol. 35, 1956, pp.
         307-325, 5 figs., 4 tables.
             This article presents the investigation of the
         biology of the hydroids including their growth and
         regeneration. The findings are a) the growth is
         seasonal, occurring mostly in the summer months and
         b) the regeneration of cut stems and detached side
         branches are possible.

[22]   Poreh, M. and Hefez, E., "Initial Scour and Sediment
         Motion Due to an Impinging Submerged Jet." Pro-
         ceedings, Twelfth Congress of the International As-
         sociation for Hydraulic Research, Fort Collins,
         Colorado, September 11-14, 1967, Vol. 3, pp. 9-16,
         10 figs.
             A theoretical analysis and experimental study
         of the initial sediment motion and scour caused by
         a circular submerged jet impinging on a flat erodible
         boundary is presented. The region in which initial
         motion of sediments may occur is predicted by gener-
         alizing Shields' criterion for the critical shear
         stress in open channel flows.

[23]   Westrich, B. and Kobus, H., "Erosion of a Uniform Sand
         Bed by Continuous and Pulsating Jets." Proceedings,
         Fifteenth Congress of the International Association
         for Hydraulic Research, Turkey, 1973, Vol. 1, pp.
         91-98, 8 figs.
             An experimental investigation of erosion of a
         uniform sand bed by a vertical submerged jet is pre-
         sented. Analysis of results show that the momentum
         flux of the jet and the distance between jet nozzle
         and sediment bed determines the rate of scour.

[24] Kobus, H., Leister, P., and Westrich, B., "Flow Field and
        Scouring Effects of Steady and Pulsating Jets Imping-
        ing on a Movable Bed." Journal of Hydraulic Research,
        Vol. 17, No. 3, 1979, pp. 175-192, 12 figs.
            The flow field and erosion pattern of a continuous
      and pulsating impinging jet were studied experimentally.
      The mean velocity field as well as the turbulent and
      pulsation components, wall pressure and wall shear
      stress distributions are reported.

[25] Yalin, M. S. and Karahan, E., "Inception of Sediment
        Transport." ASCE Journal of the Hydraulics Division,
        Vol. 105, No. HY11, November, 1979, pp. 1433-1443,
        5 figs., 1 table.
            This article presents the investigation on the
      mass transport of sediments in open channel having
      movable boundaries. The prediction of the critical
      shear stress corresponding to the inception of sedi-
      ment transport in fluvial hydraulics is reported.
      An extended Shields' diagram is also included in this
      paper.

[26] Tani, I. and Komatsu, Y., "Impingement of a Round Jet on
        a Flat Surface." Proceedings, Eleventh International
        Congress of Mechanics, Munich, 1964, pp. 672-676,
        7 figs.
            An experimental study of circular jet impinge-
      ment on a flat surface is reported. The experimental
      analysis was performed using similarity solution for
      calculating jet centerline velocity and radial veloc-
      ity. The study also compares analytical results
      with experimental findings.

[27] Rajaratnam, N., "Plane Turbulent Compound Wall Jets."
        Journal of Hydraulic Research, Vol. 10, No. 2, 1972,
        pp. 189-203, 10 figs.
            Reports a simple method of predicting the varia-
      tion of the velocity and length scale and the wall
      shear stress for the problem of the plane wall jet.
      This method was based on similarity analysis, inte-
      gral momentum equation, dimensional analysis and
      available experimental data.

[28] Beltaos, S. and Rajaratnam, N., "Impinging Circular Tur-
bulent Jets." ASCE Journal of the Hydraulics Divi-
sion, Vol. 100, No. HY10, October, 1974, pp. 1313-
1328, 15 figs., 1 table.
      Presents an analytical and experimental study
of the impingement region of circular turbulent im-
pinging jets. Wall pressure and velocity fields are
reported. A semi-empirical method developed to pre-
dict the variation of the axial velocity is discussed
as well as an analytical method developed to assess
the wall shear stress profile.

[29] Beltaos, S. and Rajaratnam, N., "Impingement of Axisym-
metric Developing Jets." Journal of Hydraulic Re-
search, Vol. 15, No. 4, 1977, pp. 311-326, 8 figs.,
2 tables.
      An experimental and analytical study of develop-
ing jets, impinging on a smooth wall, is presented.
Measurements of the velocity field and static pres-
sure in excess of ambient and wall shear stress are
reported.

[30] Kline, S. J., Abbott, D. E., and Fox, R. W., "Optimum
Design of Straight-Walled Diffusers." Journal of
Basic Engineering, Vol. 81, No. 9, September, 1959,
pp. 321-331, 8 figs., 1 table with discussion.
      This article discusses four common optimum prob-
lems in diffuser design. Included in the discussion
are the effects of geometrical and non-geometrical
parameters. Derivation of diffuser head losses and
the minimization of this head loss are also provided.

[31] Ho, G. C., Diaz, R. J., and Neilson, B. J., "Evaluation
of Ventra Vacs at Pier 12 Naval Base, Norfolk, Vir-
ginia." Special Report No. 228 in Applied Marine
Science and Ocean Engineering, Virginia Institute of
Marine Science, Gloucester Point, Virginia, September,
1979, 12 figs., 8 tables.
      The authors summarize the field and flume study
of the Ventra Vac units to resolve suction fouling
problems on deep-draft vessels. Field study of cur-
rents, water quality, bathymetry and the distribution
and entrainment of marine organisms at Pier 12 area
is reported. Flume tests to determine the character-
istics of the marine organisms are also described.

[32] Diaz, R. J. <u>Distribution and Hydrodynamic Properties of Fouling Organisms in the Pier 12 Area of the Norfolk Naval Station</u>. Virginia Institute of Marine Science, Gloucester Point, Virginia, 1980, 1 fig., 5 tables.
       This article reports the distribution and hydro-dynamic properties of the silver hydroid and fleshy bryozoans in Hampton Roads area of the Norfolk Harbor, Virginia.

Appendix F,
User's Manual–Numerical Program

APPENDIX F
USER'S MANUAL
NUMERICAL PROGRAM

F.1 ORIGIN OF THIS PROGRAM

The program documented herein was developed by Hydro Research Science (HRS, Inc.) of Santa Clara, California under ONR contract Number N00014-80-C-0395 dated 80 MAR 17.

F.2 PURPOSE OF THE PROGRAM

This simulation program has been designed to analyze under-keel flow field characteristics under the influence of combined sea chest discharge jet and suction. The purpose of the analysis is to assist in judging CVN class sea chest ingestion of suspended sediments.

The two bottom boundary conditions simulated were flat and movable bottoms. The bottom materials involved in the simulations were sand and mud.

F.3 HARDWARE AND SOFTWARE REQUIREMENTS

This numerical model has been written for standard FTN compiler executions of the CDC 7600 machine. These codes can also be compiled and executed on other machines such as IBM computer systems. The CPU time is about 5 seconds for the flat-bottom problem, and 0.7 seconds for the movable-bottom problem.

F.4 GENERAL DESCRIPTION OF THE PROGRAM

The present flat-bottom numerical model will simulate the flow field of combined jet and suction. It also simulates the bottom pressure and the bottom shear stress under the impingement of a discharger jet. The input data for the model includes: (a) the diameters of the jet and the suction, (b) the distance

from the jet center to the suction center, and (c) the flow rate
and depth from the jet (or suction) to the bottom.

The jet and suction are treated separately in computation
procedures. The advantage of this approach is the use of an
axisymmetrical flow field assumption, which is good for both
jet and suction problems.

Based on the numerical results, which showed that if the
radial distance from the center of the jet (or suction) to the
point of interest is greater than three jet (or suction) diam-
eters, then the kinematics are negligible. This was also sup-
ported by the HRS physical model test results. In the present
problem, the distance from the jet center to the suction cen-
ter is much greater than triple the diameter of the jet (or
suction).

The flow field for a movable-bottom boundary was simulated
under the impingement of a jet. The numerical model is based
on HRS laboratory results. This model is for water depths of
5- and 13-ft, and for two different bottom materials (mud and
sand). The diameter of the jet is 16-in., and the flow rate is
5890 gpm.

F.5 LIMITATIONS OF THE PROGRAM

Two different bottom boundary conditions are simulated:
the flat bottom, and the movable bottom. The flat bottom
numerical model does not have limitations. It is a general
model, and can provide flow field, bottom pressure, and bottom
shear stress information for any conditions.

For movable bottom boundary problems, on the other hand,
this model can only provide flow field information for four
different cases, including: two different depths (5- and 13-
ft), and two different bottom materials (sand and mud). These
conditions were based on HRS laboratory results.

F.6 INPUT REQUIREMENTS

Input requirements are summarized in the following table.

TABLE F-1

Input Requirements for Numerical Model

Card number and format	Fortran variables	Description
1 2I2	LTYPE	= 1 Flat bottom = 2 Movable bottom
1 2I2	LMAT	= 1 Bottom material is mud = 2 Bottom material is sand
1 1X, F10.7	CONCEN	The concentration of bottom material sucked into the suction
2 F6.3, 3(2X, F6.3), 2X, F8.3	DJ	The diameter of the jet (the unit is inches)
	DS	The diameter of the suction (the unit is inches)
2 F6.3, 3(2X, F6.3), 2X, F8.3	DEPTH	The axial distance from the jet (or suction) opening to the bottom (the unit is feet)
	DIS	The radial distance from the jet center to the suction center (the unit is feet)
	Q	The absolute flow rate of the jet or suction (the unit is gpm = gallons per minute)

Figure F-1 illustrates a typical input card.

Where LTYPE   = 2

LMAT   = 1

CONCEN   = 0.00013

DJ   = 16 inches

DS   = 37.125 inches

DEPTH   = 13 feet

DIS   = 12.85 feet

G   = 5890 CPM

Figure F-1

Typical Input Card for Numerical Program

F.7 OUTPUT FORMATTING

The output first lists all the information described in the input. Then for the movable-bottom problems, it prints the axial and radial velocity field of the impingement of the jet in dimensionless form. The common denominator is the average velocity at the opening of the jet.

For the flat-bottom problems, the output shows the flow-field results under the impingement of the jet in dimensionless form, and the common denominator is the average velocity at the opening of the jet. The flow-field results under the suction are also reported in dimensionless form, which is normalized by the average velocity at the opening of the suction. The total flow-field results present the flow-field under the combination of the impingement of the jet and suction expressed in feet per second. Finally, the bottom-pressure and shear stress distribution along the radial direction is printed.

F.8 FLOW CHART

Figure F-2 illustrates the logic setup of the program.

F.9 PROGRAM LISTING

A numerical model program listing follows (refer to the following 16 pages).
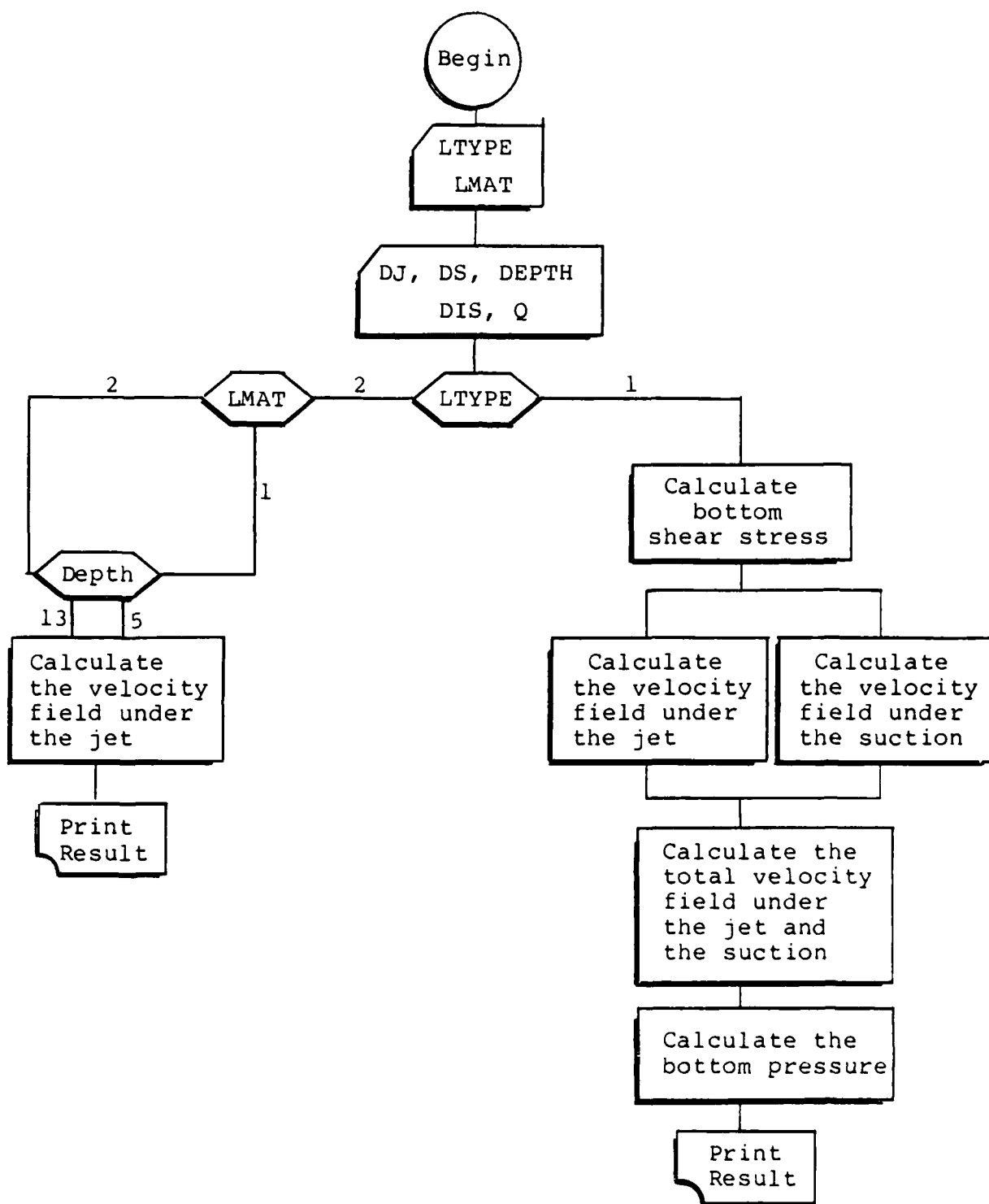
Figure F-2

Flow Chart

```
HRSSC

  1.  000000B        **PROGRAM HRSSC(INPUT,OUTPUT,TAPE5=INPUT,TAPE6=OUTPUT)**

                C***  PROGRAM HRSSC(INPUT,OUTPUT,TAPE5=INPUT,TAPE6=OUTPUT)
                C***  THIS NUMERICAL MODEL IS TO DEFINE THE THE GENERALIZED VELOCITY FIELDS
                C***  UNDER CAPITAL SHIPS DURING PIERSIDE STEAMING EVOLUTIONS FOR THE
                C**   CONTRACT OF NAVAL FACILITIES ENGINEERING COMMAND.
                C**

  2.  001103B       DIMENSION UZJ(101,81),URJ(101,81),UZS(101,81),URS(101,81),
                   *STR(101,81),UC(101),VM(81),VP(81),RR(81),RZ(81),
                   *RAD(81),ZDE(101),PR(81),SH(81),PRDI(81),UMO(41,4),VMO(34,4)

  3.  001103B       DIMENSION NU(3),NV(3),PU(3),PV(3)
  4.  001103B       DATA (UMO(I,1),I=1,32)/3.,7.13,8.63,10.13,9.,11.,5.,0.57,
                   *0.5,0.13,0.03,0.017,0.014,0.011,0.009,0.0,0.54,0.48,0.21,
                   *0.077,0.0,-0.049,-0.066,-0.057,-0.046,-0.03,-0.02,0.2,0.15,
                   *0.0,-0.063,-0.074/

  5.  001103B       DATA (UMO(I,2),I=1,41)/3.,7.5,9.32,11.19,12.,16.,6.,0.642,
                   *0.368,0.165,0.037,0.025,0.025,0.024,0.023,0.017,0.0099,0.0049,
                   *0.0,0.518,0.443,0.226,0.049,0.033,0.03,0.026,0.025,0.017,0.,
                   *-0.015,-0.035,-0.047,-0.051,-0.047,-0.037,0.318,0.21,0.099,
                   *0.049,-0.064,-0.151/

  6.  001103B       DATA (UMO(I,3),I=1,13)/2.,2.63,3.75,4.,4.,0.73,0.37,-0.012,0.,
                   *0.71,0.046,0.0014,0./

  7.  001103B       DATA (UMC(I,4),I=1,32)/3.,1.875,3.038,4.54,8.,11.,6.,0.894,
                   *0.855,0.684,0.179,0.053,0.0105,0.0053,0.0,0.795,0.752,0.566,
                   *0.137,0.021,0.,0.,-0.0013,-0.0092,-0.0237,-0.0263,0.71,0.566,
                   *0.016,-0.16,-0.113,-0.026/

  8.  001103B       DATA (VMO(I,1),I=1,34)/3.,5.,8.75,10.86,5.5,11.,7.,8.,-0.029,
                   *3.,0.,-0.009,-0.011,-0.029,0.043,0.054,0.06,0.051,0.031,-0.0036,
                   *0.0027,0.011,0.017,0.026,0.031,0.049,0.0045,0.014,0.023,
                   *0.02,0.014,0.0029,0./

  9.  001103B       DATA (VMO(I,2),I=1,34)/3.,3.75,6.,8.25,5.,11.,9.,6.,0.,0.,-0.012,
                   *-0.0049,0.0049,0.0142,0.,0.0099,0.0173,0.0839,0.0938,0.,0.,0.,
                   *0.0099,0.0173,0.0259,0.0494,0.0642,0.0074,0.0099,0.0235,0.0222,
                   *0.0074,0./

 10.  001103B       DATA (VMO(I,3),I=1,30)/3.,4.125,7.35, 8.81,0.5,11.,5.,6.,0./
```

```fortran
            *-0.0015,-0.0091,-0.0121,-0.0061,0.0053,0.033,0.051,0.051,0.033,
            *30.,0.,...,0.006,0.0212,0.033,0.0182,0.0242,0.0208,0.0242,0.0074,
            *0./
11.  001103B
12.  C011038        DATA (VMU(I,4),I=1,21)/2.5,0.7.25,0.7.8,...,0.0015,
                   *0.0158,0.0342,0.0635,0.0039,0.0053,0.066,0.0552/
13.  123237B        READ(5,5)LTYPE,LMAT,CONCEN
                  5 FORMAT(2I2,1X,F10.7)
          C** LTYPE=1, IT IS FOR THE FLAT BOTTOM
          C** LTYPE=2, IT IS FOR THE MOVABLE BOTTOM
          C** LMAT=1, THE BOTTOM MATERIAL IS WALNUT SHELL
          C** LMAT=2, THE BOTTOM MATERIAL IS SAND
14.  123237B        IF(LTYPE.EQ.1) WRITE(6,7)
15.  123247B      7 FORMAT(//2X,*----FLAT BOTTOM----*,//)
16.  123247R        IF(LTYPE.EQ.2) WRITE(6,8)
17.  123257R      8 FORMAT(//,2X,*----MOVABLE BOTTOM----*,//)
18.  123257R        IF(LTYPE.EQ.1) GO TO 9
19.  123260R        IF(LMAT.EQ.1) WRITE(6,12)
20.  123271R     12 FORMAT(/,2X,*----THE BOTTOM MATERIAL IS WALNUT SHELL----*,//)
21.  123271R        IF(LMAT.EQ.2) WRITE(6,14)
22.  123301R     14 FORMAT(/,2X,*----THE BOTTOM MATERIAL IS SAND----*,//)
23.  123.018      9 CONTINUE
24.  123302R        READ(5,10)DJ,DS,DEPTH,DIS,Q
25.  123315R     10 FORMAT(F6.3,2X,F6.3,2X,F6.3,2X,F6.3,2X,F6.3)
26.  123315B        WRITE(6,20)DJ,DS,DEPTH
27.  123326R     20 FORMAT(///,2X,*THE JET DIAMETER IS *,F6.3,1X,*IN*,//,2X,
                   * *THE SUCTION DIAMETER IS *,F6.3,1X,*IN*,//,2X,
                   * *THE WATER DEPTH IS *,F6.3,1X,*FEET*)
28.  123326R        WRITE(6,30)DIS,Q
29.  123336B     30 FORMAT(//,2X,*THE DISTANCE BETWEEN THE JET AND SUCTION IS *,
                   * 1X,F6.3,* FEET*,//,2X,
                   * *THE FLOW RATE OF THE JET AND SUCTION IS *, F8.3,* GPM*,//)
          C** CHANGE INCH TO FOOT
30.  123336R        DJ=DJ/12.
31.  123337R        DS=DS/12.
          C** CHANGE GPM TO CFS
32.  123340H        Q=Q/448.2
```

```
33.  123342B    PI=3.1415927
34.  123343B    RJ=.5*DJ
35.  123344B    RS=.5*DS
36.  123345B    VOJ=Q/(PI*RJ*RJ)
37.  123350B    VOS=-Q/(PI*RS*RS)
38.  123352B    DR=DIS/80.
39.  123354B    DZ=DEPTH/100.
40.  123356B    DRE=DEPTH/DJ
41.  123357B    IF(ILTYPE.EQ.2) GO TO 6000
                C** CALCULATE THE SKIN FRICTION (PSI) ON THE BOTTOM
                C** ALONG THE RADIAL DIRECTION
42.  123362B    TMO=PI*VOJ*VOJ*RJ*RJ*(.3048)**4
43.  123365B    DEN=1000.
44.  123367B    CHON=2.2/(3.2808*12.)**2
45.  123370B    TMOV=SQRT(TMO)/(10.**(-5)*.3048*.3048)
46.  123375B    DIVP=(.3/1270.*TMOV**.2)**(1./3.3)
47.  123405B    DLP2=1./(DEPTH*.3048)**2
48.  123407B    DO 90 I=1,81
49.  123413B    RD=DR*(I-1)
50.  123415B    RDD=RJ/DEPTH
51.  123416B    IF(RDD.GT.DIVP) GO TO 85
52.  123421B    SH(I)=DEN*TMO*DEP2*1270.*(TMOV)**(-.5)*RDD*CHON
53.  123435B    GO TO 90
54.  123440B 85 SH(I)=DEN*TMO*DEP2*.3*(TMOV)**(-.3)*RDD**(-2.3)*CHON
55.  123460B 90 CONTINUE
56.  123465B    DEN=1.93
                C** TO CALCULATE THE GENERALIZED VELOCITY FIELDS UNDER THE
                C** JET CONDITION.
                C*
                C*
                C** TO CALCULATE THE JET CENTERLINE VELOCITY ALONG THE AXIAL DIRECTION
                C**
                C**
57.  123466B    IF(DRE.LT.6.) GO TO 150
58.  123471B    DRSUB=0F.E-2.
59.  123472B    UKE=VOJ*(.8C5-.065*(DRSUB-7.))
```

```
60.  1234768   IF(DRSOB.LE.7) URE=VOJ*EXP(-0.054173*(DRE-5.))
61.  1235123   IF(DRSUE.GE.10.) URE=VOJ*EXP(-0.07048*(DRE-5.))
62.  1235525R  II=(DEPTH-2.*DJ)/DZ
63.  1735308   I3=(3.*DJ)/DZ+1
64.  1235338   DC 110 I=1,I3
65.  1235542H 110 UC(I)=VOJ
66.  1235560R  DO 120 I=I3+1,II
67.  1235728   Z=DZ*(I-1)/DJ

68.  1235758   UC(I)=VOJ*(.805-.065*(Z-7.))
69.  1236058   IF(Z.LE.7.) UC(I)=VOJ*EXP(-0.054173*(Z-3.))
70.  1236248   IF(Z.GE.10.) UC(I)=VOJ*EXP(-0.07048*(Z-3.))
71.  1236438 120 CONTINUE
72.  1236478   DO 130 I=II+1,I31
73.  1236563   Z=DRE-DZ*(I-1)/DJ
74.  1236628 130 UC(I)=URE*(1.5574*Z-1.0776*Z*Z+.2742*Z**3)
75.  1236758   GO TO 190
76.  1236768 150 URE=VOJ*EXP(-0.054173*(DRE-4.11))
77.  1237108   IF(DRE-1.1 .LE. 3.) URE=VOJ
78.  1237158   II=(DEPTH-1.1*DJ)/DZ
79.  1237208   DC 160 I=1,II
80.  1237278   Z=DZ*(I-1)
81.  1237318   IF(Z/DJ.LE.3.) GO TO 155
82.  1237348   UC(I)=VOJ*EXP(-0.054173*(Z/DJ-3.))
83.  1237518   GC TO 160
84.  1237548 155 UC(I)=VOJ
85.  1237628 160 CONTINUE
86.  1237708   DO 170 I=II+1,I01
87.  1237778   Z=DZ*(I-1)
88.  1240018   Z=(DEPTH-Z)/(1.1*DJ)
89.  1240058 170 UC(I)=URE*(Z*(2.-Z))
90.  1240178 190 CONTINUE
          C** TO CALCULATE THE VERTICAL VELOCITY ALONG THE RADIAL DISTANCE
          C** FOR A GIVEN VERTICAL LOCATION.
          C**
          C**
91.  1240208   IF(DRE.LT.6) GO TO 250
```

```
124023B    92.         RIR=6.*DJ
124024B    93.         DO 240 I=1,101
124027B    94.         Z=DZ*(I-1)
124031B    95.         R1=DJ*0.35-0.065*Z
124034B    96.         IF(Z.GE.RIR) R1=0.
124040B    97.         B1=0.115*DJ+0.087*Z
124042B    98.         DO 220 J=1,81
124045B    99.         R=DR*(J-1)
124047B   100.         IF(R.LT.R1) GO TO 210
124052B   101.         ET=(R-R1)/B1
124054B   102.         UZJ(I,J)=UC(I)*EXP(-0.693*ET*ET)
124075B   103.         GO TO 220
124076B   104.  210    UZJ(I,J)=UC(I)
124113B   105.  220    CONTINUE
124117B   106.  240    CONTINUE
124123B   107.         GO TO 290
124124B   108.  250    RIR=DEPTH-1.1*DJ
124131B   109.         CLN=0.5-0.069*(DEPTH/DJ)
124134B   110.         DO 280 I=1,101
124137B   111.         Z=DZ*(I-1)
124141B   112.         R1=.39*DJ-0.065*Z
124144B   113.         IF(Z.GE.RIR) R1=DJ*CUN*(Z/DJ)**(-0.25)
124156B   114.         B1=0.115*DJ+0.387*Z
124161B   115.         UMM=UC(I)
124166B   116.         IF(Z.GE.DEPTH-0.7*DJ) UMM=1.15*UC(I)
124176B   117.         DO 270 J=1,81
124200B   118.         R=DR*(J-1)
124202B   119.         IF(R.LT.R1) GO TO 260
124205B   120.         ET=(R-R1)/B1
124207B   121.         UZJ(I,J)=UMM*EXP(-0.693*ET*ET)

124225B   122.         GO TO 270
124226B   123.  260    IF(UMM.EQ.UC(I)) GO TO 265
124236B   124.         R2=(R/R1)**2
124240B   125.         UZJ(I,J)=UC(I)+(UMM-UC(I))*R2*(2.-R2)
```

```
126.   1242575B          GO TO 270
127.   1242618    205 JZJ(I,J)=UMM
128.   124272H    270 CONTINUE
129.   1242776    280 CONTINUE
       C**
       C**
       C** CALCULATE THE RACIAL VELOCITIES FOR THE JET PROBLEM
       C**
       C**
130.   1243028    290 IF(DRE.LT.6.) GO TO 350
131.   1243068        DO 310 J=1,81
132.   1243118        R=(DR*(J-1))/CJ
133.   1243146        IF(R.LE.1.2) VM(J)=URE*(1.070848*R-0.5313*R*R+.1042*R**3)
134.   1243318        IF(R.GT.1.2 .AND. R.LE.3.2) VM(J)=URE*(.2120061+
       *      .8004053*R-.3953057*R*R+.0559883*R**3)
135.   1243478        IF(R.GT.3.2) VM(J)=URE*(.56-.075*(R-3.2))
136.   1243608    310 CONTINUE
137.   1243638        GO TO 390
138.   1243648    350 DO 360 J=1,81
139.   1243718        R=(DR*(J-1))/CJ
140.   1243748        IF(R.LE.1.2) VM(J)=URE*(1.05*R+.40625*R*R-.54675*R**3)
141.   1244118        IF(R.GT.1.2 .AND. R.LE.2.4) VM(J)=URE*(.9-.25*(R-1.2))
142.   1244256        IF(R.GT.2.4) VM(J)=URE*(.6-.1875*(R-2.4))
143.   1244368    360 CONTINUE
144.   1244418    390 DO 400 I=1,101
145.   1244468        DO 400 J=1,81
146.   1244516    400 URJ(I,J)=0.
147.   1244758        B2=.444*DJ
148.   1244768        IY=(DEPTH-2.6*B2)/DZ+1
149.   1245038        DO 410 J=1,81
150.   1245068        VMA=VM(J)
151.   1245128        DO 410 I=IY,101
152.   1245248        Y=(DEPTH-DZ*(I-1))/B2
153.   1245306        IF(Y.GE.1.5 .AND. Y.LE.2.6) URJ(I,J)=VMA*(.579-.004*Y+.0697*Y*Y)
```

```fortran
154.   12457R      IF(Y.GE..25 .AND. Y.LT.1.5) URJ(I,J)=VMA*(.3900465+.8873704*Y-
                  *  1.9748200*Y*Y+.6967529*Y**3)
155.   12456R      IF(Y.GF.0. .AND. Y.LT..25) URJ(I,J)=VMA*(.47+6.9450522*Y-
                  *  31.2256568*Y*Y+47.692356*Y**3)
156.   124636R  410 CONTINUE
                  C**
                  C**
                  C** TO CALCULATE THE GENERALIZED VELOCITY FIELDS UNDER THE
                  C** SUCTION CONDITION (BASED ON POTENTIAL THEORY).
                  C**
                  C**
                  C** SET INITIAL CONDITION
                  C**
157.   124614R      SM=-VOS*RS*RS*.5
158.   124616R      DO 415 I=1,101
159.   124622R      DO 415 J=1,81
160.   124625R      UZS(I,J)=0.
161.   124633R  415 STR(I,J)=.5*SM

162.   124642R      DO 420 I=1,101
163.   124644R  420 STR(I,1)=0.
164.   124662R      DO 430 J=1,81
165.   124664R  430 STR(101,J)=0.
166.   124670R      DO 440 J=1,81
167.   124706R      R=DR*(J-1)
168.   124710R      STR(1,J)=-VOS*R*R*.5
169.   124720R  440 IF(R.GE.RS) STR(1,J)=SM
170.   124730R      DZ2=1./(DZ*DZ)
171.   124731R      DR2=1./(DR*DR)
172.   124734R      DZR=.5/(DZ2+DR2)
173.   124736R      DO 460 J=2,81
174.   124740R      R=DR*(J-1)
175.   124742R      RZ(J)=.5/(R*DZ)
176.   124750R  460 RR(J)=.5/(R*DR)
177.   124757R      RR(1)=0.
178.   124757R      API=(COS(PI/101.)+COS(PI/81.))**2
179.   124775R      OMI=(8.-4.*SQRT(4.-API))/API
180.   125005R      ITR=0
181.   125006R      DO 600 L=1,200
```

F-13

```
182.  1250012R       DO 550 J=2,80
183.  1250015R       IF(J.EQ.80) GO TO 520
184.  1250016R       DO 510 I=2,100
185.  1250214    510 STR(I,J)=(1.-OMI)*STR(I,J)+OMI*DZR*(DZ2*(STR(I+1,J)+STR(I-1,J))
                    * +DR2*(STR(I,J+1)+STR(I,J-1))-RR(J)*(STR(I,J+1)-STR(I,J-1)))

186.  125067R         GO TO 550
187.  1250071R    520 DO 530 I=2,100
188.  1250075R    530 STR(I,J)=(1.-OMI)*STR(I,J)+OMI/(2.*DZ2+DR2+RR(J))*(DZ2*
                    * (STR(I+1,J)+STR(I-1,J))+DR2*STR(I,J-1)+RR(J)*STR(I,J-1))

189.  1251151R    550 CONTINUE
190.  1251155R        ITR=ITR+1
191.  1251156R        IF(ITR.LE.50) GO TO 580
192.  1251159         ERR=0.
193.  1251160R        DO 560 I=2,100
194.  1251163P        DO 560 J=2,80
195.  1251166R    560 ERR=ERR+(STR(I,J)-UZS(I,J))**2
                   C** UZS(I,J) REPLACED THE PREVIOUS STREAM FUNCTION VALUE TO SAVE THE
                   C** MEMORY, LATER UZS(I,J) WILL BECOME THE VERTICAL VELOCITY

196.  1252215R        ERR=SQRT(ERR/(59.*79.))
197.  1252222R        IF(ERR.LT.0.01) GO TO 650
198.  1252274R    580 DO 590 I=2,100
199.  1252330B        DO 590 J=2,80
200.  1252333R    590 UZS(I,J)=STR(I,J)
201.  1252360B    600 CONTINUE
202.  1252363R    550 WRITE(6,670)ITR,ERR
203.  1252375R    670 FORMAT(/,1X,*TOTAL INTERATION = *,I4,* ERROR = *,E15.6)
204.  1252375R        DO 690 I=1,101
205.  1252377R    690 STR(I,81)=STR(I,80)
206.  1253322R        DO 700 I=2,100
207.  1253325R        II=I
208.  1253325R        DO 700 J=2,80
209.  1253310         JJ=82-J
210.  1253322         UZS(II,JJ)=-RR(J)*(STR(I,J+1)-STR(I,J-1))
211.  1253356R    700 URS(II,JJ)=RZ(J)*(STR(I+1,J)-STR(I-1,J))
212.  1254000B        UZS(I,81)=V0S
213.  1254010         URS(I,81)=0.
```

```
       **PROGRAM HRSSC(INPUT,OUTPUT,TAPE5=INPUT,TAPE6=OUTPUT)**

214.   1254028     UZS(1,1)=0.
215.   1254028     URS(1,1)=(STR(2,81)-STR(1,81))*RZ(81)*2.
216.   1254058     UZS(101,1)=0.
217.   1254068     URS(101,1)=(STR(101,81)-STR(100,81))*RZ(81)*2.
218.   1254118     UZS(101,81)=0.
219.   1254128     URS(101,81)=0.
220.   1254128     DO 710 I=2,100
221.   1254158     UZS(I,81)=-STR(I,2)/(DK*DK)*2.
222.   1254268     URS(I,81)=0.
223.   1254328     UZS(I,1)=UZS(I,2)
224.   1254428  710 URS(I,1)=URS(I,2)
225.   1254558     DO 720 J=2,80
226.   1254608     JJ=82-J
227.   1254618     UZS(101,JJ)=0.
228.   1254668     UZS(1,JJ)=-RR(J)*(STR(1,J+1)-STR(1,J-1))
229.   1255108     URS(1,JJ)=RZ(J)*2.*(STR(2,J)-STR(1,J))
230.   1255238  720 URS(101,JJ)=RZ(J)*2.*(STR(101,J)-STR(100,J))
       C** CALCULATE THE BOTTOM PRESSURE (PSI) DISTRIBUTION ALONG
       C** THE RADIAL DISTANCE DUE TO THE EXISTANCE OF THE JET
231.   1255428     IF(URE.LT.6.) GO TO 850
232.   1255448     DO 840 I=1,81
233.   1255478     RD=DK*(I-1)
234.   1255518     RDD=RD/DJ
235.   1255528     IF(RDD.LE.1.6) VP(I)=URE*(1.07084B*RDD-.5313*RDD*RDD+.1042*RDD**3)
236.   1255578     IF(RDD.GT.1.6 .AND. RDD.LE.2.8) VP(I)=URE*(1.72112-.09726*RDD+
       *     .1256*RDD*RDD-.026125*RDD**3)
237.   1256058     IF(RDD.GT.2.3) VP(I)=URE*.86
238.   1256148  840 CONTINUE
239.   1256179     GO TO 870
240.   1256238  850 DO 860 I=1,81
241.   1256258     RD=DK*(I-1)
242.   1256278     RDD=RD/DJ
243.   1256338     IF(RDD.LE.2.) VP(I)=URE*(1.0729167*RDD+1.0729167*RDD**3+1.1230469*RDD**4-.2034565*RDD**5)
       *     2.0639321*RDD**3+1.1230469*RDD**4-.203+565*RDD**5)
```

F-15

```
244.  1256651B        IF(RDD.GT.2.) VP(I)=URE
245.  1256661B   860  CONTINUE
246.  1256666B   870  VIN=VUJ*VLJ
247.  1256667B        DO 880 I=1,81
248.  1256723        880  PR(I)=.5*DEN*(VIN-VP(I)**2)/144.
249.  1257138        DIPR=.5*DEN*VIN/144.
250.  1257158B        DO 1000 I=1,81
251.  1257238        PRDI(I)=(PR(I)-PR(81))/DIPR
252.  1257258        PR(I)=PRDI(I)*DIPR
253.  1257328  1000  RAD(I)=DR*(I-1)
254.  1257448  1100  DO 1100 I=1,101
255.  1257468        ZDE(I)=DZ*(I-1)
256.  1257658        WRITE(6,1810)VCJ
257.  1257748  1810  FORMAT(//,2X,*THE JET ENTRANCE CENTRAL VELOCITY = *,E12.5,
                     ** FEET/SEC*,//)
258.  1257748        WRITE(6,1850)
259.  1260028  1850  FORMAT(//,2X,*--THE VERTICAL VELOCITY DISTRIBUTION FOR THE *,
                     **JET (DIMENSIONLESS FORM)--*,///)
260.  1260028        DO 1860 I=1,101
261.  1260048        DO 1860 J=1,81
262.  1260078        UZJ(I,J)=UZJ(I,J)/VCJ
263.  1260168  1860  URJ(I,J)=URJ(I,J)/VCJ
264.  1260248        DO 2000 K=1,5
265.  1260248        I1=18*(K-1)+1
266.  1260353        I2=18*K-1
267.  1260328        IF(I2.GT.81) I2=81
268.  1260368        WRITE(6,3000)(RAD(J),J=I1,I2,2)
269.  1260668        DO 1900 I=1,101,2
270.  1260708  1900  WRITE(6,3100)ZDE(I),(UZJ(I,J),J=I1,I2,2)
271.  1261348  2000  CONTINUE
272.  1261438        WRITE(6,2040)
273.  1261478  2040  FORMAT(//,2X,*--THE RADIAL VELOCITY DISTRIBUTION FOR THE *,
                     **JET (DIMENSIONLESS FORM)--*,///)
274.  1261478        DO 2100 K=1,5
275.  1261518        I1=18*(K-1)+1
276.  1261538        I2=18*K-1
277.  1261558        IF(I2.GT.81) I2=81
278.  1261618        WRITE(6,3000)(RAD(J),J=I1,I2,2)
```

```
279.  1262111B         DO 2050 I=1,101,2
280.  1262133     2050 WRITE(6,3150)ZDE(I),(URJ(I,J),J=I1,I2,2)
281.  1262257B    2100 CONTINUE
282.  1262262B         WRITE(6,2110)VCS
283.  1262273B    2110 FORMAT(//,2X,*-THE SUCTION ENTRANCE CENTRAL VELOCITY = *,E12.5,
                      ** FEET/SEC*,//)
284.  1262273B         DO 2120 I=1,101
285.  1262275B         DO 2120 J=1,81
286.  1263000B         UZJ(I,J)=UZJ(I,J)*VCJ
287.  1263007B         URJ(I,J)=URJ(I,J)*VCJ
288.  1263010B         UZS(I,J)=UZS(I,J)/VOS
289.  1263127B    2120 URS(I,J)=-URS(I,J)/VOS
290.  1263209B         WRITE(6,2140)
291.  1263273B    2140 FORMAT(///,2X,*--THE VERTICAL VELOCITY DISTRIBUTION FOR THE*,
                      ** SUCTION (DIMENSIONLESS FORM)--*,///)
292.  1263327B         DO 2200 K=1,5
293.  1263313B         I1=18*(K-1)+1
294.  1263334B         I2=18*K-1
295.  1263350B         IF(I2.GT.81) I2=81
296.  1263418B         WRITE(6,3000)(RAD(J),J=I1,I2,2)
297.  1263710B         DO 2150 I=1,101,2
298.  1263730B    2150 WRITE(6,3150)ZDE(I),(UZS(I,J),J=I1,I2,2)
299.  1764378B    2200 CONTINUE
300.  1264436B         WRITE(6,2240)
301.  1264528B    2240 FORMAT(///,2X,*--THE RADIAL VELOCITY DISTRIBUTION FOR THE *,
                      ** SUCTION (DIMENSIONLESS FORM)--*,///)
302.  1264528B         DO 2300 K=1,5
303.  1264549B         I1=18*(K-1)+1
304.  1264456B         I2=18*K-1
305.  1264604B         IF(I2.GT.81) I2=81
306.  1264646B         WRITE(6,3000)(RAD(J),J=I1,I2,2)
307.  1265104B         DO 2250 I=1,101,2
308.  1265168B    2250 WRITE(6,3150)ZDE(I),(URS(I,J),J=I1,I2,2)
309.  1265562B    2300 CONTINUE
310.  1265664H         DO 2320 I=1,101
311.  1265718B         DO 2320 J=1,81
312.  1265744H         UZS(I,J)=UZS(I,J)*VOS
313.  1266044H         URS(I,J)=URS(I,J)*VOS
```

```
314.   126E04H       UZJ(I,J)=UZJ(I,J)+UZS(I,J)
315.   126E05H  2320 URJ(I,J)=URJ(I,J)+URS(I,J)
316.   126E14R       WRITE(6,2340)
317.   126E24B  2340 FORMAT(//,2X,*--THE VERTICAL VELOCITY DISTRIBUTION FOR THE*,
                     */,2X,*--SUM OF THE JET AND THE SUCTION (FT/SEC)--*,///)
318.   126E23H       DO 2400 K=1,5
319.   126E25H       I1=18*(K-1)+1
320.   126E27H       I2=18*K-1
321.   126E31H       IF(I2.GT.81) I2=81
322.   126E35B       WRITE(6,3000)(RAD(J),J=I1,I2,2)
323.   126E65B       DO 2350 I=1,101,2
324.   126E67R  2350 WRITE(6,3100)ZDE(I),(UZJ(I,J),J=I1,I2,2)
325.   126733B  2400 CONTINUE
326.   126737H       WRITE(6,2440)
327.   126746B  2440 FORMAT(//,2X,*--THE RADIAL VELOCITY DISTRIBUTION FOR THE *,
                     */,2X,*--SUM OF THE JET AND THE SUCTION (FT/SEC)--*,///)
328.   126746R       DO 2500 K=1,5
329.   126750H       I1=18*(K-1)+1
330.   126752R       I2=18*K-1
331.   126754B       IF(I2.GT.81) I2=81
332.   126760R       WRITE(6,3000)(RAD(J),J=I1,I2,2)
333.   127010H       DO 2450 I=1,101,2
334.   127012H  2450 WRITE(6,3100)ZDE(I),(URJ(I,J),J=I1,I2,2)
335.   127056H  2500 CONTINUE
336.   127062B       WRITE(6,2600)
337.   127071B  2600 FORMAT(//,2X,*LIST THE BOTTOM PRESSURE AND THE SKIN FRICTION *,
                     * *ALONG THE RADIAL DISTANCE*,//,2X,*RADIAL DISTANCE*,4X,
                     * *  PRESSURE (PSI) *,4X,* SKIN FRICTION (PSI)*,//)
338.   127071B       DO 2700 I=1,81
339.   127073B       RD=DR*(I-1)
340.   127075H       RDD=RD/UJ
341.   127076H  2700 WRITE(6,3200)RD,PR(I),SH(I),RDD,PRDI(I)
342.   127133H  3000 FORMAT(//,15X,*RADIAL DISTANCE (FOOT)*,//,1X,
                     * * VER. DIS. *,9(1X,E12.5),//)
343.   127133H  3100 FORMAT(10(1X,E12.5))
344.   127133H  3200 FORMAT(3X,E12.5,9X,E12.5,12X,E12.5,5X,E12.5)
345.   127133H       GO TO 9000
346.   127133B  6000 CONTINUE
```

```
C**
C**
C** CALCULATE THE VELOCITY FIELD FOR A MOVABLE BOTTOM UNDER A JET
C**
C**

347.    1271368      IF(DEPTH.EQ.13.) I=LMAT
348.    127142A      IF(DEPTH.EQ.5.) I=LMAT+2
349.    1271468      KUT=UMU(1,I)+0.2
350.    127156R      KVT=VMU(1,I)+0.2
351.    1271658      DO 6100 J=1,KUT
352.    1271753      J1=J+1
353.    1271175A     J2=J1+KUT
354.    1271768      PU(J)=UMO(J1,I)*DJ
355.    1272116      J3=UMO(J2,I)+0.2
356.    1272228 6100 NU(J)=J3
357.    1272316      DO 6200 J=1,KVT
358.    1272408      J1=J+1
359.    1272498      J2=J+2+KVT
360.    1272428      PV(J)=VMO(J1,I)*DJ
361.    1272558      J3=VMU(J2,I)+0.2
362.    1272668 5200 NV(J)=J3
363.    1272758      STV=VMO(2+KVT,I)
364.    1273048      KMAX=0
365.    1273058      DO 6210 J=1,KUT
366.    1273158 6210 IF(KMAX.LT.NU(J)) KMAX=NU(J)
367.    1273328 6210 IF(DEPTH.EQ.5.) GO TO 6500
368.    1273338      ITUL=3
369.    1273348      DZ=2.*DJ
370.    1273358      R1R=6.*DJ
371.    1273378      DO 6300 J=1,ITUL
372.    1273478      Z=DZ*J
373.    1273508      R1=0.39*DJ-0.065*Z
374.    1273538      IF(Z.GE.R1R) R1=0.
375.    1273578      H1=0.115*DJ+0.087*Z
376.    1273618      ZC=7/DJ
377.    127?026      IF(ZC.LT.3.) UCV=VOJ
```

```
378.   1273668   IF(ZD.GT.3. .AND.ZD.LE.7.) JCV=VOJ*EXP(-0.054173*(ZD-3.))
379.   1274028   DO 6220 J1=1,KMAX
380.   1274118   R=0.5*DJ*(J1-1)
381.   1274148   IF(R.LT.R1) GO TO 6215
382.   1274178   ET=(R-R1)/B1
383.   1274218   UZJ(J1,J)=UCV*EXP(-0.693*ET*ET)/VOJ
384.   1274418   GO TO 6220
385.   1274428  6215 UZJ(J1,J)=UCV/VOJ
386.   1274548  6220 CONTINUE
387.   1274618  6240 CONTINUE
388.   1274658   GO TO 6550
389.   1274668  6500 ITOL=1
390.   1274678   DZ=DJ
391.   1274718   Z=DZ
392.   1274718   R1=0.39*DJ-0.065*Z
393.   1274748   B1=0.115*DJ+0.087*Z
394.   1274778   DO 6510 J=1,KMAX
395.   1275078   R=0.5*DJ*(J-1)
396.   1275128   IF(R.LT.R1) GO TO 6520
397.   1275158   ET=(R-R1)/B1
398.   1275178   UZJ(J,1)=VOJ*EXP(-0.693*ET*ET)/VOJ
399.   1275348   GO TO 6510
400.   1275358  6520 UZJ(J,1)=1.
401.   1275448  6510 CONTINUE
402.   1275528  6550 CONTINUE
403.   1275538   WRITE(6,1810)VOJ
404.   1275628   WRITE(6,1850)
405.   1275708   DO 6600 J=1,KMAX
406.   1275778  6600 RAD(J)=0.5*DJ*(J-1)
407.   1276178   KP4A=9
408.   1276178   IF(KMAX.LT.9) KPMA=KMAX
409.   1276238   WRITE(6,3000)(RAD(J),J=1,KP4A)
410.   1276508   DO 6620 J=1,ITOL
411.   1276578   Z=DZ*J
412.   1276608  6620 WRITE(6,3100)Z,(UZJ(J1,J),J1=1,KPMA)
413.   1277158   I1=8
414.   1277168   I2=I1+NU(1)
415.   1277178   I3=I2+NU(2)
```

```
416.   DO 6630 J=1,KUT
417.   IF(J.EQ.1) IST=11
418.   IF(J.EQ.2) IST=12
419.   IF(J.EQ.3) IST=13
420.   IUD=9+IS1-1
421.   IF(NU(J).LT.9) IEND=NU(J)+IST-1
422.   6630 WRITE(6,3100)PU(J),(UMU(J1,I),J1=IST,IEND)
423.   IF(KMAX.LL.9) GO TO 700C
424.   KST=10
425.   WRITE(6,3000)(RAC(J),J=KS1,KMAX)
426.   DO 6650 J=1,ITCL
427.   L=DZ*J
428.   6650 WRITE(6,3100)IZ,(UZJ(J1,J),J1=KS1,KMAX)
429.   I1=17
430.   I2=I1+NU(1)
431.   I3=I2+NU(2)
432.   DO 6683 J=1,KUT
433.   IF(NU(J).LE.9) GO TO 6670
434.   IF(J.EQ.1) IST=11
435.   IF(J.EQ.2) IST=12
436.   IF(J.EQ.3) IST=13
437.   IEND=IST+NU(J)-10
438.   WRITE(6,3100)PU(J),(UMU(J1,I),J1=IST,IEND)
439.   GO TO 668C
440.   6670 WRITE(6,3100)PU(J)
441.   6680 CONTINUE
442.   7000 CONTINUE
443.   WRITE(6,7100)
444.   7100 FORMAT(///,2X,*--THE RADIAL VELOCITY DISTRIBUTION UNDER THE *,
       * *JET (DIMENSIONLESS FORM)--*,//,15X,
       * *RADIAL DISTANCE (FOOT)*,/)
445.   WRITE(6,7110)(PV(J),J=1,KVT)
446.   7110 FORMAT(/,1X,* VER. DIS. (FT) *,8(1X,E12.5))
447.   IF(KVT.EQ.2) GO TO 7260
448.   I1=9
449.   I2=I1+NV(1)
450.   I3=I2+NV(2)
451.   DO 7250 J=1,11
```

```
452.    1303148    POS=(STV+0.5*(J-1))*DJ
453.    1303320B    I4=I1+J-1
454.    1303321B    I5=I2+J-1
455.    1303323B    I6=I3+J-1
456.    1303325B    A=VMQ(I4,1)
457.    1303335B    B=VMQ(I5,1)
458.    1303345B    IF(NV(3).GE.J) C=VAQ(I6,1)
459.    1303361B    IF(NV(3).GE.J .AND. NV(2).GE.J .AND. NV(3).GE.J)
                  *  WRITE(6,7400)POS,A,B,C
460.    1304018    IF(NV(1).GE.J .AND.NV(2).LT.J .AND. NV(3).GE.J)
                  *  WRITE(6,7410)POS,A,C
461.    1304218    IF(NV(1).GE.J .AND. NV(2).GE.J .AND. NV(3).LT.J)
                  *  WRITE(6,7400)POS,A,B
462.    1304418    IF(NV(1).GE.J .AND. NV(2).LT.J .AND. NV(3).LT.J)
                  *  WRITE(6,7430)POS,A
463.    1304608   7250 CONTINUE
464.    1304638   7400 FORMAT(3X,E12.5,6X,E12.5,1X,E12.5,1X,E12.5)
465.    1304638   7410 FORMAT(3X,E12.5,6X,E12.5,1+X,E12.5)
466.    1304638   7420 FORMAT(3X,E12.5,19X,E12.5)
467.    1304638        GO TO 8000
468.    130464E   7260 I1=7
469.    1304668        I2=I1+NV(1)
470.    1304708        DO 7270 J=1,7
471.    1304738        POS=(STV+0.5*(J-1))*DJ
472.    1304778        I4=I1+J-1
473.    1305008        I5=I2+J-1
474.    1305028        A=VMQ(I4,1)
475.    1305118        B=VMQ(I5,1)
476.    1305208   7270 WRITE(6,7400)POS,A,B
477.    1305378        I5=I2+7
478.    1305418        POS=(STV+0.5*7.)*DJ
479.    1305438        B=VMQ(I5,1)
480.    1305528        WRITE(6,7420)POS,B
481.    1305648   8000 SUVOL=Q*CUHEN*60.
482.    1305678        WRITE(6,8010)SUVOL
483.    1306028   8010 FORMAT(///,3X,*THE SUCTION RATE OF THE BOTTOM MATERIAL IS *,
                  *  E13.6,* CU. FT. / MIN. *)
484.    1306008   9000 CONTINUE
485.    1306018        END
```

F-22

Appendix G,
Conversion Factors, Customary to
SI Units of Measurements

APPENDIX G

CONVERSION FACTORS, CUSTOMARY
TO SI UNITS OF MEASUREMENTS

Units of measurement used in this report can be converted as follows:

Multiply	By	To Obtain
inch	2.540* – 02	meter
foot	3.048* – 01	meter
micron	1.000* – 06	meter
foot/second	3.048* – 01	meter/second
centimeter/second	1.000* – 02	meter/second
pound	4.537* – 01	kilogram
gram/cubic centimeter	1.000* + 03	kilogram/cubic meter
cubic foot/second	2.832* – 02	cubic meter/second
gallons/minute	6.310* – 05	cubic meter/second

END

FILMED

9-83

DTIC